Control of Size and Charge Selectivity in Amphiphilic Graft Copolymer Nanofiltration Membranes

by

Nathan Gary Lovell

B.S. Chemistry, University of Utah, 2001
B.C.S. Computer Science, University of Utah, 2002

S.M. Materials Science and Engineering,
Massachusetts Institute of Technology, 2005

Submitted to the Department of Materials Science and Engineering in Partial Fulfillment of the Requirements for the Degree of

Doctor of Philosophy in Materials Science and Engineering

at the

Massachusetts Institute of Technology

September 2010

Signature of Author:_____
Department of Materials Science and Engineering
June 28, 2010

Certified by:_____
Anne M. Mayes
Toyota Professor of Materials Science and Engineering
Thesis Co-Advisor

Certified by:_____
Michael F. Rubner
TDK Professor of Materials Science and Engineering
Thesis Co-Advisor

Accepted by:_____
Christopher Schuh
Danae and Vasilios Salapatas Associate Professor of Metallurgy
Chair, Departmental Committee on Graduate Students

Control of Size and Charge Selectivity in Amphiphilic Graft Copolymer Nanofiltration Membranes

by

Nathan Gary Lovell

Abstract

The throughput and efficiency of membrane separations make polymer filtration membranes an important resource for the pharmaceutical, food and wastewater treatment industries. Nanofiltration (NF) membranes fill an important niche between nonporous reverse osmosis membranes, which have comprehensive solute rejection and low solvent permeability, and porous sieving ultrafiltration membranes. However, challenges in NF membrane design remain outstanding. At the effective pore size of NF membranes (~0.5 nm-2 nm), both electrostatic and steric factors determine membrane selectivity. Most NF membranes are charged under a wide range of environmental conditions and thus preferentially exclude charged solutes. This charge selectivity precludes separation of molecules based solely on size. An additional limitation of NF membranes is the tendency to foul by adsorption of feed components. The purpose of this thesis is to demonstrate control of membrane selectivity in fouling resistant membranes via manipulation of the chemistry of a specific copolymer system, polyacrylonitrile (PAN)-based poly(ethylene oxide) (PEO) graft polymers.

Previous work with amphiphilic graft copolymers as membrane materials has included PAN-*g*-PEO with an average graft length of 9 (PAN-*g*-PEO9). PAN-*g*-PEO9 was shown to have excellent fouling resistance as an antifouling additive in porous ultrafiltration membranes and as a dense selective layer coated onto a support base membrane—a thin-film composite (TFC) NF membrane. The comb morphology of the polymer imposes high interfacial area on the microphase-separated domains, resulting in a bicontinuous structure consisting of a glassy PAN matrix interpenetrated by PEO-filled "nanochannels" that can act as *via*s for water and small solutes (with a size cutoff of ~0.8 nm). It also presents a PEO brush on the comb surface which acts as a steric barrier to resist irreversible fouling of the membranes. The understanding from previous work on PEO comb NF membranes is that the pore size is determined by the nanochannel's size, *i.e.* the PEO domain size.

Because the graft characteristics (spacing and length) of comb copolymers determine the domain size, it was expected that varying the graft length would allow broad, precise control of the size cutoff of the TFC membranes, a concept demonstrated previously with amphiphilic graft copolymer NF membranes of poly(vinylidene fluoride)-*graft*-poly(oxyethylene methacrylate) (PVDF-*g*-POEM). The first aim of this thesis was to tailor the retention properties of PAN-*g*-PEO TFC NF membranes by modifying the chemistry to tune the electrostatic and steric properties sufficiently to enable complex separations, particularly of solutes with high fouling potential. Comb copolymers incorporating ~40 weight % PEO with side chains varying from 5-40 EO units were synthesized by free radical methods and compared as selective-layer coatings on PAN UF membranes.

Membranes incorporating combs with 9 EO units or more were shown to resist irreversible fouling when challenged by a model protein feed solution (bovine serum albumin) for 24 hours. Fouling resistance was found to be compromised, however, upon exposure to acid (pH 2) solution, used to simulate chemical cleaning procedures in industry. Thickness-normalized permeabilities of these PAN-*g*-PEO*n* NF membranes exceeded those of commercially available NF membranes by approximately an order of magnitude. A systematic effect of side chain length on permeability was seen when varying temperature, ionic strength, and pressure.

Contrary to expectations, the membrane size cutoff (~0.8 nm) for charged rigid molecular probes in deionized water was independent of the comb side chain length. This new finding can be explained by modeling the hydrophilic domains as opposing swollen polymer brushes of uniform density acting as a physical gel. The gel mesh size (distance between chains) is independent of side chain length, and controls the size cutoff in good solvent conditions matching those in which the membrane was equilibrated during fabrication. In poorer solvent conditions, a decrease in the brush height, progressing to complete collapse of the PEO gel, can be expected to create differentiation based on domain size (*i.e.* side chain length). This is consistent with the finding that retentions of dyes increased with decreasing side chain length in saline solution, as salt is known to reduce PEO-water miscibility.

Fluorescently labeled peptides germane to proteomics research were filtered and both chromatographic and size-selective membrane behavior was observed—the first demonstration of size-based nanofiltration of peptides. Based on this finding, two different peptides of molecular weights 1.3kDa and 1.5kDa were fractionated to achieve a six-fold increase in the concentration of the larger peptide relative to the smaller peptide in two filtration steps.

The electrostatic selectivity of the PEO comb membranes could also be varied. Terpolymers consisting of PAN-*g*-PEO with 1-2% charged sulfopropyl acrylate (SPA) or 5% *N*,*N*-dimethyl-*N*-(2-methacryloyloxyethyl-*N*-(3-sulfopropyl) ammonium betaine (SPE) were synthesized and coated onto PAN base membrane. The divalent salt (Na_2SO_4) retention of the resulting TFC membranes increased from ~20% for the PAN-*g*-PEO copolymer to ~45% and 82% for the SPE and SPA terpolymers, respectively. Retention of monovalent NaCl was substantially lower, characteristic of commercial NF membranes. The charged comb membranes did not completely resist fouling by a 1 g/L BSA solution, losing 2% of the initial flux after 24 h exposure. Forming a trilayer TFC, with a layer of PAN-g-PEO coated over a charged terpolymer, reduced membrane fouling compared to the charged layer alone.

In summary, the goal of this study was to demonstrate control of membrane selectivity in fouling-resistant PAN-*g*-PEO NF membranes. An important finding was that the PEO gel created in the hydrophilic domains leads to similar size cutoffs over a wide range of side chain length. To access the desired spectrum of size cutoffs, the quality of solvent for the swollen PEO brush must be reduced. In spite of these limitations, the membrane was shown to have useful fractionating properties as demonstrated with labeled peptides of varying molecular weight. The retention of salts was enhanced by incorporating small amounts of charged monomer into the comb backbone, but at the expense of fouling resistance.

Thesis Supervisor: Anne M. Mayes

Table of Contents

List of Figures

List of Tables

Acknowledgements

I would like to acknowledge and extend thanks to some key people who have shaped my experiences here. First, to Professor Anne Mayes for her patience and unflagging attention to detail, for the high standards she holds herself to and expects from others, and for her candid observations. She has been a loyal advocate and a blunt critic, an insightful advisor and an endless optimist;

Second, to Professor Michael Rubner for taking the Mayes refugees under his wing, for dispensing regular doses of reality into my perspective, and for being an excellent administrator of so many important programs, particularly the CMSE/MPC summer internship that introduced me to Materials Science and MIT;

To Ayşe Asatekin Alexiou, who is appropriately first in so many alphabetical lists of friends, and never accepts without a fight the stolid, silent passing of friends (or strangers) in the hallway that so many of us take for granted; who knows, like only a few do, what it is to be "insane in the membrane", and who successfully grants respect and dignity to those she meets without feeling her own considerable competence is threatened thereby;

To Al for passing on such crucial wisdom as the art of playing dart; to Will for peptides and quiet brilliance; to Bill Phillip for “forcing” the issue; to Randy Carney for reigning over his fiefdom with great wisdom and order, and nanostuff; to the Cohen/Rubner collective and the former Mayes group members for their insights; to my committee for making time and taking the position seriously in spite of hectic schedules;

To Brian Kinghorn for his tireless friendship through thick and thin and many miles;

To Carolee and Gary Lovell, for their habitual inability to conceive of me failing, and puzzled but unquestioned love when i so often do;

To Professor J. Walter Woodbury and Grandma Betty the entomologist, who are behind whatever principle of intelligence i have attained. Grandpa: in a most unexpected way, the “family business” of membrane research passed to another generation…

To Patrick Boisvert and Dr. Shiahn Chen for their assistance with electron microscopy;

And finally, to the many friends who have so frequently brightened Boston's greyer days.

The financial support for this work was provided by the WaterCAMPwS, a Science and Technology Center of Advanced Materials for the Purification of Water with Systems under National Science Foundation agreement number CTS-0120978. Funding was also provided *via* NSF fellowship and DuPont-MIT Alliance, for which i am most grateful. The MRSEC Shared Experimental Facilities were vital for characterization. They are supported by the National Science Foundation under Award DMR-0213282.

1. Overview

This thesis is about the basis and control of the properties of filtration membranes[*] based on amphiphilic graft copolymers. The membranes have been a topic of some extended focus in our group which applied principles of polymer morphology to important engineering challenges. These challenges and the motivation for the work will be discussed presently, complemented by a discussion of membrane filtration processes. After this context is established, the history of amphiphilic graft copolymer materials in membranes will be reviewed as a preface for the research presented herein. The aim of the project was to control the steric (size) and charge selectivity of polyacrylonitrile-*graft*-poly(ethylene oxide) membranes and characterize their filtration properties for new applications.

1.1. Introduction

Two important trends, the exponentially growing global demand for fresh water and the rapid advances in biotechnology, are motivating interest in technologies that can selectively remove components of aqueous feeds. Because of their scalability and versatility, polymer filtration membranes have been employed across the spectrum of applications, from those characterized chiefly by volume and cost considerations (*e.g.* textile dye recovery [1,2] municipal wastewater treatment [3] and seawater desalination for municipal potable water [4]) to the precision fractionation of organic molecules and biocomponents in complex feeds for the pharmaceutical industry [5,6].

The charged, aromatic polyamide (PA[†]) selective layers of membranes used in current practice have limited utility for fractionating output streams from industrial processes and retaining small, uncharged contaminants. Increasing public interest in natural food additives, awareness of deleterious compounds in the environment, and pressure to reduce pollutants in industrial waste streams point to a need for new membrane technologies with controlled size-based separation capability at the molecular scale. Moreover, future biochemical therapies and

[*] A membrane can be generally defined as a thin discrete barrier with selective permeability.
[†] A glossary of abbreviations and terms is found on page 98.

assays will require ever more precision, scalability, and speed in processing solutions of very small organic molecules, such as protein digests inherent to proteomics technologies.

1.2. Water and Sustainability

A dependable supply of water has been a vital issue in human history, prompting such basic inventions as dams, canals, wells, and aqueducts. Water quality is also important, with many pathogens using it as a vector for infection. A significant fraction of the over one million annual deaths due to diarrheal diseases are attributed to contaminated water, and nearly one billion people lack access to clean water [7]. The developed world expends substantial resources to create and maintain its supply: in the United States, business-as-usual infrastructure upgrades are expected to cost over $1 trillion over the next 15 years using present technology and neglecting growth; yet, many parts of the country already face anthropogenic water supply-related problems and fully developed resources, even as the population continues to expand [8]. Improvements are needed in water treatment technology.

An adequate water supply represents, then, a sustainability challenge on par with energy. The demand and provision of the two resources are inextricably linked. For example, over 50 percent of water withdrawals in the states of New Hampshire, Massachusetts, Rhode Island, and Connecticut are used for energy production purposes [8], while an estimated 24 MW of power will be consumed by a new seawater desalination plant in San Diego to produce 50M gallons fresh water per day.

1.3. Water Purification and Membranes

The significant energy cost of water purification is one of the drivers of interest in alternative technologies. Installations of thermal-based seawater desalination plants proliferated *e.g.* in the Middle East during the second half of the last century due to a lack of effective and competitive options. The advent of the Loeb-Sourirajan process in 1963 made polymer membranes an alternative industry for the first time [9,10]. The innovation consisted of a phase inversion precipitation of cellulose acetate which formed the bulk of the membrane material into a porous support with a thin, dense selective skin layer on one face (Figure

1.1.A). This *asymmetric* membrane structure had much greater permeability than the symmetric membranes produced previously.

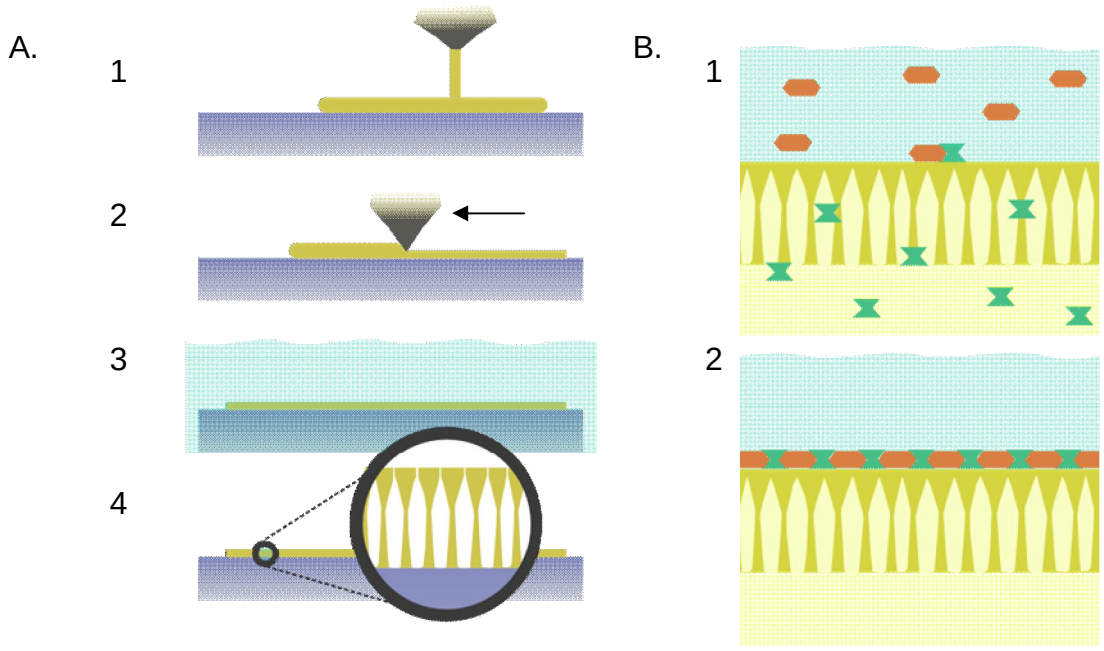

Figure 1.1. Breakthrough polymer membrane fabrication schemes include the Loeb-Sourirajan phase inversion process (A) and interfacial polymerization (B); A: a polymer solution (1) is formed into a thin, uniform layer (2) on a flat surface and immersed into a nonsolvent bath (3). An *asymmetric membrane* is formed as the nonsolvent wave front advances inward from the top of the polymer solution layer, causing a porous support to form under a thin skin (4). B: a *thin-film composite* membrane (2) can be formed via interfacial polymerization as a porous base membrane is first infiltrated with an aqueous solution containing one monomer, and then transferred to a solution of a second monomer in an organic solvent (1).

The cellulose acetate membrane had two shortcomings that limited its utility: sensitivity to acid, base[*] and elevated temperature, and insufficient salt retention to make seawater potable in a single pass. Nevertheless, a membrane industry developed around cellulose acetate reverse osmosis membranes and the phase inversion process, which was soon adapted to synthetic polymers such as polyacrylonitrile and polysulfone for other applications.

A second important membrane innovation was the interfacially-polymerized, thin-film composite (TFC) membrane, which was stable over a greater pH range, but with the tradeoff of susceptibility to oxidative attack by *e.g.* chlorine. The FT-30 developed at FilmTec by Cadotte in the late 1970s [11] made single-stage seawater reverse osmosis (SWRO) possible.

[*] The operating range for cellulose acetate is pH 4-6 [9].

The process was widely adopted and is well represented in contemporary product lines (Figure 1.1.B).

1.4. Membranes

A membrane can be abstracted as a sieve. In this context, the fundamental characteristic is the size of the grating, or the smallest solute that it prevents from passing through. This is the basis for membrane classification. In microfiltration (MF, size cutoff 0.1 to 10 μm) and ultrafiltration (UF, 2-200 nm) membranes, the molecular weight cutoff (MWCO[*]) is determined by the size and shape of discrete pores in the membrane selective layer. Their range of MWCO makes them suitable for removing particulates, macromolecules and microorganisms, and these membranes are commonly used for the sterilization of water and clarification of beverages [9].

Reverse osmosis (RO) membranes have no discrete pores. The selective (or "active") layer is a dense polymer film that allows water to permeate by diffusion through the free volume between the polymer chains. The effective size cutoff is less than half a nanometer, making reverse osmosis membranes capable of retaining even small salts (*e.g.* sodium and chloride ions in seawater, with hydrated radii of ~0.7 nm [13]). However, molecules with a high affinity for the membrane material may dissolve into the thin selective layer itself and diffuse across, a process known as solution-diffusion [14].

The most recent category of membranes fills the gap between RO and UF, that is, from 0.5 nm to 2 nm. Although these nanofiltration (NF) membranes may be considered to have discrete pores, these are not directly formed by the phase inversion process introduced in the previous section, which is used for UF and MF membranes [15]; typically, the membranes are created by the interfacial polymerization of an aromatic polyamide on the microporous surface of an asymmetric UF or MF base (Figure 1.1.B) [9], a structure referred to as a thin-film composite (TFC). Although NF membranes span the continuum from dense RO to microporous UF, the combination of small scale, charged groups in the active layer, and

[*] The molecular weight or size cutoff is commonly defined as the size of the smallest molecule which is retained 90% by the membrane.[12]

microporosity lead to different barrier characteristics than either RO or UF. Salts which are excluded by RO membranes are selectively retained in NF through a combination of electrostatic forces and steric repulsion. As a consequence, the ionic strength of the solution and the ion valences are cofactors with hydrated ionic radii (*i.e.* size) [16,17], and NF membranes are capable of passing small, uncharged solutes while retaining salts.

This two-dimensional (electrostatic and steric) parameter space for NF membrane selectivity holds much potential for precise separations in the biotechnology and chemicals industries which has yet to be fully realized [5,6]. Present NF applications include the recovery of dyes from textile wastewater [1,2], various food component fractionations and concentration of juice and dairy products [18-21], and water purification. Existing water purification processes implemented with RO or UF, such as ultrapure water for the semiconductor industry, seawater desalination, and membrane bioreactors, are also being enhanced by the improved permeability or better selectivity of NF membranes [3,4,22].

1.5. Metrics of Membrane Performance

It has been seen that solute retention and solvent permeability are important metrics for a membrane; a molecular weight cutoff (MWCO) has been defined as the smallest molecule that is retained 90% by a membrane. In the context of this thesis, retention or rejection is defined as:

$$R = \left(1 - c_{per} / c_{ret}\right) \qquad (1),$$

where c_{per} is the concentration of the solute in the permeate (that which permeates through the membrane), and c_{ret} is the concentration of the solute remaining in the retentate. This represents the effective selectivity of the membrane in the system; the intrinsic retention by the membrane will be higher due to concentration polarization (1.5.1), and higher or lower due to the finite permeation time of a membrane with finite thickness in a changing system.

Permeability is the pressure-normalized flux of solution across the membrane. There is a

bewildering and bizarre array of units used for permeability and flux in the membrane industry. Here, permeability will be reported as liters permeate per square meter of membrane per hour per megapascal, L/m^2hMPa (also LMH/MPa). Thickness-normalized permeabilities are also reported for various TFC membranes in units of LMH-μm/MPa.

1.6. Membrane and Membrane Process Limitations

1.6.1. Concentration Polarization

When a solvent is selectively removed from a thin layer of solution at the surface of the membrane, the retained solutes are concentrated and begin to diffuse away from the membrane into the bulk of the solution. The greater the flux across the membrane, the higher the polarization becomes. This buildup at the membrane surface decreases its selectivity and permeability. The phenomenon can be mitigated by not relying on diffusion to mix the solution—by designing the process to have a cross-flow of feed solution or agitation.

1.6.2. Fouling

A more general problem for membranes is the reduction of permeability over time due to clogging by the feed solution. This *fouling* may be caused by the precipitation of insoluble compounds as they are concentrated by filtration (scaling), the consolidation of retained feed components into a compacted gel layer (caking), the adhesion and growth of microorganisms on the surface (biofouling), or the adsorption of solutes directly onto the surface [23].

The latter is known as *adsorptive fouling*. When a hydrophobic membrane surface is presented with an aqueous feed of organic components, it may be thermodynamically favorable for the solutes to adsorb on the membrane, thereby reducing the energy of the interface [24]. Adsorption is a particularly challenging problem in membrane systems because it is not subject to reversal by mere mechanical means, such as back-flushing [23]. Therefore, a regimen of chemical cleaning has become a part of many membrane processes, balancing the costs of decreased membrane permeability (*e.g.* lower capacity, higher energy consumption) with the reduction of membrane lifetime and system downtime necessary for a regular cleaning step.

The hydrophobicity of synthetic polymer membranes developed since the original cellulose acetate membranes has made adsorption an increasingly important problem, while membrane inefficiency due to fouling has motivated much research [25-28]. Other membrane properties that affect fouling are roughness and charge density, both important characteristics of polyamide TFC NF membranes.

Biofouling is a more complex process due to the active antagonists (microbes). After initial adhesion to the surface, bacteria may form a biofilm and specialize to produce additional components that will accelerate membrane fouling and, particularly in the case of natural polymer-based membranes such as cellulose acetate, membrane decomposition [29-31]. Strategies for preventing biofouling have targeted prevention of initial adhesion and targeted antimicrobial agents to prevent proliferation [32-34].

1.6.3. Fouling and Selectivity

The problem with fouling is the effect it has on membrane permeability. This has been introduced simplistically as an impediment to the passage of solvent, but it is in reality much more complex. For example, hydrophilic foulants may in fact increase solvent permeability under certain conditions [24]. Equally important is the way that fouling affects the selectivity of the membrane. One intuitive effect is the narrowing or partial blockage of pores in microporous membranes, which reduces the size cutoff [26,27,35]. This effect is predominant in MF and UF membranes, but extends even to the NF regime, where it can increase the size-based rejection of salts [27]. Competing effects make NF fouling more complex, depending not just on solute size but on the chemical properties of the membrane, the foulant, the solute, and the solution. In direct competition to pore size reduction is cake-enhanced concentration polarization, wherein cake fouling on the surface hinders the diffusion of concentrated solutes back into the bulk solution. This leads to a reduction in retention for molecules compatible with the membrane material (*i.e.* those that may follow a solution-diffusion mechanism) due to the relative decrease in water flux to solute flux [14,36], but may reduce the MWCO of charged species and those incompatible with the membrane (*e.g.* hydrophilic or hydrophobic) [26].

1.6.4. Selectivity

Regarding the nanofiltration realm, it has been observed that the methods for producing these membranes (*i.e.,* interfacial polymerization to create a thin film composite) provide little control over the size and distribution of the nanopores, leaving a gap in the continuum of membranes with precise size cutoffs between ~1 nm and ~10 nm [16]. Van Der Bruggen *et al.* reviewed several models of nanofiltration membrane selectivity in the context of small organic molecule solutes and polyamide TFC NF membranes and found that some common models (that assume a uniform pore size) are overly idealized [12]. They concluded that a model based on a log-normal distribution of pore sizes is the most useful to predict retention in practical applications. Another study that found the log-normal model a best fit for the experimental data measured pore radii for two TFC membranes to range from 0.26–0.73 nm [37]. In general, uniformity of pore size is desirable as it increases membrane selectivity and permeability [38].

1.7. Improving Membranes

1.7.1. Fouling Resistance

Resistance to many foulants can be imparted by a coating or surface modification that decreases membrane roughness and increases hydrophilicity, but the additional membrane resistance may not be compensated by the averted fouling [39-41], and may decrease pore size [39]. For example, Ulbricht *et al.* used a low temperature plasma to etch or graft 2-hydroxy-ethyl methacrylate (HEMA) onto UF membrane surfaces. They found that the etch decreased the retention while increasing the permeability and hydrophilicity of the polysulfone membranes. By grafting hydrophilic polymer onto the membrane after activation by the plasma, they were able to improve the fouling resistance and permeability of both polysulfone and polyacrylonitrile membranes, while also increasing retention [33].

Kochkodan *et al.* modified polysulfone and poly(vinylidene fluoride) membranes by grafting on hydrophilic, charged or quaternized ammonium moieties. This versatility was used to make general observations about biofouling of membranes. They found that smoothness and hydrophilicity reduce fouling, while the absence of charge makes bacteria more easily detach.

The most effective modifier to prevent biofouling was the quaternized ammonium group, which disrupts directly the development of the bacteria into a biofilm [34].

To avoid modifying the membrane permeability or selectivity, antifouling components can be directly incorporated during the membrane production process. In an early example, Nunes *et al.* started with a hydrophilic PVDF ultrafiltration membrane and produced a fouling-resistant membrane of the desired size cutoff by coating it with a nylon-poly(ethylene oxide) (PEO) block copolymer [42]. By varying the blend of two copolymers and concentration of the coating solution, they were able to adjust the MWCO down to 900 g/mol. This active layer reduced the permeability to 64 LMH/MPa, one tenth that of the base membrane, but gave the membrane comparable permeability and fouling resistance to a control hydrophilic acetate UF membrane. In the intended application, the filtration of oily water, the coated membrane maintained a higher permeability than the base membrane within minutes of starting the filtration.

Later studies on the mechanics of fouling found that end-attached PEO brushes of sufficient density can completely inhibit protein binding to a surface over a finite period of observation [43-45]. Both Irvine *et al.* and Sofia *et al.* evaluated inhibition of protein adsorption by surface-grafted linear and star PEO, and reported complete protein resistance in higher density grafts [43,45]. Irvine also used neutron reflectometry to find the volume fraction of PEO at different distances from the surface. From this information an explanation could be given for imperfect protein resistance by a dense star PEO-grafted surface: the PEO density at the star-grafted surface was lower than at larger distances from the surface due to the branched star, thus allowing proteins to adsorb onto the surface after permeating through the denser region.

Norde and Gage elaborated on the role of PEO graft spacing and brush thickness using bovine serum albumin and human blood plasma proteins as probes [44]. They confirmed the importance of graft spacing less than the size of the protein for effective resistance, but also observed a decrease in protein resistance for thicker brushes at a given graft density, and enhanced protein adsorption with tenuous (sparse) brushes. They hypothesize that there is a weak attractive interaction between PEO and the proteins, and that the widely known protein

resistance of dense PEO brushes is due to a high activation energy to enter the brush. Bosker *et al.* reached the same conclusion about the weak attraction of PEO to a model protein after characterizing the resistance of bimodal PEO brushes to bovine serum albumin [46]. The strong steric hindrance that PEO brushes pose to permeating solutes will be important in this study.

PEO remains one of the most effective anti-fouling materials today [39], and is frequently studied as a means to impart fouling resistance to membrane surfaces as a cross-linked gel [47-49], grafted layer [32,39,50-52], or self-organizing additive or coating [53-63]. A subset of the latter group will be addressed in more detail in section 1.8.

1.7.2. Controlled and Uniform Pore Size

Researchers have attempted to address the limitations of polyamide NF membranes using selective layers that exploit self-assembly phenomena, such as the coordination of metal ligands into molecular squares [64] or the morphologies of liquid crystalline [16], graft copolymer [54,55,53], and block copolymer materials [65,66], and the regular packing of a protein in space [67]. Others have created membrane pores using discrete structures such as carbon nanotubes [17] and aquaporin proteins [68], and by etching radioactively-ionized tracks in dense films [69] or patterned silicon substrates [38].

The pore sizes available using these techniques range from the reverse osmosis regime (< ~0.7 nm) to ultrafiltration (> 2 nm). The membrane pore size of interest for this work is ~1-5 nm, the interface between nano- and ultrafiltration. One of the precise pore fabrication methods that covers that range is the technique of Martin and coworkers [70,71], which can create pores from 50 nm to 1 nm by narrowing polycarbonate track-etched membrane[*] pores *via* electroless deposition of gold to a desired aperture. Different size-based separations have been demonstrated, including small organic molecules and large proteins. The researchers also adsorbed thiol-terminated PEO chains on the gold and found that it prevented the pores

[*] The work in the early 1970s on track-etched membranes [69] is another breakthrough in the field due to its ability to produce regular pores down to nanometers in diameter by exposing polymer films to ionizing radiation and then etching the resulting damaged tracks. The main disadvantages to the membranes are due to the stochastic mechanism for creating the pores: a tradeoff must be made between low porosity and many connected pores (*i.e.* increased size dispersity).

from clogging due to protein adsorption [70].

Another interesting example is the recent work of Peng *et al.* [67], in which crosslinked stacks of the 12 nm globular ferritin protein were used to create membranes with 1.7-2.2 nm effective pore size and extremely high pure water permeability (90,000 LMH/MPa compared to 8,000 LMH/MPa for the Sepro PS-20 UF membrane and 75 LMH/MPa for the FilmTec NF-90). The membranes were stable across a high range of pH and many solvents. Because the protein in the membrane is inherently charged, they filtered both charged proteins and uncharged cyclodextrins to estimate the size cutoff, and found that the electrostatic repulsion decreased the effective pore size for charged probes by ~0.2 nm (*i.e*. about 10%). The "ultrafast permeation" was attributed to a combination of the thin (40 nm) membrane, and the order-of-magnitude smaller effective thickness due to the reduced transition length of the smallest "pore": the narrowest point in the interstitials of the proteins. A defect-free membrane so thin was possible due to the way the proteins are assembled, and is a strength of membrane designs that assemble macromolecules directly into a selective layer [67,72]. It is reasonable to assume that different effective pore sizes could be achieved through the use of different proteins, but no specific statements were made by the researchers regarding that, the scalability of the process, or the fouling resistance of the membranes.

1.8. Amphiphilic Graft Copolymer Nanofiltration Membranes

Because selectivity and fouling resistance remain two of the most important challenges to membrane science [73], efforts have been made in our lab to combine self-assembly and PEO brushes to create precision nanosieves [55,53,56,57]. The NF membrane designs were based on amphiphilic comb copolymers (Figure 1.2 (A)) incorporating PEO as the comb "teeth", and poly(vinylidene fluoride) (PVDF), or polyacrylonitrile (PAN), as the hydrophobic spine.

PVDF-*graft*-polyoxyethylene methacrylate (PVDF-*g*-POEM) and polyacrylonitrile-*graft*-poly(ethylene oxide) (PAN-*g*-PEO) (Figure 1.3) were both shown to microphase separate into a bicontinuous network structure at the 1 nm scale. The PEO side chains fill the "nanochannels" that interpenetrate the rigid PVDF or PAN matrix (Figure 1.2 (B)), allowing

the passage of water molecules and retention of solutes larger than the nanochannel diameter.

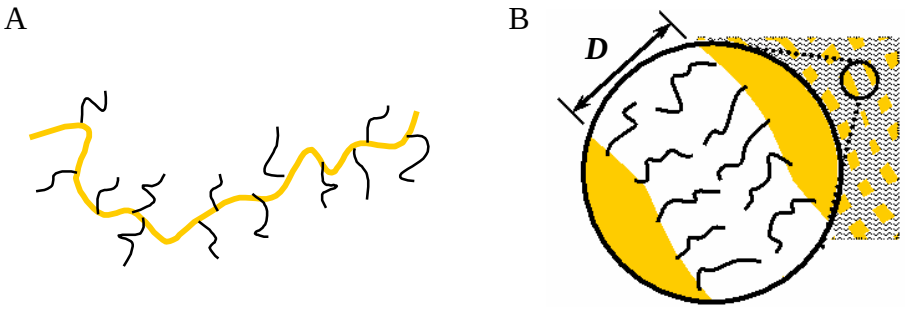

Figure 1.2. A conceptual representation of a single amphiphilic comb copolymer chain (A) with hydrophilic PEO side chains in black and hydrophobic backbone in orange; in bulk (B), the two microphase separate into a bicontinuous structure with PEO-lined "nanochannels" acting as pores for water transport through the rigid matrix.

Nanosieving with a PVDF-*g*-POEM-coated PVDF ultrafiltration (UF) membrane was demonstrated through the separation of like-charged molecular dyes [53]. It was also shown that reducing the solvent quality of the feed solution for PEO increases the effective size cutoff of the NF membrane by collapsing the swollen PEO chains within the nanochannels [56,57]. PAN-*g*-PEO comb copolymers could likewise be formed into thin film composite (TFC) NF membranes when coated onto a commercial PAN UF support. The PAN-based NF membranes exhibited separation capability similar to their PVDF analogues [55]. Both comb chemistries displayed complete resistance to irreversible fouling in dead-end filtration studies with model organic foulants at concentrations of 1g/L and above [55,53,58,59,74]. Other researchers have created PEO graft copolymers for use as biocompatible materials [32,75], electrolytes [76], medical imaging contrast [77], etc.

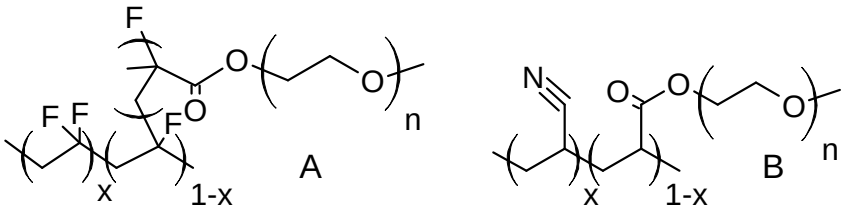

Figure 1.3. Amphiphilic graft copolymers incorporating poly(ethylene oxide) in the side chains: (A) poly(vinylidene fluoride)-*graft*-poly(oxyethylene methacrylate) (PVDF-*g*-POEM) and (B) polyacrylonitrile-*graft*-poly(ethylene oxide) (PAN-*g*-PEO).

PVDF is a more thermally and chemically robust material than PAN, but carries a higher cost[*]. Synthesis of PVDF-*g*-POEM is *via* an atom transfer radical polymerization (ATRP)-like mechanism [79], which requires a copper complex catalyst that can be difficult to remove from the product [80] and is difficult to scale up. Due to its more facile free radical synthesis, the PAN-based comb copolymer was studied in this work.

1.9. Outline

Because the fouling resistance, permeability and regular pore size of amphiphilic graft copolymer membranes show promise to overcome the greatest limitations of NF membranes, the technology has the potential to improve established membrane systems and open applications not possible with existing membranes. The utility of these membranes will hinge upon the degree to which membrane selectivity can be specified and retained during filtration operations. This work explores the control of PAN-*g*-PEO NF membrane steric and electrostatic selectivity, and the possible applications these enable.

Chapter 2 describes the experimental methods, including synthesis, polymer characterization, membrane fabrication, and membrane characterization.

Chapter 3 investigates the role of PEO side chain length, PEG casting additive, and filtration feed solvent quality on the permeability and effective pore size of PAN-*g*-PEO NF membranes through the filtration of rigid dyes of varying size from ~0.6-1.2 nm [55,53,57]. The fouling resistance of these membranes is further assessed by filtration of bovine serum albumin (BSA) and supplemental colloidal force spectroscopy studies measuring the attraction of a carboxylate-modified latex particle, as a model foulant [58,59,74], to the membrane coatings. Bacterial adhesion tests are conducted to compare the short-term biofouling resistance of the membranes with the adsorptive fouling [81]. The membranes are also subjected to acidic and basic conditions typical of those used to clean industrial membrane systems to ascertain the susceptibility of the PEO linkage, an ester bond, to hydrolysis under those conditions.

[*] Resin prices are reported to be $7.2/lb for PVDF and $1.3/lb for general acrylics at annual volumes of 200,000 lbs and 2 million lbs, respectively [78].

In Chapter 4, potential applications of the membrane are demonstrated using two types of probes increasingly important in biotechnology: metal nanoparticles and fluorophore-labeled peptides.

Chapter 5 reports modifications to the comb copolymer chemistry that change the electrostatic component of its selectivity. The charged terpolymer membranes so produced have greatly increased salt retention properties but reduced fouling resistance.

Finally, Chapter 6 summarizes the findings and concludes the discussion with a review of potential applications for the membranes.

2. Experimental Methods

2.1. Introduction

The experimental portions of this work can be divided into three categories: material synthesis and characterization, membrane fabrication and characterization, and application development. A brief summary of each follows.

2.1.1. Material Synthesis Considerations

Amphiphilic graft copolymers with PEO side chains can be produced *via* a "grafting from" process, requiring activation of a site on the polymer backbone and extension of the chain with monomer, or by "grafting through", which uses a PEO *macromonomer (*a macromolecule with a pendant group that can participate in a polymerization (Figure 2.1)) in the synthesis of the backbone [82]. The latter approach has as an outcome grafted PEO of consistent length, an important characteristic for this project. PEO macromonomers have been studied for several decades [83-87] due to the interesting and useful properties of PEO and PEO copolymers as coatings [43,88,44,89], catalyst media [90], emulsifiers [91], electrolytes [92], and membranes [55,53,57,58,81,93,60].

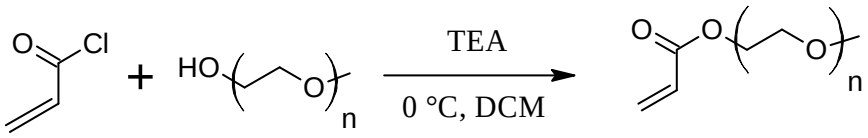

Figure 2.1. Synthesis scheme for an acrylate-based PEO macromonomer in triethylamine and dichloromethane.

PEO macromonomers can be prepared directly by the reaction of *e.g.* acryloyl chloride with monofunctionalized PEG* (Figure 2.1) [87,94,82]. This approach was pursued initially in this project to produce a PEO4 acrylate macromonomer, which was used to make PAN-*g*-PEO with monodisperse tetrameric side chains of PEO (PAN-*g*-PEO4). Though the monodispersity

* Traditionally poly(ethylene glycol) (PEG) has been used to refer to shorter chains of ethylene oxide, and PEO for high molecular weight macromolecules. The terms will be used accordingly here except when referring to grafted chains.

was ideal to permit exact comparison of combs of different side chain length, the lack of availability of longer monodisperse PEG chains and the commercial availability of (polydisperse [88]) methacrylate-capped PEO macromonomers (POEM) in a range of molecular weights eventuated a change to POEM. While this change was consistent with the underlying motivations for using PAN (industrial scalability and cost), it produces a different PAN-*g*-PEO backbone than that studied previously as an antifouling water filtration membrane [55,57,58,74]. Acrylates and acrylonitrile have similar activities and the acrylate PEO macromonomer can be expected (and seen [95]) to form a random copolymer with acrylonitrile. The higher activity of methacrylate ester is one possible source of trouble, as blockiness in the copolymer could introduce defect sites in a membrane surface that nucleate fouling. However, due to reduced mobility and steric hindrance, solvent quality can be as significant as monomer moiety reactivity in determining the outcome of copolymer synthesis with macromonomers [96]. An important observation to be made is whether POEM-based PAN-*g*-PEO has the same desirable properties as acrylate-based PAN-*g*-PEO.

2.1.2. Membrane Fabrication Considerations

The many relevant parameters in the membrane casting and fabrication process have led to a common perception that it is a "black art" [9]. The conceptually simple but similarly nuanced coating process used to make TFC membranes is also prone to inconsistencies due to similar factors: variation in polymer properties, coating solution concentration and viscosity, coagulation bath composition, temperature, humidity, contaminants, airflow, etc. The optimization of this process was not a focus of this work; however, it is of more than academic interest due to the proposed application of the described membranes, where existing (and optimized) commercial membranes may already be available. Accordingly, properties that are dependent on such an optimization (*e.g.* permeability) will be discussed in that context. In general, the experimental approach was to err on the side of thicker coatings to minimize defects and produce reliable retention data.

2.1.3. Applications

Although nanotechnology has entered the common vernacular, the touted convergence of molecular and mesoscopic scale has not (and cannot) lead to a completely smooth continuum

from nano- to mesoscopic materials and methods. For example, coated nanoparticles, which are commonly available in > 5 nm suspensions, are not found in subnanometer sizes. Uncoated particles (available down to ~0.6 nm diameters) readily aggregate when concentrated. At the other side of the divide is the rigid molecular dye which, at sizes larger than a nanometer, tends to be insoluble or aggregate.

Many self-assembly phenomena that might be used in fabricating a membrane selective layer also tend to one extreme. At the angstrom length scale are voids in molecular assemblies [64] and between liquid crystalline domains [16], while etched, microphase separated block copolymers [65] have pores tens of nanometers in diameter. A similar gap exists in dimensional analysis (*e.g.* dynamic light scattering, small- vs. wide-angle x-ray scattering (SAXS/WAXS) and (as has been discussed) polymer membranes.

As will be seen, by virtue of the grafted morphology, this gap is the regime where the PAN-*g*-PEO NF membranes operate, making them valuable for separations intended to provide strictly nanoscopic products.

2.2. Materials

2.2.1. Monomers, Reagents and Polymeric Casting Additives

The initiator and monomers, azobisisobutyronitrile (AIBN), acrylonitrile (AN), poly(ethylene glycol) methyl ether methacrylate, also known as poly(oxyethylene) methacrylate (*M*n~300 g/mol, POEM5 (5 EO repeats); *M*n~475 g/mol, POEM9 (9 EO repeats); *M*n~1,100 g/mol, POEM23; *M*n~2080, POEM45), potassium 3-sulfopropyl acrylate (SPA), *N*,*N*-dimethyl-*N*-(2-methacryloyloxyethyl-*N*-(3-sulfopropyl) ammonium betaine (SPE), and casting additives poly(acrylic acid) (PAA) and oligimeric PEO (poly(ethylene glycol) (*M*n~400 g/mol, PEG9; *M*n~1,000 g/mol, PEG23; *M*n~2000 g/mol, PEG45)), were purchased from Sigma-Aldrich (St. Louis, MO). POEM and AN were passed through a column of basic alumina to remove inhibitor before use.

The solvents—dimethyl formamide (DMF), dimethyl sulfoxide (DMSO), deuterated dimethyl sulfoxide (DMSO-d_6), isopropanol, ethanol, methanol, acetic acid, pH 11 buffer, and phosphate buffered saline (PBS, pH 7.4) —were purchased from VWR (West Chester, PA) and used as received. Pre-synthesis nitrogen purge gas was of high purity grade (AirGas).

2.2.2. Membrane Characterization Probes

Rigid molecular probes Acid Fuchsin, Alizarin Yellow GG (AY), Amaranth, Direct Red 80 (DR80), Chicago Sky Blue (CSB), Reactive Red 120 (RR120), Acid Blue 45, Methyl Orange, 4-(phenylazo)benzoic acid, and benzoic acid were also purchased from Sigma-Aldrich.

Peptides labeled with 5-carboxytetramethylrhodamine (5-TAMRA) or 5-carboxyfluorescein (5-FAM)—p60c-src Substrate 1, Glycogen Synthase derived peptide, Abltide, Tyrosine Kinase Peptide 3, Tyrosine Kinase Peptide 1, Bak - BH3, Bid BH3, Peptide II, and Neuropeptide Y (13 - 36)—were purchased from Anaspec (Fremont, CA).

Bovine serum albumin was purchased from SeraCare (Milford, MA). Sodium chloride, sodium sulfate and calcium chloride were purchased from VWR (West Chester, PA). Deionized (DI) water was obtained from a Millipore Milli-Q system.

Water dispersions of metal nanoparticles were acquired in the form of 2 nm gold colloid (British Biocell International), 0.7 nm silver colloid (Colloidal Science Laboratory, Westampton, NJ) and ~2 nm gold nanoparticles coated with sodium 11-mercaptoundecanesulfonate and octanethiol ligands in a 2:1 ratio (prepared by Randy Carney in the lab of Prof. F. Stellacci at MIT) [97]. An aliquot of gold colloid was dried under vacuum and redispersed in methanol using a Branson 2210 sonicator (Danbury, CT). The rest of the probes were used as received.

2.2.3. Membranes

PAN-400 ultrafiltration and NF-20 nanofiltration flat sheet membranes were purchased from Sepro Membranes, Inc. (Oceanside, CA) and used as the base membrane and control, respectively. NF-90 flat sheet membrane was obtained from FilmTec (Dow; Edina, MN). All

control membranes were soaked in DI water for 48 hours to hydrate them prior to use. The NF controls are both thin-film composite membranes with interfacially polymerized charged polyamide active layers.

2.3. Synthesis and Characterization of Comb Copolymers

2.3.1. Synthesis of Polyacrylonitrile-graft-poly(ethylene oxide)

Polyacrylonitrile-*graft*-poly(ethylene oxide) (PAN-*g*-PEO) was synthesized by free radical polymerization using AIBN as an initiator (Figure 2.2). The monomers, 30 ml DMSO, AIBN, and a stir bar were added to a round bottom flask, which was then sealed with a rubber septum and purged with nitrogen gas for 20 minutes while stirring. The flask was moved to an oil bath regulated to 60 °C and stirred for 20 hours. The reaction was quenched with excess 4-methoxyphenol (MEHQ) and then the polymer was precipitated by pouring the solution gradually into 10 times the volume of water. The precipitant was collected by vacuum filtration and dried in a vacuum oven at 50 °C, then redissolved in sufficient DMSO to permit free flowing of the solution (~30 ml) into water to purify the product.

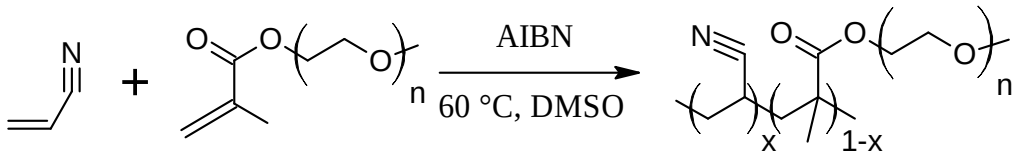

Figure 2.2. Synthesis of PAN-*g*-PEO*n* by free radical polymerization via the poly(oxyethylene) methacrylate (POEM) macromonomer route.

Because the resulting copolymer was consistently enriched in macromonomer, monomer ratios were initially chosen to contain 35% PEO, and then adjusted in subsequent syntheses as needed to obtain combs with ~39 wt.% PEO content. Approximately 100 mg (0.5 mol%) initiator was used except in the case of POEM5-based reactions, which tended to form a cross-linked gel (due to difunctionalized macromonomers [83]) unless the initiator and monomer concentration were reduced by half. This alteration reduced the yield substantially (consistent with the findings of Garcia *et al.* using DMF [84]). It also increased the molecular weight of the PAN-*g*-PEO5, relative to the other comb copolymers, as expected for a free radical synthesis with radical-radical annihilation as the predominant termination step.

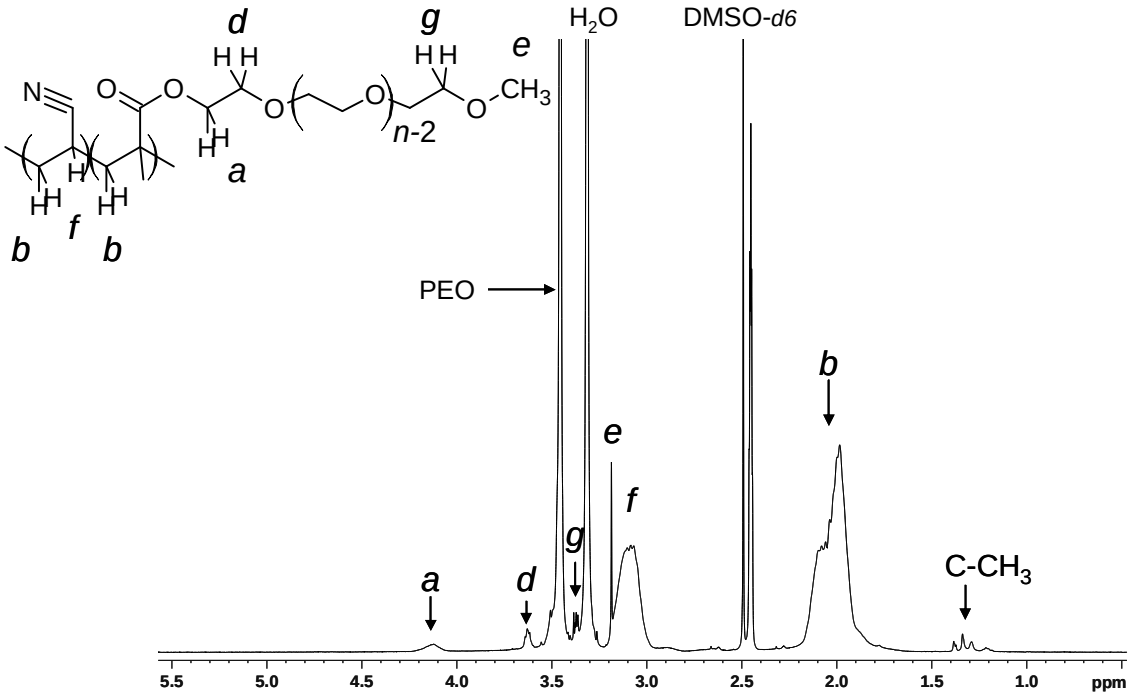

Figure 2.3. ^{1}H Nuclear Magnetic Resonance (NMR) spectrum of PAN-*g*-PEO with all peaks matched to their corresponding protons; the ester protons (a), backbone tail protons (b), and PEO protons are sufficient to obtain the PEO content and average PEO side chain length.

2.3.2. Chemical Characterization

The PEO content was determined by ^{1}H nuclear magnetic resonance (NMR) spectroscopy with a Bruker DPX 400 spectrometer (Figure 2.3). DMSO-d_6 was used as the solvent. Peak assignment follows from expected chemical shifts, known solvent shifts [98], and observation of the peak-broadening effect that proton attachment to kinetically slow chains causes (see *e.g.* the sharp singlet for the terminating PEO ether methyl group (e) and the resolution of the triplet for the relatively unhindered last methylene of the PEO (g) compared to the broadened first (a) and second (d) PEO methylenes). The ratio of the ester ($COOCH_2$) protons (~4.2 ppm) of POEM to the PEO protons (3.5, 3.6 ppm) was used to find the average side chain length. The ratio of total PEO protons to total backbone tail protons (1.7-2.2 ppm) was used to calculate the PEO content, which was maintained at ~40 wt.% for the different side chain lengths. The molecular weight was measured by gel permeation chromatography (GPC) using a Waters Breeze 1525 HPLC system equipped with two Polypore columns operated at 75 °C, series 2414 refractive index detector, series 1525 binary HPLC pump, and 717plus autosampler with DMF as the eluent, calibrated with poly(methyl methacrylate) (PMMA)

standards. PEO contents and molecular weights of the comb polymers are reported in Table 2.1.

Table 2.1. Monomer composition and purified PAN-*g*-PEO product characteristics

Mass POEM (g)	Mass AN (g)	Nominal Side chain EO units	Actual side chain EO units‡	Backbone mers per graft	Wt.% PEO‡	Mw* (kg/mol)	Mw/ Mn*	Yield (%)	Grafts per chain
3.7†	6.3	45	40	57	37	240	2.3	81	51
3.9	6.1	23	22	25	41	250	2.7	77	110
4.4	5.6	9	9	11	38	240	2.7	85	240
4.8	5.2	9	9	8	44	240	2.5	72	290
2.4	2.4	4.5	4.5	4	44	280	1.9	54	620

† 1:1 water solution; ‡ ^{1}H NMR; * DMF GPC, PMMA standards

2.3.3 Physical Characterization

The thermal properties of the neat polymers was investigated using a Q100 TA Instruments differential scanning calorimeter (DSC) in modulated mode. A ~10 mg sample was hermetically sealed in an aluminum pan and subjected to a preparatory heating-cooling cycle (190 °C to -95 °C), and then modulated 1.27 °C/min while ramping the temperature by 2 °C/min. The TA Universal Analysis software was used to extract the reversible heat flow and report first and second-order transitions.

The water swelling ratio of the polymers was measured gravimetrically. A dry ~1 g sample was weighed and placed in deionized water for twelve hours. The swollen sample was left exposed to dry air until the polymer surface appeared dry, whereupon it was weighed again. The experiment was repeated twice for each sample.

2.4. Synthesis and Characterization of Comb Terpolymers

2.4.1. Synthesis

Comb terpolymers were synthesized from acrylonitrile, POEM, and either zwitterionic *N*,*N*-dimethyl-*N*-(2-methacryloyloxyethyl-*N*-(3-sulfopropyl) ammonium betaine) (SPE) (Figure

2.4 (A)) or negatively charged 3-sulfopropyl acrylate (SPA) (Figure 2.4 (B)) by free radical polymerization (2.3.1). The resulting polymers, poly(acrylonitrile-*co*-*N*,*N*-dimethyl-*N*-(2-methacryloyloxyethyl-*N*-(3-sulfopropyl) ammonium betaine)-*graft*-poly(ethylene oxide) (P(AN-*r*-SPE)-*g*-PEO)) and poly(acrylonitrile-*co*-3-sulfopropyl acrylate)-*graft*-poly(ethylene oxide) (P(AN-*r*-SPA)-*g*-PEO)) are described in Table 2.2.

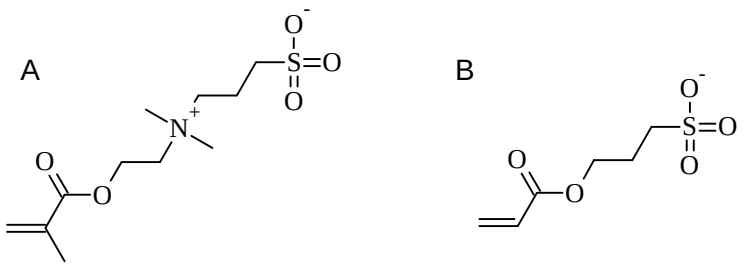

Figure 2.4. Zwitterionic *N*,*N*-dimethyl-*N*-(2-methacryloyloxyethyl-*N*-(3-sulfopropyl) ammonium betaine (A) and negatively charged 3-sulfopropyl acrylate (B) monomers used in the synthesis of amphiphilic graft terpolymers.

Table 2.2. Monomer composition and purified comb terpolymer product characteristics

Side chain EO units	Mass POEM (g)	Mass AN (g)	Mass SPA/SPE (g)	Wt. % PEO* (Product)	Wt. % SPA/SPE*	Mw‡ (kg/mol)	Mw/ Mn‡
P(AN-*r*-SPA)-*g*-PEO							
9	4.2	5.6	0.3	36	1	490	3.9
9	4.8	5	0.3	46	2	490	3.8
45	3.3	6.6	0.2	47	1	420	4.0
P(AN-*r*-SPE)-*g*-PEO							
9	4.6	5	0.4	41	5	490	3.7
45	4.6	5	0.4	50	4	400	3.6

* ^{1}H NMR; ; ‡ DMF GPC, PMMA standards

2.4.2. Terpolymer Characterization

The PEO and SPA/SPE content of the terpolymer combs were determined by ^{1}H nuclear magnetic resonance (NMR) spectroscopy with a Bruker DPX 400 spectrometer (Figure 2.5). The peak for the ester ($COOCH_2$) protons of the SPE moiety is more highly shifted (4.4 ppm) than for the POEM ester (4.1 ppm). Together with the integration of the broad peak representing the backbone tail protons (1.7-2.2 ppm), the PEO content and SPE content can be calculated. PEO side chain length can be calculated from the ratio of the PEO peaks (Figure

2.3) to the PEO ester peak, subtracting the known contribution due to the SPE tether protons. The SPA ester proton peak overlays that of the POEM ester protons (spectrum not shown, but qualitatively equal to that of PAN-*g*-PEO (Figure 2.3)), so the integration of the methacrylate (C-H_3) proton peak is used to disambiguate the contribution of SPA and POEM to that peak. The molecular weight was measured by GPC (2.2.2). These properties are reported in Table 2.2.

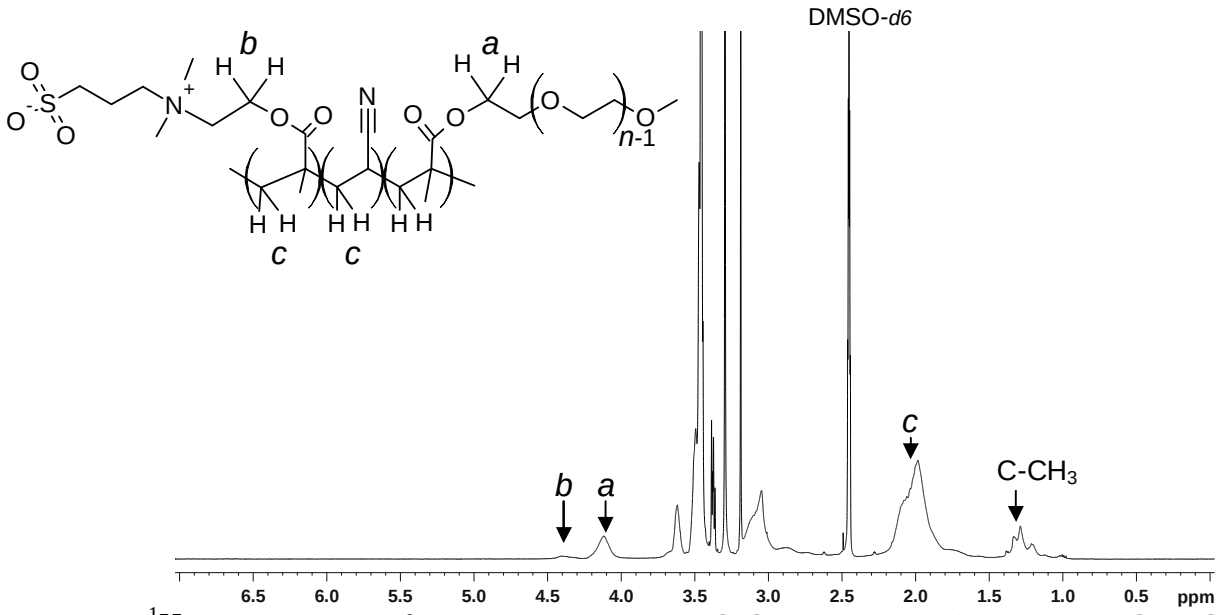

Figure 2.5. ^{1}H NMR spectrum of P(AN-*r*-SPE)-*g*-PEO with the POEM ester (a), SPE ester (b) and backbone tail hydrogens (c) and corresponding peaks labeled; these are sufficient to calculate the content of both PEO and SPE.

2.5. Membrane coating

2.5.1. Coating Method

Solutions of each polymer were prepared by dissolving 1 g dry polymer in 4 ml DMSO (Figure 2.6). For membranes fabricated with PEG additive, ~4 wt. % PEG9, PEG23, or PEG45 was added to the solution of the respective PAN-*g*-PEO*n* comb (a concentration of 10 wt. % within the ~40 wt. % PEO domain of the combs). The solutions were filtered through a 1 µm glass syringe filter (Whatman) and degassed at 70 °C for approximately 1 h. A 12x30 cm section of PAN-400 membrane was fixed to the coater (Testing Machines, Inc., Ronkonkoma, NY) and the doctor blade was set to 30 µm height and fixed to the motorized

arm. The surface was briefly blasted with a gas duster (Dust-Off, VWR) and a small bead of ~45 °C polymer solution was poured in front of the blade on the base membrane. The coater motor speed selector was set to 3.5, and activated. After one minute, the coated membrane was immersed in an isopropanol bath at room temperature. After 10 minutes, the membrane was transferred to a deionized water bath, also at room temperature, then stored in DI water in sealed polyethylene containers until use.

Membranes with double layers of comb polymer were made by drying the membrane after the isopropanol coagulation step for five minutes in air and repeating the coating process with a second solution.

Figure 2.6. Polymer-to-membrane illustrated (from left): P(AN-*r*-SPA)-*g*-PEO polymer as precipitated into water, dried, dissolved in DMSO, and being coated onto a PAN base membrane.

2.5.2. Coating Thickness and Contact Angle

Samples of the thin film composite membranes were prepared for characterization by quick freezing in liquid nitrogen and freeze-fracturing. The cleaved samples were affixed to a sample holder with carbon tape and the edges were imaged with an FEI/Philips XL30 environmental scanning electron microscope (ESEM) at 1500-6500× magnification and 15kV potential using both back-scattering and gaseous secondary electron detectors. The operational pressure was 0.5 Torr and the spot size was set to 3. The thickness of the coating was measured at intervals across the membrane sample using instrument software. At least 10 measurements were made of three separate portions of the membrane and the results averaged. The swelling behavior of the PAN-*g*-PEO coating in dry and hydrated conditions was measured in wet mode using a 0.3 mm pressure-limiting aperture and a cold stage to control the relative humidity (RH). Prepared PAN-*g*-PEO9 and PAN-*g*-PEO40 membrane samples were transferred directly from water to the stage and imaged at ~90% RH (10 °C and 8.8

Torr) and then by briefly reducing the pressure to ~2.5 Torr (~30% RH) to improve clarity. The samples were then dried for 6 to 10 hours (2.5% RH humidity; 30 °C and 0.7 Torr) before returning to 10 °C and imaging at ~2.5 Torr (30% RH). The experiment was repeated in reverse by starting with a membrane sample dried for 48 hours in a vacuum oven at 35 °C and then imaged before and after being exposed to 100% RH for 8 hours (12.9 Torr, 15C).

The static contact angle of DI water with the coated surface was measured at 23 °C and <20% relative humidity by the sessile drop method using an Advanced Surface Technologies, Inc. VCA2000 contact angle system. Two membrane samples for each comb tested were dried in air for six hours and fixed to a microscope slide with double-sided tape. Four or more droplets of ~4 µl were placed on the surface and the angle formed after 5 seconds was measured with the instrument software. The UF base membrane was subjected to the coating procedure using pure solvent before testing it for a controlled comparison with the polymer coatings.

2.6. Atomic Force Microscopy Colloidal Probe Measurements

Atomic force microscopy (AFM) was used to characterize the interfacial forces between the comb copolymer or comb-based membranes and a model organic foulant, employing a MultiMode AFM connected to a Nanoscope IIIa controller (Veeco Metrology Group, Santa Barbara, CA). A carboxylate-modified latex (CML) particle (Interfacial Dynamics Corp., Portland, OR) was used as the AFM probe due to the ubiquity of carboxylate functional groups in most common organic foulants. The CML particle (3.9 µm in diameter) was attached by Norland optical adhesive (Norland Products, Inc., Cranbury, NJ) to a tipless SiN cantilever having a spring constant of 0.06 N/m (Veeco Metrology Group, Santa Barbara, CA) and cured under UV light for 20 min. Measurements were carried out in a fluid cell under solutions of 10 mM NaCl, 100 mM NaCl and also PBS at four different locations on the membrane in each solution, and at least 10 force measurements were analyzed for each location. This experiment was conducted by William Phillip in the Elimelech group at Yale.

2.7. Membrane Bacterial Adhesion

The adhesion of Escherichia coli K12 MG1655 to the surface of the membranes was used as a probe to characterize their ability to resist biofouling [81]. The bacterial strain was tagged with a plasmid coding for green fluorescent protein to facilitate identification of adhered bacteria. Two 1 cm by 1 cm coupons of each membrane were incubated in 20 mL of a suspension of the bacteria (4×10^7 cells/mL) in solution (10 mM NaCl, 100 mM NaCl, and PBS) in a shaker (Lab-line 4631 Maxi Rotator) at 20 rpm and room temperature (22 °C). After 1 hour, the coupons were rinsed with the same solution to remove loose bacteria, and then observed under a fluorescent microscope (Olympus BX41, Japan). At least 10 images were taken across the membrane surface and the average number of cells on the membrane was normalized by the observed membrane area (0.145 mm^2). This experiment was also conducted by William Phillip at Yale.

2.8. Membrane Filtration Experiments

2.8.1. Permeability

A circular coupon was cut from the coated membrane and installed in an Amicon 8050 or 8010 stirred, dead-end filtration cell (Millipore), or a Sepa ST high pressure cell (Osmonics). The Amicon cells have effective filtration areas of 13.4 cm^2 and 4.1 cm^2 and volumes of 50 ml and 10 ml, respectively. Care was taken at all times to prevent the membrane surface from drying out. The cells were filled with either deionized water, 0.2 M NaCl solution, 0.4 M NaCl solution, ethanol, water and ethanol, or methanol. Temperature was controlled using a hot plate (Corning) and water bath, and measured using a Traceable temperature probe (VWR). Sepro specifies 50 °C as the maximum operating temperature for the PAN-400 base membrane, and significant permanent reduction of the permeability occurred above this temperature; to compensate for this effect, minimal time was spent above this temperature and multiple temperature sweeps were made to compare fluxes for repeatability. The cells were pressurized using compressed nitrogen. Pure solvent permeabilites were calculated gravimetrically from the mass of permeate collected three or more times over a period of 10 minutes each, measured after at least 0.5 h of equilibration at the test pressure (0.34 MPa; 50 psi) when the flux (and temperature) was found to be stable over multiple collections. Membrane permeability is reported as the volume of solvent that permeates the membrane,

normalized by time, pressure, and membrane area (see sec. 1.5). To account for the effect of coating thickness differences on membrane permeability, the thickness-normalized permeability was also calculated as the membrane permeability times the coating thickness [16,99].

2.8.2. Fouling

Fouling resistance was tested using a model protein foulant solution consisting of 1 g/L BSA in PBS. The pure water permeability of the membrane was measured in an Amicon 8050 cell for at least 3 hours until the flux appeared constant. The cell was then depressurized and immediately filled with buffered BSA solution and repressurized. A reservoir maintained the solution level during 24 hours, while permeate was collected by a FRAC-100 sample collector (Pharmacia) in timed mode. The BSA concentration in the permeate was measured spectrophotometrically (2.8.3) after 3 hours of BSA filtration using the λ_{max}=279. After 24 h, the cell was emptied and rinsed for 10 seconds with a fine stream of deionized water from a laboratory water bottle (VWR) to remove any BSA not adsorbed on the surface, and then filled with water and stirred for 15 minutes, replacing the water three times. The cell was refilled with DI water and repressurized to measure the permeability again.

2.8.3. Molecular Probe Retention

Charged, rigid dyes and other small organic molecular probes (Table 2.3), shown in Figure 2.7, were added to the chosen aqueous solvents at a concentration of 50 ppm. The cell and membrane were flushed with clean solvent for 0.5 h between each retention test. Permeability and dye retention tests were conducted on at least two coupons from each membrane. Each was preceded by at least 0.5 h equilibration period at the testing pressure of 0.34 MPa (50 psi) or 0.03 MPa (5 psi) for the PAN-400 base membrane, and the order of dyes tested was reversed to reveal any persistent effects on the membrane. To ensure steady state was reached, samples of permeate were collected and compared in solute concentration with the retentate until their ratio was constant. Dye concentration was measured in PMMA semimicro cuvettes (Plastibrand, VWR) using a GENESYS 10 UV spectrophotometer (Thermo Scientific) according to the Beer-Lambert Law,

$$A = \varepsilon l c \qquad (2),$$

Table 2.3. Water-soluble molecular probes and their properties

Molecule	**Charge**	**λ_{max}**	**MW**	**Diameter (nm)***
Chloride	-1	-	36	-
Benzoic acid	0	338	122	0.60
4-(phenylazo)benzoic acid	0	345	226	0.73
Alizarin Yellow GG	-1	362	286	0.76
Methyl Orange	-1	462	304	0.79
Acid Blue 45	-2	595	428	0.84
Amaranth	-3	520	536	0.90
Acid Fuchsin	-2	549	540	0.93
Chicago Sky Blue	-4	616	901	1.08
Direct Red 80	-6	528	1235	1.20
Reactive Red 120	-6	552	1332	1.21

* Of sphere of equivalent volume to modeled molecular volume; † Because of a strong sensitivity of Acid Blue 45 absorbance to [NaCl], it was only used in DI water experiments.

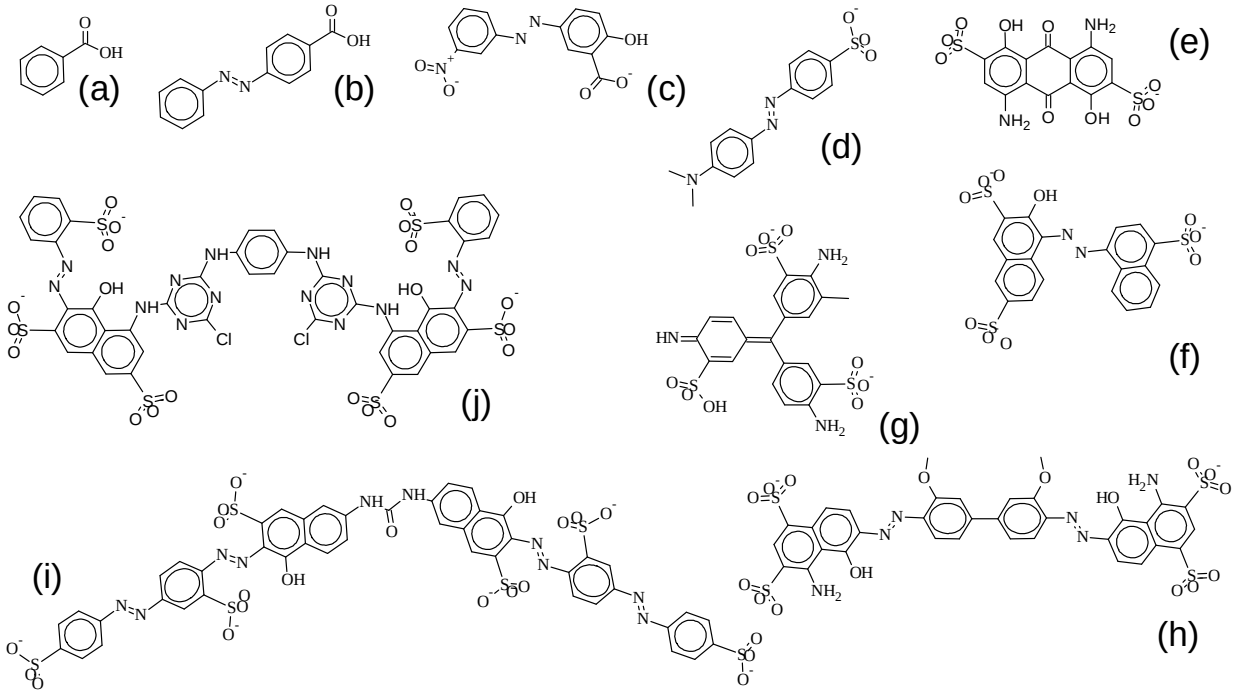

Figure 2.7. Rigid molecular probes in order of increasing diameter (a) benzoic acid, (b) 4-(phenylazo)benzoic acid, (c) Alizarin Yellow, (d) Methyl Orange, (e) Acid Blue 45, (f) Amaranth, (g) Acid Fuschin, (h) Chicago Sky Blue, (i) Direct Red 80, and (j) Reactive Red 120.

where A is the absorbance, ε is the molar absorptivity, / is the path length, and c is the molar concentration. Dye standard solutions were successively diluted and measured to find an absorbance-concentration regression. Any experimental solutions with dye concentrations above the linear region were diluted as needed. The probe concentration in the permeate and retentate were used to find the retention (Eq. 1). The molecular diameter of the dyes was estimated as the diameter of a sphere having an equivalent volume to the molecular volume as calculated by Molecular Modeling software (ChemSW, Fairfield, CA). Molecular probe characteristics are given in Table 2.3. Unless otherwise noted, all retentions given are the mean of three measurements, and the given error is the standard deviation.

2.8.4. Peptide Retention

Fluorescently labeled peptides (Table 2.4) were dissolved at a concentration of 10 mg/L in aqueous solutions of either 6.6 g Na_2SO_4 and 3.3 g NaCl per liter or 0.1 M NaCl. The Amicon 8010 cell was filled with the peptide solution and operated at a ΔP of 0.34 MPa (50 psi). For the individual peptide permeation experiments, the filtration was halted after each ~10% reduction in cell volume (~1.2 ml) and the peptide retention was determined by the spectrophotometric method (2.4.2). Then the permeate was returned to the cell, thus maintaining the total concentration of peptide in the system constant, much like a recirculating crossflow setup. This was repeated until the retention reached a steady state.

For the peptide separation, the cell was charged with a feed of equal concentrations of two peptides. The same method was followed to reach equilibrium, at which point the permeate was retained and the cell recharged instead with the two-peptide feed solution. After collecting ~15 ml of permeate this way, the retentate was set aside, the membrane flushed. The retentate was then added to the cell and the equilibration procedure followed. The cell volume was then allowed to reduce to 50% (~5 ml) and the retentate concentration measured for comparison. After flushing the cell, the process was repeated for the collected permeate from the first filtration, with a fraction of the permeate being collected after equilibration for comparison.

Table 2.4. Fluorophore-labeled peptide probes

Peptide	Charge[a]	Charged Residues	Hydro-philicity[b]	MW[c] (Da)	Dia-meter[d] (nm)	Sequence[e]
P60c-src Substrate 1	1	1	-0.8	1290	1.45	YIYGSFK-OH
Glycogen Synthase derived	2	3	0.3	1542	1.54	KKLNRTLSVA-OH
Abltide	1	3	0	1677	1.58	KKGEAIYAAPFA-NH_2
Tyrosine Kinase Peptide 3	0	6	0.8	1931	1.66	RRLIEDAEYAARG-NH_2
Tyrosine Kinase Peptide 1	0	4	0.2	2083	1.7	KVEKIGEGTYGVVYK-OH
Bak BH3	1	5	0.4	2266	1.75	GQVGRQLAIIGDDINR(K)-NH_2
Bid BH3	-1.9	8	0.5	2722	1.84	EDIIRNIARHLAQVGDSMDR-OH
Neuropeptide Y (13 – 36), human, rat	2.1	7	-0.1	3413	2.0	PAEDMARYYSALRHYINLITRQRY-NH_2

a. At neutral pH; b. Hopp-Woods algorithm; c. Including 430 Da TMR dye; d. Equivalent sphere with ρ=1.35 g/cm^3.; e. Beginning with labeled end except for Bak BH3, which is labeled on the pendant lysine.

Salt retention was measured in an analogous way to peptide retention, using instead a conductivity probe (VWR Traceable).

2.8.5. Nanoparticle Retention

For 2 nm gold nanoparticle permeation tests, the Amicon 8010 cell was charged with a few ml of gold colloid solution. The permeate was collected until the cell was dry. A few ml pure solvent were then added to the cell, flushed through and collected, and then the permeate was vacuum concentrated at room temperature to 1-2 ml. Membrane permeation of 0.7 nm silver colloid was tested by the same procedure and also with an additional prefiltering step, using a PAN-400 UF membrane, to remove aggregates. Permeate and feed solution samples were prepared for imaging by dropping solution onto the surface of a carbon-coated copper grid (400 mesh, Electron Microscopy Science, Hatfield, PA) and letting the solvent evaporate. A JEOL 2010 CX transmission electron microscope in bright field mode at 200 keV was used to capture images magnified 67k times.

2.8.6. Salt Retention

Individual solutions of 0.1% (1 g/L) sodium chloride and sodium sulfate were filtered by first rinsing the prepared dead-end cell with 20 ml solution and then filling it. The solutions were filtered for 0.5 h to equilibrate, and then two fractions of permeate were collected and compared in salt concentration to the retentate using a conductivity probe (VWR Traceable). The cell was then filled with fresh solution and the procedure repeated.

2.9. Membrane pH Stability

To test the effect of acidic and basic conditions typical of membrane cleaning cycles on PAN-*g*-PEO, membrane coupons were immersed in 25% acetic acid solution (pH 2.1) or pH 11 buffer for specific periods of time and then transferred to DI water for an hour before loading into a filtration cell to test permeability and dye retention.

2.10. Summary

Amphiphilic graft copolymers and terpolymers of 37-50 wt.% PEO were synthesized using free radical polymerization of acrylonitrile, poly(oxyethylene) methacrylate macromonomers of different PEO chain lengths, and, for terpolymers, a third acrylate or methacrylate monomer. The prepared terpolymers incorporated negatively charged (sulfopropyl acrylate) or zwitterionic (*N*,*N*-dimethyl-*N*-(2-methacryloyloxyethyl-*N*-(3-sulfopropyl) ammonium betaine). The molecular weight polydispersity was ~2 for the copolymers and ~4 for the terpolymers. Preferential addition of the lower molecular weight fraction of POEM45 macromonomer may have occured in the PAN-*g*-PEO40 copolymer synthesis, as the average side chain length was found to be 40 EO mers by NMR; in the case of the POEM23, POEM9 and POEM5 macromonomers, the average PEO length in the resulting copolymer were in excellent agreement with the manufacturer's specified molecular weights. In the case of the terpolymers, the PEO length of each comb was consistent with monomer specifications.

Each polymer was used to fabricate a thin-film composite nanofiltration membrane by solution coating onto a PAN-400 base membrane. Size progressions of rigid molecular probes and labeled peptides were obtained to characterize the membranes' selectivity.

3. Fouling-resistant Nanofiltration Membranes with Controlled Size Cutoff

3.1. Introduction

It has been found that pore-size control in the NF range (~0.8-2 nm) is limited by the morphological features that govern membrane selectivity in NF and UF commercial membranes. At one extreme is the nanoporosity of NF membranes, explained as the free volume both between the crosslinked chains and between nanoscale aggregates of polymer developed during membrane production [100,15]; at the other extreme is the broad pore distribution within an UF membrane selective layer due to coarsening during its fabrication by phase inversion [101]. Amphiphilic graft copolymer NF membranes, with an effective pore size in this intermediate regime [53,55-57], occupy an uncrowded niche that few novel fabrication techniques address.

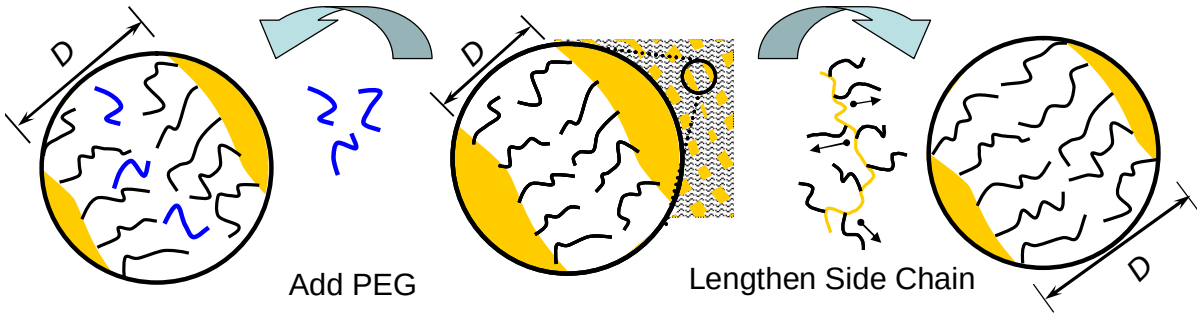

Figure 3.1. Schematic illustration of PAN-*g*-PEO microstructure showing two methods of controlling nanochannel diameter; (left) PEG segregated to and swelling the PEO domain during coagulation is free to elute out; (right) side chain length and frequency on the backbone determine the surface/volume ratio of the domains, controlling the periodicity of the microphase separation.

In this chapter, the direct control of size cutoff of uncharged PAN-*g*-PEO amphiphilic graft copolymer membranes will be explored through changes in the chemistry and membrane fabrication steps (Figure 3.1). The fouling resistance of the resulting membranes, tested by direct and predictive methods, is reported, as is the size cutoff determined through the filtration of rigid molecular probes. The response of the PEO-filled channels to environmental conditions is also described.

3.2. PAN-*g*-PEO Combs with Varied Side Chain Lengths

The useful barrier properties and fouling resistance of amphiphilic graft copolymer NF membranes depend on the microphase separation of the hydrophilic PEO side chains and hydrophobic backbone to form a bicontinuous structure [53,56]. In this morphology, the hydrophilic nanochannels are lined with a PEO brush tethered to the backbone at the domain interface, and the thermal transitions of both component polymers should be observable in a DSC thermograph. Figure 2 is a composite of reversible heat flow DSC thermographs of the combs synthesized. For the PAN-*g*-PEO40[*] comb, a sharp endotherm corresponding to the melting of PEO crystallites is seen at 28 °C [53], along with two second-order transitions attributable to PAN at ~90 and 150 °C [55,102] . The PAN-*g*-PEO22 comb exhibits these same transitions, but with a broader PEO melting endotherm at 5 °C and an additional glass transition for PEO at -60 °C. For the PAN-*g*-PEO9 combs, glass transitions at -60 and 150 °C verify a microphase-separated morphology. A transition at ~10 °C is additionally seen, consistent with the glass transition of a third, mixed phase, which might be expected given the increased proportion of interface to volume in this material. A comparison of the two POEM9 combs shows a stronger PEO glass transition in the comb with higher PEO content, as would be expected. Further shortening the PEO side chains to 5 EO units results in the disappearance of the characteristic thermal transitions for PAN and PEO, suggesting the PAN-*g*-PEO5 comb resides in a mixed state. Consistent with this is the observation that the polymer flows; it showed poor durability and low permeability as a membrane coating. Hence no membrane data are reported for it.

[*] For consistency, PAN-*g*-PEO polymers are named according to the nominal length of the side chain; thus, the copolymer of acrylonitrile and POEM45 is PAN-*g*-PEO45, regardless of the actual side chain length.

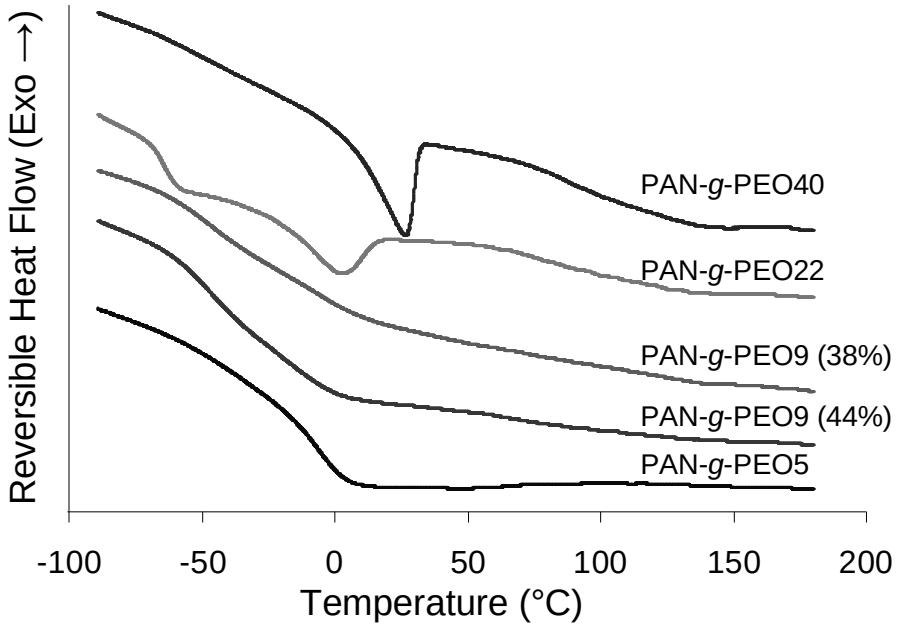

Figure 3.2. Overlaid modulated differential scanning calorimetry (DSC) thermographs of PAN-*g*-PEO copolymers. Scan temperature modulated by 1.27 °C/min while ramping by 2 °C/min. Characteristic thermal transitions for distinct PAN and PEO domains are observed for all materials but PAN-*g*-PEO5.

Another important parameter in the performance of PAN-g-PEO membranes is the PEO composition. With too little PEO, the coverage of the brush is incomplete and the fouling resistance impaired; with too much PEO, the polymer becomes water soluble. In previous studies, ~40% PEO content was found to be sufficient for fouling resistance [58]. The upper limit of PEO content was not investigated, but PAN-*g*-PEO40 combs with greater than 50% PEO content were found to be unsuitable as membrane selective layers due to partial solubility.

Table 3.1. PAN-*g*-PEO polymer characteristics

Side chain EO units	**Wt.% PEO***	**Mass swelling ratio (water)**	**Molar swelling ratio (water/EO)**
40	37	2.9 ± 0.2	13 ± 1
22	41	3.6 ± 0.2	15 ± 1
9	38	2.3 ± 0.2	8.3 ± 0.5
9	44	2.7 ± 0.2	9.2 ± 0.5
5	44	1.7 ± 0.1	4.0 ± 0.3

* ^{1}H NMR

The side chain length and PEO content are seen to affect the swelling behavior of the combs (Table 3.1). Similar effects were observed in PVDF-*g*-POEM copolymers [101], but in that polymer an upper limit of ~11 water molecules/EO appears to have been reached. Each repeat unit in PEG5 and PEG9 usually coordinates 4 water molecules, while PEG23 and PEG45 may form trihydrates or hexahydrates [103], so this degree of swelling leaves many water molecules "free" to conduct water flux. It is also interesting to note that, existing as it does in the mixed state, PAN-*g*-PEO5 only absorbs enough water to directly coordinate the PEO.

3.3. Thin-film Composite Nanofiltration Membranes: PAN-*g*-PEO Coatings on PAN Base Membrane

3.3.1. SEM Micrographs of Membranes

The thickness of the PAN-*g*-PEO selective layer of the thin film composite membranes after coagulation and drying was found by SEM to be between 0.6 and 2.8 μm (Figure 3.3). The thickness varied by less than 1 μm in each individual sample imaged (~1 cm span). Coatings of several hundred nanometers thickness are commonly applied in commercial membrane fabrication *via* such techniques as spray coating, and have been found to be adequate for membrane selectivity [9]. Because the permeability of a membrane is inversely proportional to its thickness [9], there is substantial potential for enhancing intrinsic flux by optimizing this step of the membrane fabrication process.

The change in coating thickness when hydrated was measured as described in section 2.5.2 by starting with hydrated or dried membranes and measuring the coating thickness in an appropriate relative humidity before promoting drying or hydrating, respectively, and then repeating the measurements. Figure 3.4 shows two micrographs taken this way. The dried membrane is on the left and the same membrane after 8 hours at 100% humidity is on the right. No evidence of a change in coating thickness was found, suggesting that the morphology is established and fixed during the coagulation step.

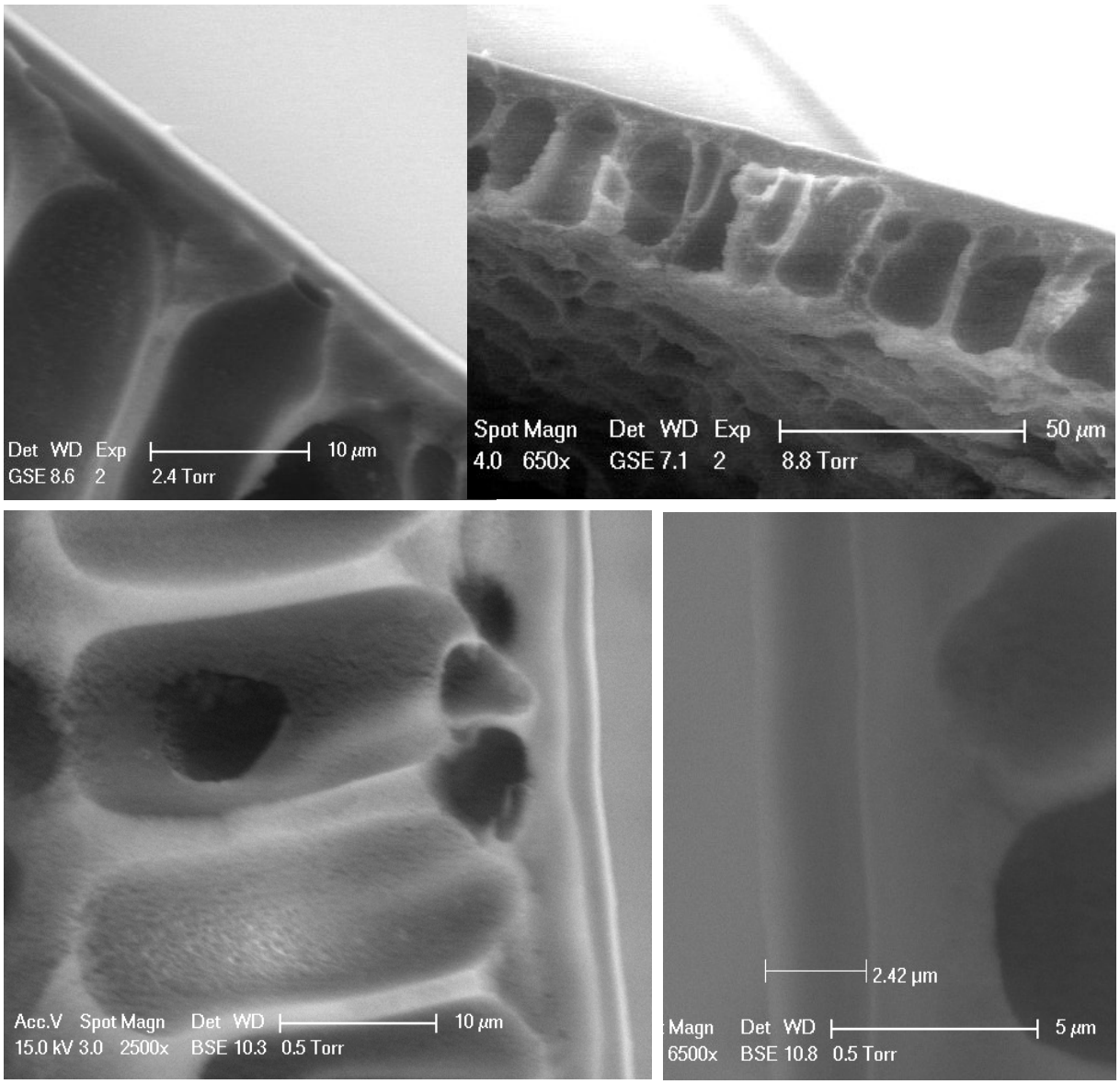

Figure 3.3. Environmental scanning electron microscopy (ESEM) images of cross sections of a thin film composite membranes comprising PAN-*g*-PEO comb coatings on an asymmetric porous PAN-400 ultrafiltration membrane using (top) 10kV beam potential and a gaseous secondary electron detector (GSE) showing (left) the coating bridging a pore in the UF base membrane at 2500× magnification and (right) the thin-film composite structure of asymmetric porous base membrane with a thin coating on top at 650× magnification; (bottom) 15kV beam potential and a back-scattered electron detector (BSE) at (left) 2500× magnification; (right) 6500× magnification; these membranes are oriented with the coated top surface facing the other image.

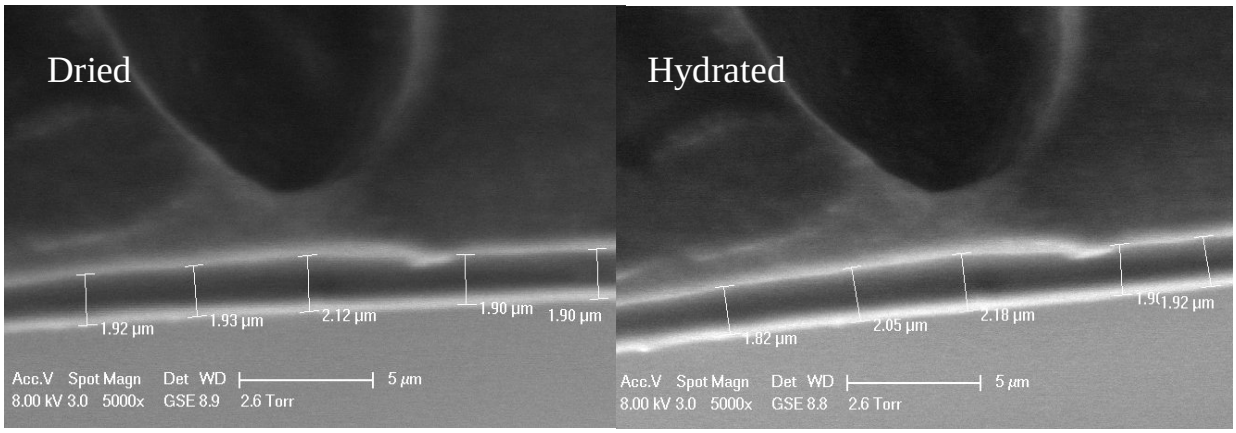

Figure 3.4. GSE ESEM images of cross sections of PAN-g-PEO comb coatings at 10 °C and 2.6 Torr water pressure showing that no change in thickness occurs when the dried (left) coating is hydrated (right).

3.3.2. Contact Angle

The SEM results suggest that the comb copolymers fully coat the underlying PAN-400 membranes such that wettability, resistance to fouling and size cut-off of the TFC NF membranes should replicate those of each comb. Water contact angles measured on the coated membranes varied systematically according to PEO side chain length (Figure 3.5). The comb with the longest PEO side chains (PAN-*g*-PEO40) had the lowest contact angle (36°), followed by the POEM23 comb (39°) and the POEM9 comb (50°), with no detectable difference between PAN-*g*-PEO9 coatings having 44 wt% PEO and 38 wt% PEO. These numbers are in close agreement with the findings of Fan *et al.*, who polymerized POEM9 and POEM23 brushes from initiators immobilized on a titanium substrate and measured the contact angles as 49 and 40, respectively [88]. The results suggest that the combs contain sufficient POEM content to achieve complete coverage of the membrane surface by the corresponding PEO brush. For membranes cast with PEG additive, there was no change in contact angle. The contact angle values are consistent with those of Asatekin *et al.* for PAN-*g*-PEO9 combs prepared from the more hydrophilic acrylate macromonomer [58]; they reported a contact angle of 39° for a 40 wt.% PEO comb. That comb was shown to exhibit no attraction to a carboxylate-modified AFM probe tip and complete resistance to irreversible fouling in biofoulant filtration studies [55,74].

To make a more direct comparison to the material used in that study, acrylate-based PAN-*g*-PEO9 combs were synthesized according to the method reported and coated onto PAN-400

membranes. The static contact angle of those membranes was found to be 46 ± 2°, higher than reported but intermediate to the POEM9 and POEM23 PAN-*g*-PEO combs. When Fan *et al.* encountered an unexpectedly high carbon-to-oxygen ratio in their POEM brushes, and also found the POEM macromonomer to be polydisperse, they hypothesized that the former was due to preferential polymerization of the low molecular weight fraction of POEM [88]. It is possible that the difference between the methacrylate- and acrylate-based PAN-*g*-PEO9 contact angle is due to the same phenomenon, amplified by the difference in reactivity of methacrylates and acrylates, or simply due to the difference in backbone chemistry.

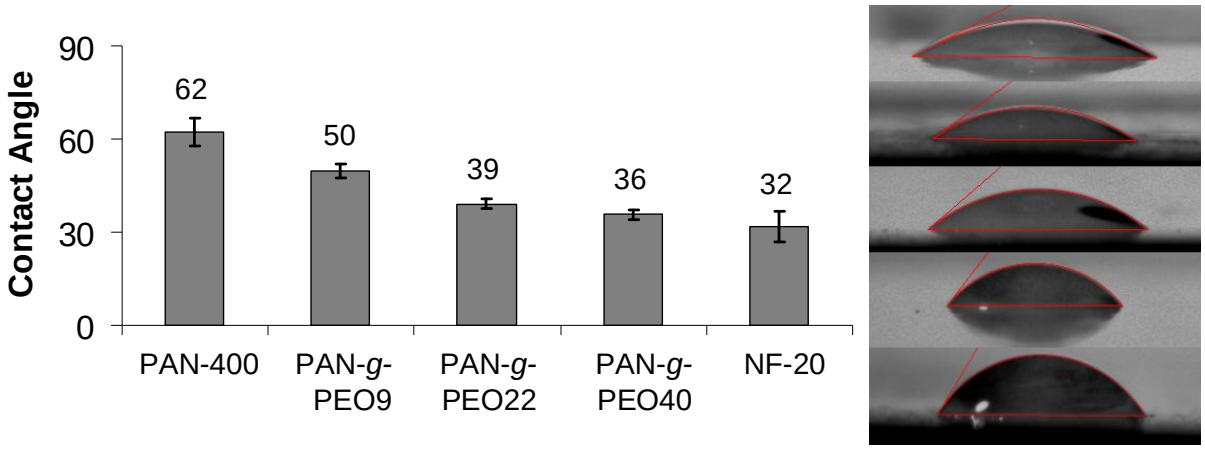

Figure 3.5. Static water contact angles with PAN-*g*-PEO coated membrane surfaces and the Sepro NF-20 TFC membrane. The control for the coated membranes, the porous PAN-400 UF base membrane, was subjected to the same coating process as for the comb polymers (Section 2.3.1) using pure DMSO solvent. For the PAN-*g*-PEO membranes, contact angle decreases with increasing PEO side chain length.

3.4. Membrane Fouling Resistance

3.4.1. AFM Force Measurements: Carboxylate-Modified Particle Adhesion

In previous work, it was shown that force measurements employing a charged colloidal AFM tip could be used as a predictor for fouling performance of filtration membranes [55,74]. Membranes incorporating PEO comb copolymers were found to have a net repulsive force on the probe tip due to the hydrophilic brush on the surface. Figure 3.6 shows that the POEM-based PAN-*g*-PEO NF comb membranes also exhibit this behavior in their as-coated state except the 38 wt.% PEO PAN-*g*-PEO9. In the case of this membrane, annealing for four hours in 90 °C water increased the mean adhesive force to 0.95 ± 1.64 mN/m in PBS, an overall repulsive effect. Annealing increases the mobility of the copolymer, thus allowing the

further promotion of hydrophilic PEO chains to the surface. However, the annealing temperature used exceeded Sepro's published range for the PAN-400 base, and resulted in a large loss of membrane permeability.

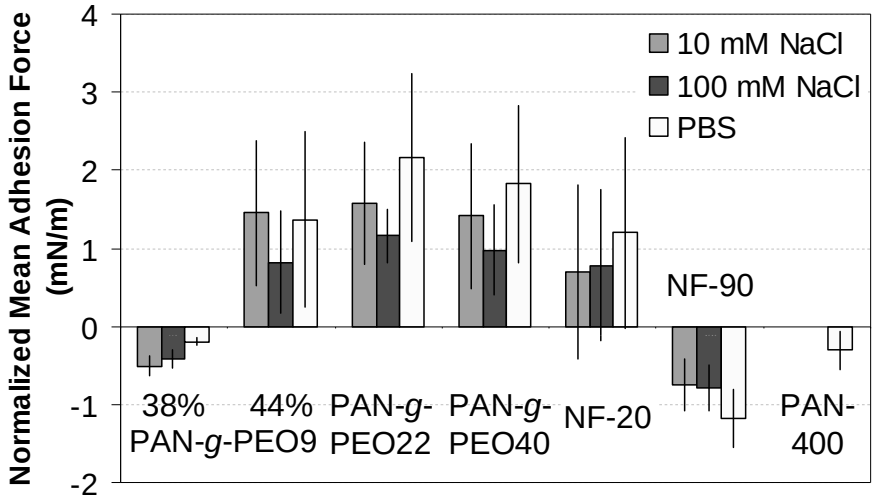

Figure 3.6. PAN-*g*-PEO and control membrane surface adhesion forces to a carboxylate-modified AFM colloidal tip showing a net repulsion for most of the comb membranes and an adhesive force for the controls. AFM experiments conducted by William Phillip from the Elimelech group at Yale University.

The comb membrane adhesion force results contrast with those of the control membranes, which (at least partially) adhered to, rather than repelled, the tip. These experiments were performed by William Phillip in the Elimelech group at Yale University.

3.4.2. Bacterial Adhesion

The ability of bacteria to adhere to surfaces is influenced by many factors including roughness, hydrophilicity, and charge. In this specific case of fouling, the predominance of negatively charged bacteria makes negative charge an effective mechanism for reducing adhesion; however Kochkodan *et al.* reported that, once adhered, negative surface charge makes bacteria adhere more tightly [34].

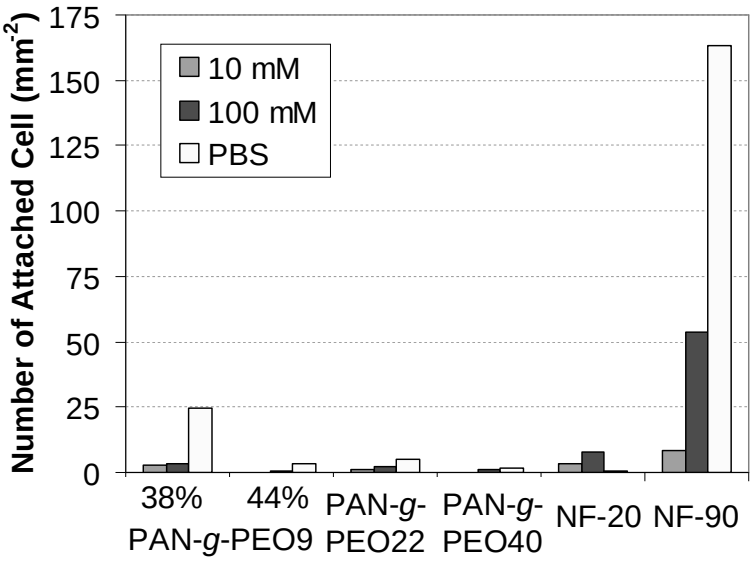

Figure 3.7. Comparison of *Escherichia coli* adhesion to membrane surfaces after 1 hour in 10 mM and 100 mM NaCl and PBS solution showing resistance of PAN-*g*-PEO surfaces; compare with 1100 cells/mm^2 for Osmonics PAN UF membrane in 100 mM NaCl [81].

Figure 3.7 shows the results of experiments at Yale to measure the resistance of the membranes to bacterial adhesion. Only a few bacteria adhered to the comb membranes and NF-20 control, while the more highly-charged NF-90 was less able to resist adhesion (Figure 3.8). In a previous study by Adout *et al.*, a PAN UF membrane specially treated to increase hydrophilicity was found to host ~35 cells/mm^2 (in 10 mM NaCl) and 1100 cells/mm^2 (in 100 mM NaCl) after the same procedure [81]. The resistance of the combs to tight adhesion appears to be weakly related to PEO content and side chain length, which parallels closely the results of the AFM experiments.

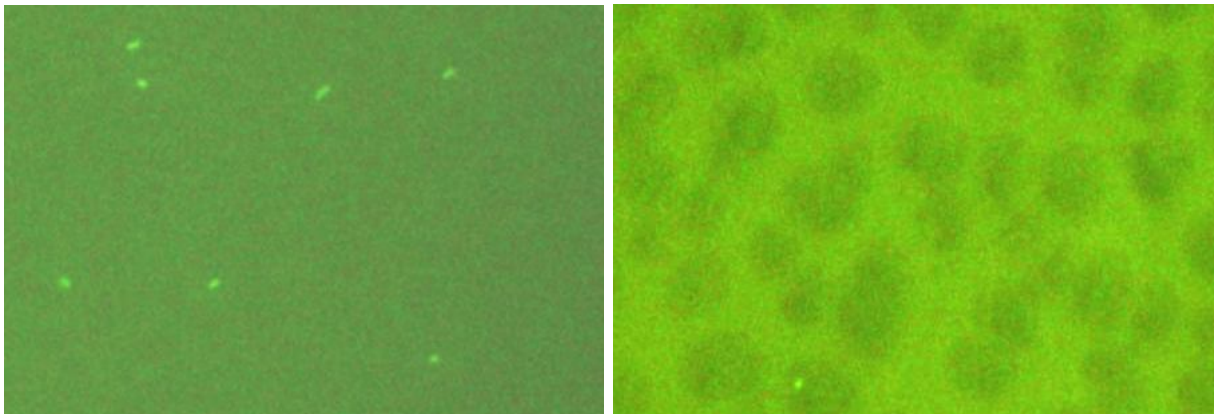

Figure 3.8. Fluorescence microscopy images of NF-90 (left) and PAN-*g*-PEO22 membrane (right) surfaces showing fewer adhered bacteria (bright) on the comb membrane; the large-scale porosity of the asymmetric PAN-400 base membrane is visible through the comb coating.

3.4.3. 24 Hour Bovine Serum Albumin Filtration

Based on the AFM and bacterial adhesion data, we might expect the PAN-*g*-PEO TFC NF membranes to show limited to complete resistance to adsorptive fouling by biofoulants. Figure 3.9 shows data for 24-hour dead-end filtrations of a 1 g/L BSA solution through control membranes and the membranes made with combs of varying side chain length. Solid symbols represent the permeability of DI water through the membrane, while open symbols represent the filtration of BSA feed solutions. The osmotic pressure established by the high salt retention of the NF-90 membrane reduced its operational flux to nearly zero during filtration of the BSA/PBS feed. It was fouled by the BSA solution, irreversibly losing 20% of its initial flux. The permeability of the NF-20 membrane did not stabilize after days of operation, making its fouling resistance difficult to characterize [104]. However, with its hydrophilic surface (Figure 3.5) and low surface charge density at experimental conditions [104], little fouling would be expected. Nevertheless, a decrease of 5% permeability was measured before the steadily increasing permeability compensated.

The flux data for the comb membranes is normalized by the average value of the pure water flux after stabilization and prior to the introduction of the BSA feed. For these membranes, no statistically significant (5% level) change in permeability was observed between the DI and BSA feeds, indicating that negligible fouling occurred. No BSA was detectable in the permeate three hours into the experiment for any of the membranes, indicating 100% BSA retention, within instrument limits, as would be expected for this heart-shaped, 66 kilodalton (kDa) protein, given its reputed dimensions of ~8.4×8.4×3 nm [105]). The PAN-400 base membrane lost 76% of its initial permeability when challenged with the same 24-hour BSA solution (Appendix A).

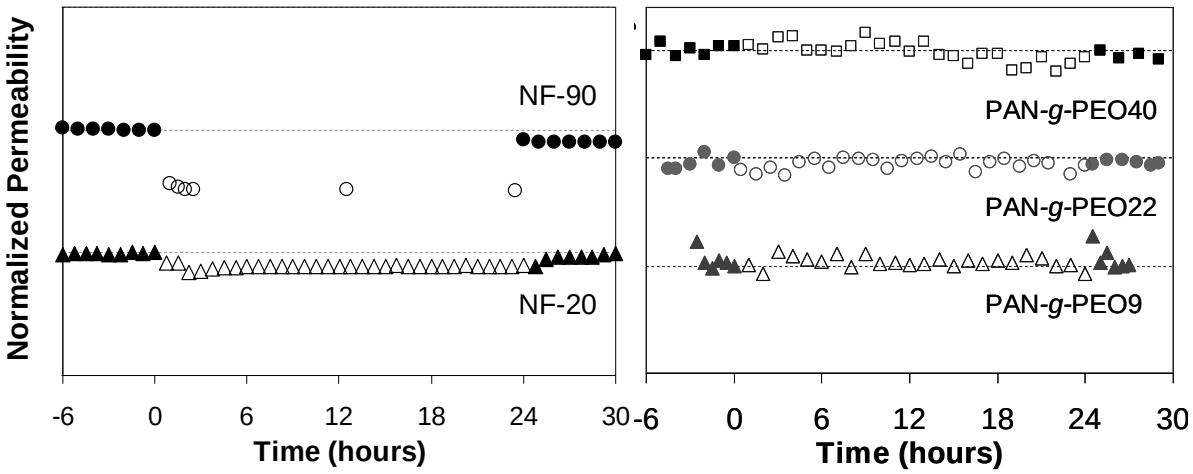

Figure 3.9. Dead-end filtration at 0.34 MPa of 1 g/L BSA solution (open symbols) and deionized water (filled) through (left) polyamide TFC NF; and (right) PAN-*g*-PEO TFC NF membranes, with permeability normalized by the initial pure water permeability. Exposure to the protein solution causes a ~5% decrease in the initial permeabilites of 65 and 10 L/m^{2}hMPa for the NF-90 and NF-20 membranes respectively, and no loss of the initial stabilized permeabilities of 9, 22 and 72 L/m^{2}hMPa for PAN-*g*-PEO9, PAN-*g*-PEO22 and PAN-*g*-PEO40 membranes, respectively. BSA retention, R_{BSA}=1 for all membranes.

3.5. Membrane Permeability

3.5.1. Contributing Factors

Fouling resistance is important, both to maintain useful fluxes and to avoid shifts in membrane selectivity due to changes in hydrophobicity [26,27,24] or partial pore blockage [26,27,35], However, order-of-magnitude trade-offs in the initial permeability of the membrane may make fouling resistance of secondary importance, particularly in commodity water purification applications. The PAN-*g*-PEO membranes in this study exhibited permeabilities in the range of 9-72 L/m^{2}hMPa at room temperature. These values are comparable to the Sepro NF-20 (12 L/m^{2}hMPa) and FilmTec NF-90 (76 L/m^{2}hMPa) membranes used here as controls or others described in manufacturer's specifications (e.g., 45 L/m^{2}hMPa at 0.655 MPa for the Koch TFC-SR 100). Differences between the combs may reflect differences in both coating morphology, governed by the comb polymer chemical architecture, and coating thickness.

Increasing PEO fraction and/or side chain length can be expected to increase permeability due to several factors: increased hydrophilicity [9,106,50], reduced boundary effects on solvent

flow [107], and increased "porosity" [9]. The latter is supported by the comb swelling results, which show a dependence on both side chain length and fraction of PEO (Table 3.1), and is consistent with the finding of Stamatialis *et al.* that solvent-resistant NF membrane permeability is proportional to the degree of swelling [108].

The role of porosity and nanochannel diameter on permeability were investigated by attempting to swell the PEO domain of the comb with PEG additive during the solution coating process. PEG molecules of the same length as the comb side chains should optimally segregate to the center of the hydrophilic domains during casting without compromising the functional morphology or aggregating [109], and then elute out.

These expected effects of comb chemistry and additive on permeability could not be verified in this study due to a large variability in coating thickness and thickness-normalized permeability (28-111 LMH-μm/MPa, Appendix B) between membrane samples. The average coating thicknesses observed by SEM were between 0.6 – 2.8 μm and the range in permeability for those membranes was 25-63 LMH/MPa at 22 °C. Approximating the polyamide TFC membrane active layer thickness as 0.1 μm [16], the control membranes NF-20 and NF-90 have thickness-normalized permeabilities of 1 and 7 LMH-μm/MPa, respectively. Based on the range of thickness-normalized permeabilites of the PAN-*g*-PEO membranes, permeabilities between 112-446 LMH/MPa should be possible by reducing the coating thickness to 0.25 μm.

3.5.2. PEO and Solvent Quality

The PEO/water system is known to have a lower critical solution temperature (LCST) where PEO becomes immiscible with water [110-112]. For example, 2.18 kg/mol PEO in water has a critical point of 177 °C [110]. It was found previously that raising the temperature in filtrations using PVDF-*g*-POEM9 NF membranes reversibly increased their molecular weight cutoff and permeability, while increasing the pressure decreased them [57]. (A qualitatively similar temperature response has been observed for certain commercial NF membranes [37], and was attributed to thermal expansion, increased activated transport, and structural changes.) The tunability of the PVDF-*g*-POEM9 membrane properties was attributed to the

progressive collapse of the water-swollen PEO brush lining the nanochannels as the interaction of PEO with water becomes less favorable, thus opening up the channels.

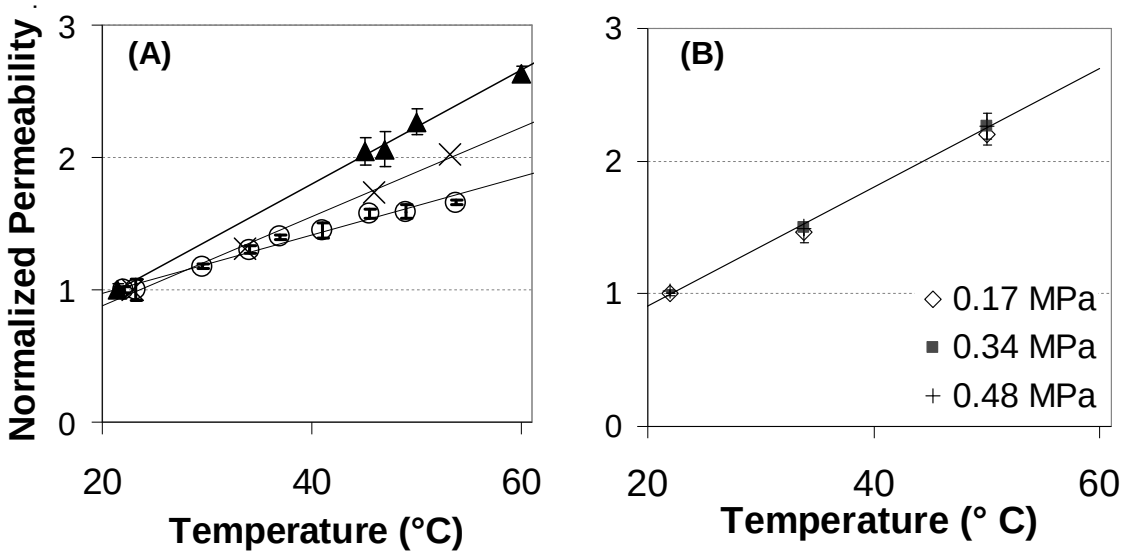

Figure 3.10. Normalized pure water flux through PAN-*g*-PEO NF membranes showing the effects of (A) temperature on PAN-*g*-PEO9 (○), PAN-*g*-PEO22 (×), and PAN-*g*-PEO40 (▲) membranes at 0.34 MPa; (B) temperature and transmembrane pressure on PAN-*g*-PEO40 membrane.

Figure 3.10.A shows the trend in PAN-*g*-PEO TCF membrane permeability with temperature, normalized by the permeability at room temperature. Permeability increases linearly for all the membranes, and the slope increases with PEO side chain length. In Figure 3.10 (B), it is seen that various applications of pressure to the PAN-*g*-PEO40 membrane do not cause notable deviation from the linear trend observed for a fixed pressure.

Saeki *et al.* found that sodium chloride has a strong effect on PEO-water miscibility (364 °C/M for 2 kg/mol PEO and increasing with decrease in PEO MW) [110], so the effect on the PEO-water system of a 0.2 M NaCl feed should be greater than raising the temperature by 70 K. Figure 3.11.A shows the effect of solvent quality on the permeability of PAN-*g*-PEO40 membrane. The permeability of methanol, a somewhat poorer solvent for PEO than water [113], is compared with that of DI water and 0.2 M NaCl at room temperature and 50 °C. Only a small increase in permeability was caused by the increased salinity; the permeability of methanol was similar to that of 50 °C water.

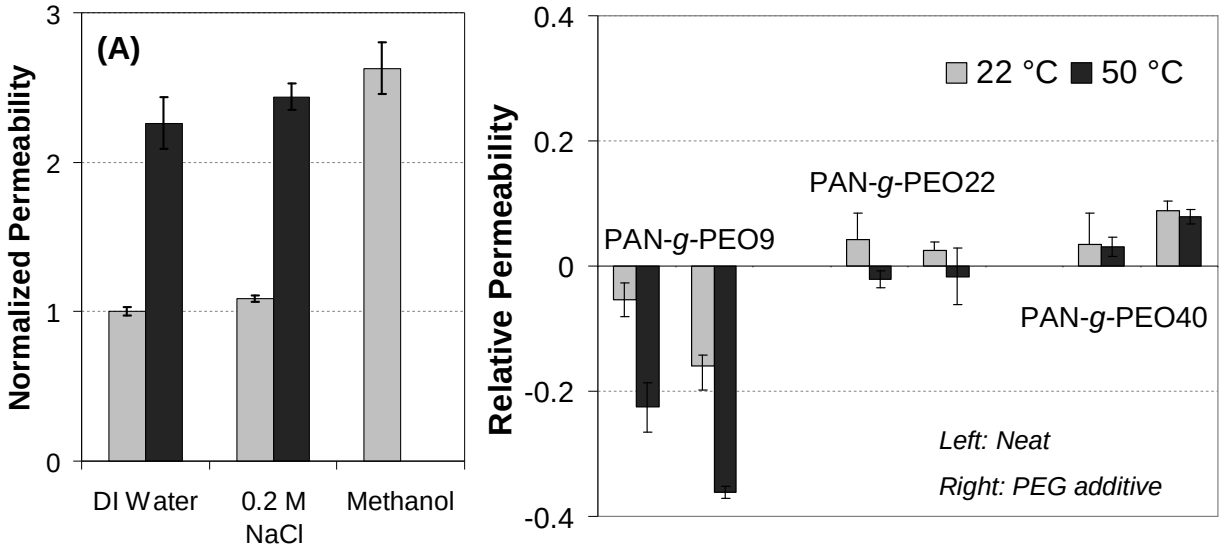

Figure 3.11. Dependence of permeability on PEO solvent quality during filtration by PAN-*g*-PEO membranes at 0.34 MPa showing a much larger response to temperature and methanol than salinity for a PAN-*g*-PEO40 membrane at both 22 °C (light) and 50 °C (dark) (A); (B) the relative change in permeability in 0.2 M NaCl for neat and PEG additive membranes is negative for PAN-*g*-PEO9 membranes, neutral for PAN-*g*-PEO22 membranes, and positive for PAN-*g*-PEO40 membranes.

3.5.3. Environmental Response

In spite of the nanoscale porosity of NF membrane functional surfaces, studies have found that bulk parameters are the most significant parameters to modeling permeability [114,115,108]. Santos *et al.* concluded that solvent flux could mainly be related to molecular weight cutoff (*i.e.* pore size) and viscosity [114], while Darvishmanesh *et al.* recently published an updated membrane model wherein both the diffusional and viscous term prefactors are inversely proportional to solvent viscosity [115].

Thus much of the effect of these solvent parameters on the membrane permeability can be explained in terms of viscosity and PEO swelling; methanol's viscosity is comparable with that of water at 50 °C, and roughly half of the 1 mPa·s of 20 °C water [116]. Additional permeability tests using ethanol-water mixtures (not shown) found water-ethanol permeability to be lower than either pure water or pure ethanol permeability, again consistent with the respective viscosities.

To eliminate the effects of viscosity in the data, a correction was made based on the temperature dependence of water viscosity. The normalized, viscosity-corrected water permeability [37],

$$p_{\mu} = p\mu / p_{\mu,0} \,, \qquad (3)$$

where p is the measured permeability, μ is the dynamic viscosity of water at the measurement temperature and $p_{\mu,0}$ is the viscosity-corrected permeability at 22 °C, is plotted in Figure 3.12 (A). A rise in permeability is seen with increasing temperature for the PAN-*g*-PEO22 and PAN-*g*-PEO40 membranes, while the trend for the PAN-g-PEO9 has downward curvature and shows a slight reduction in flux for T > 50 °C. The general trend with PEO side chain length is consistent with the expected larger diameter of the nanochannels and the closer proximity of the LCST for the longer-side chain combs.

Measurements taken at various transmembrane pressures show similar systematic behavior with side chain length. Figure 3.12 (B) plots the normalized flux of the membranes at 22 °C as a function of pressure. Interestingly, the PAN-*g*-PEO9 membrane shows a decrease in flux with increased pressure. For this system, pressure effects may be dominated by increased swelling of the PEO brush due to enhanced PEO-water miscibility at elevated pressures [117]. The result might alternatively arise from reversible base membrane compaction. A similar study on PVDF-g-POEM9 NF membranes showed the opposite trend with pressure [57].

The effect of sodium chloride in solution on PAN-*g*-PEO membrane permeability also follows the same trend with side chain length as pressure and temperature. In Figure 3.11 (B), the relative change in permeability with the addition of 0.2 M NaCl to solution at 22 °C and 50 °C is plotted for both neat and PEG additive membranes of PAN-*g*-PEO. As in the case of temperature and pressure, PAN-*g*-PEO9 flux was decreased by the change in condition, while PAN-*g*-PEO40 flux increased and PAN-*g*-PEO22 flux was nearly constant. For each comb, the additive magnified the effect. The NaCl retention of each comb membrane is very low; the development of osmotic pressure due to salt retention is thus not believed to be the cause of this phenomenon.

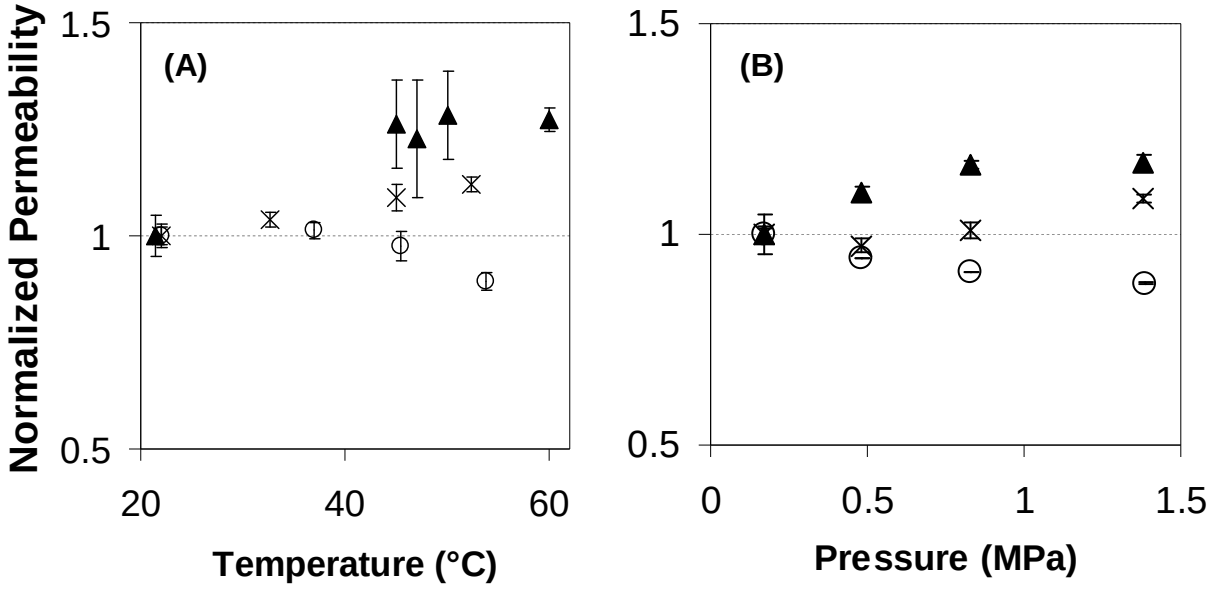

Figure 3.12. Normalized pure water flux through PAN-*g*-PEO NF membranes showing the effects of temperature and transmembrane pressure on PAN-*g*-PEO9 (○), PAN-*g*-PEO22 (×), and PAN-*g*-PEO40 (▲) membranes; (A) the viscosity-corrected permeabilities from Fig.3.10; (B) normalized flux vs. transmembrane pressure at 22 °C.

The effects of pressure, temperature, and NaCl concentration on PEO-water compatibility are known to be dependent on chain length [118,110]. The viscosity-corrected water permeability [37] of the membranes leaves a small residual that increases with side chain length, consistent with both the larger diameter of the nanochannels and the closer proximity of the long PEO chains to their LCST.

3.6. Effect of Side Chain Length on Size Cutoff

In previous studies of amphiphilic comb NF membranes, the molecular size cutoff was thought to be defined by the width of the PEO "nanochannel" network formed by the microphase-separated comb [55,53,56,57]. In this case, the size cutoff should increase systematically with increasing side-chain length of the PAN-*g*-PEO coating material from 9 to 40 EO units.

As a first estimate of the size of the water-swollen PEO domain, *D*, the PEO chains can be treated as Gaussian coils, with the RMS-average end-to-end distance given by:

$$\sqrt{\langle r^2 \rangle} = n^{1/2} a \,, \tag{4}$$

where a = 0.35 nm is the effective segment length for PEO [119], n the number of EO segments in the side chain Following this approach,

$$D \approx 2\sqrt{\langle r^2 \rangle} \tag{5}$$

yields D values of 2.1, 3.3, and 4.4 nm for PAN-*g*-PEO9, PAN-*g*-PEO22, and PAN-*g*-PEO40, respectively. The effective size cutoff for PAN-*g*-PEO9 was previously reported as ~0.8 nm using rigid molecular probes [55], roughly 40% the size of the estimated domain dimensionality. Using this scaling, the difference in size cutoff between each of the three side chain lengths is estimated to be ~0.45 nm.

The size-based selectivity of the PAN-*g*-PEO NF membranes was investigated experimentally using small molecular dyes and other aromatic compounds (Table 2.3), so chosen because of the rigidity imparted by their conjugated chemical structures, water solubility due to charged groups (on average -1 formal charge per 230 g/mol mass), and characteristic light absorption [55,53,57]. The planar, irregular molecular shapes (Figure 2.7) precluded definitive arrangement of these probes hierarchically by size. To address this issue, each probe was assigned the diameter of a sphere of equivalent volume to the dye's molecular volume [55], also reported in Table 2.3.

3.6.1. Deionized Water

Figure 3.13 plots membrane retention of charged probes in DI water *versus* the probe molecular weight for the polyamide (PA) TFC control membranes, NF-20 and NF-90 (left) and PAN-*g*-PEO membranes and PAN-400 base (right). The effective size cutoff for both of the PA membranes is ~200 g/mol (0.6-0.7 nm by our equivalent sphere metric). This value is consistent with those reported for other commercial NF membranes [37].

Compared with the commercial NF controls, the PAN-*g*-PEO NF membranes all exhibit a larger permeate size cutoff. A sharp decline in retention is observed for molecules below ~400 Da (~0.85 nm diameter) by PAN-*g*-PEO membranes, as shown in Figure 3.13 (B). Somewhat surprisingly, there was no notable dependence on comb side chain length. The observed cutoff diameter is comparable to that reported previously for PAN-*g*-PEO9 NF membranes prepared from a PEO acrylate macromonomer, which retained over 90% of an 0.84 nm (311 Da) dye in DI water at room temperature [55]. Given the large expected differences in PEO domain size for the different amphiphilic combs, the results suggest that molecular sieving by the PAN-*g*-PEO NF membranes is controlled by some other aspect of the membrane than the PEO domain width of the microphase-separated selective layer coating.

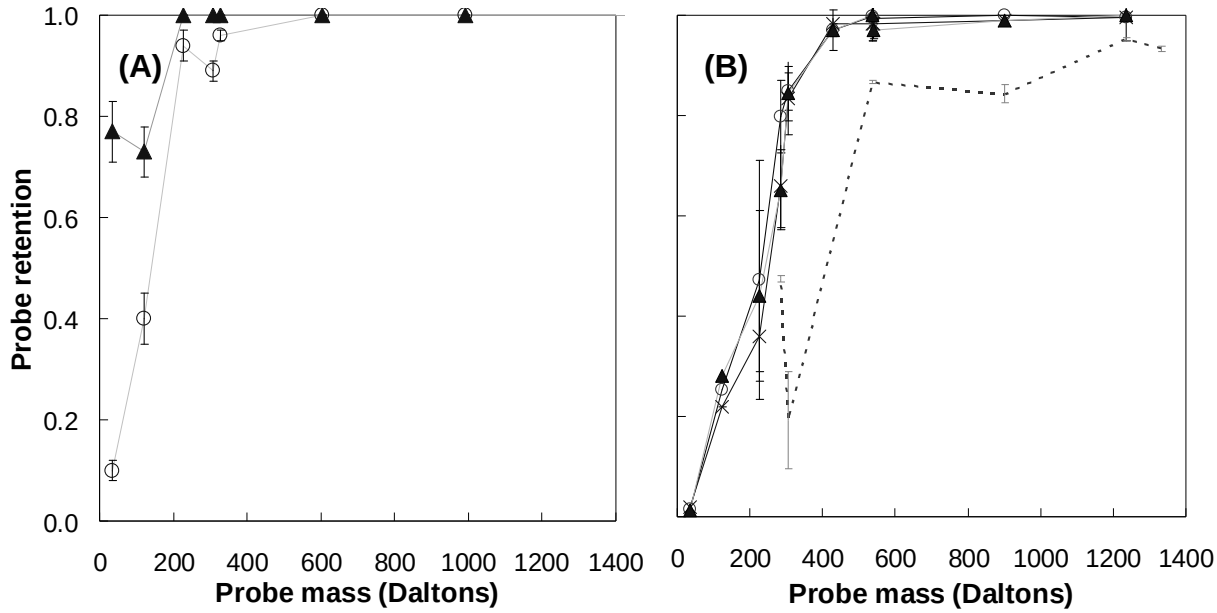

Figure 3.13. The retention of charged molecular probes in 22 °C deionized water with 0.34 MPa transmembrane pressure in dead-end mode filtration by (A) controls Sepro NF-20 (○) and FilmTec NF-90 (▲) showing a cutoff at ~200 Da; (B) PAN-400 UF base membrane (dashed line), showing effects of high polydispersity in pore size, and PAN-*g*-PEO*n* TFC membranes (solid lines), showing a size cutoff at ~400 Da (~0.85 nm), with no significant dependence on comb side chain length for *n*=9 (○), *n*=22 (×), and *n*=40 (▲).

One possible explanation is the UF support membrane, which is common to all the comb membrane systems. However, filtration of the probes through the PAN-400 base membrane alone gave retention values substantially below those of the coated membranes across the full size range of probes tested, as seen in Figure 3.13 (B). These membranes are reported by the

manufacturer to reject 75% of a 20 kDa PEO standard; one might therefore expect smaller retentions for the low molecular weight probes studied here. However, similar findings were reported for a polysulfone UF base membrane challenged with anionic dyes and monodisperse PEO standards [120]. These results can be attributed to the broad distribution of pore sizes encountered in UF membranes prepared by phase inversion, and the rigidity of the molecular dyes, which limits their entry into the smallest pores of the UF membrane selective layer.

3.6.2. 0.2 M NaCl Solutions

The observed invariance of the size cutoff with comb side-chain length in DI water would appear to limit the utility of this approach for tuning membrane selectivity. To further explore the effects of side-chain length, sodium chloride was added to the molecular probe feed solutions and the filtrations rerun. Sodium chloride substantially reduces the miscibility of PEO in water [110], dramatically decreasing the lower critical solution temperature (LCST). It was found previously that addition of 0.2 M NaCl in filtrations employing a PVDF-*g*-POEM9 NF membrane decreased the retention of Reactive Red 120 from 95% to 85% [57]. The lower rejection was attributed to a collapse of the PEO brush lining the nanochannels, thereby increasing the effective pore size. By this mechanism, one would expect the addition of salt to lower rejections more notably for membranes coated with longer side-chain combs.

Figure 3.14 shows the retention of the probes in a 0.2 M NaCl solution at room temperature for the PAN-400 base membrane and the comb-coated NF membranes. A large reduction in the probe retentions was found for the UF base compared to DI water (Figure 3.15). This phenomenon was observed previously in the ultrafiltration of charged solutes, and was ascribed to the reduced effective diameter of the charged solutes due to a reduced hydration shell and charge screening by ions in solution [121]. The retention of the polyamide membranes also decreased for similar reasons [17]. The PAN-*g*-PEO NF membranes also showed lower retentions, exhibiting the expected trend of lower rejections with increasing side chain length. Defining the cutoff as 90% retention, the PAN-*g*-PEO9 molecular weight cutoff shifted from 400 Da to ~1.2 kDa, or 0.84 nm to ~1.2 nm (Figure 3.15).

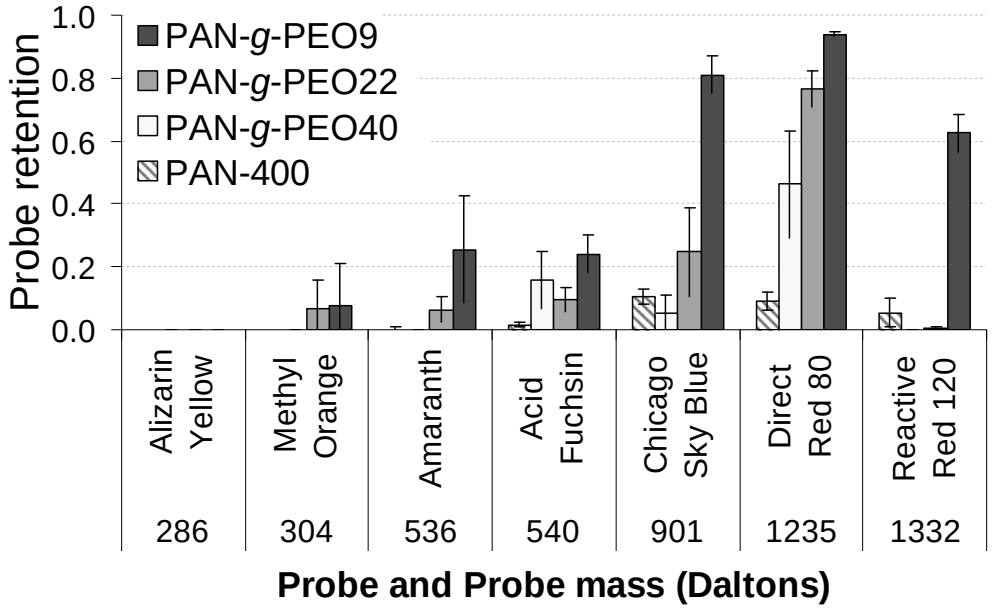

Figure 3.14. Retention of rigid molecular dyes in an aqueous 0.2 M NaCl feed by PAN-*g*-PEO NF membranes and PAN-400 UF base at 22 °C and 0.34 MPa transmembrane pressure in dead-end mode filtration showing a differentiation of retention by side chain length in the comb.

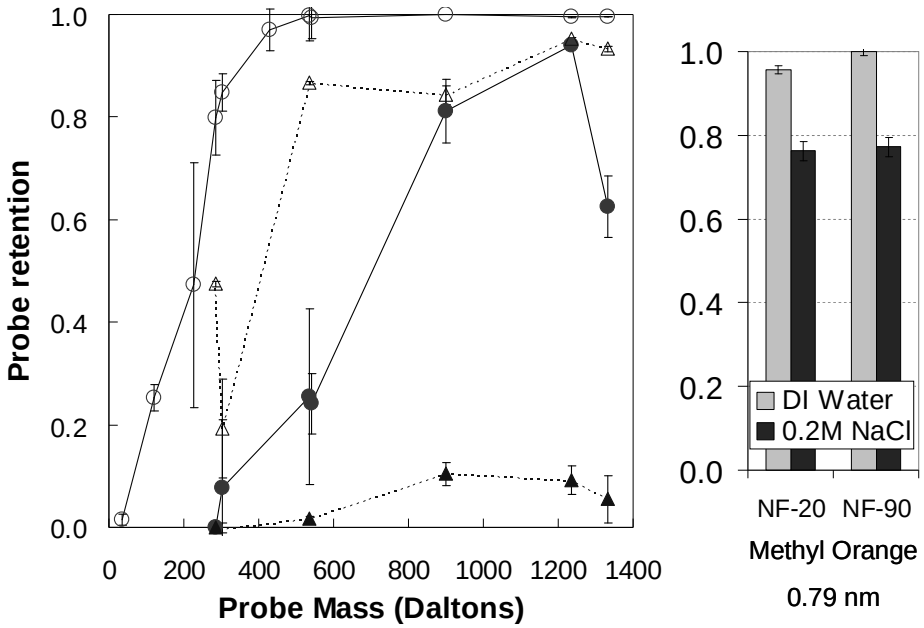

Figure 3.15. Comparison of molecular probe retention in 22 °C DI (open/grey) and 0.2 M NaCl (filled/black) feeds for (left) PAN-*g*-PEO9 (circles), PAN-400 (triangles) and (right) polyamide TFC controls NF-20 and ND-90 showing the shift in effective size cutoff.

For CSB and RR120, the PAN-400 control shows a higher retention than the PAN-*g*-PEO40 and/or PAN-*g*-PEO22. Since the PAN-400 forms the base of the TFC NF membrane, this result is not readily explained. One would expect a minimum rejection equivalent to that of the base membrane. Since the base membrane experiments were run in a different month and using membranes from a different batch than those used in the comb membranes, variations in experimental conditions such as room temperature, or in morphology might account for the discrepancy. Manufacturers commonly cite ±5-10% variance in retention and permeability. Another possible explanation is that the thick comb coating enhances concentration polarization by the same mechanism as a cake layer [14,122].

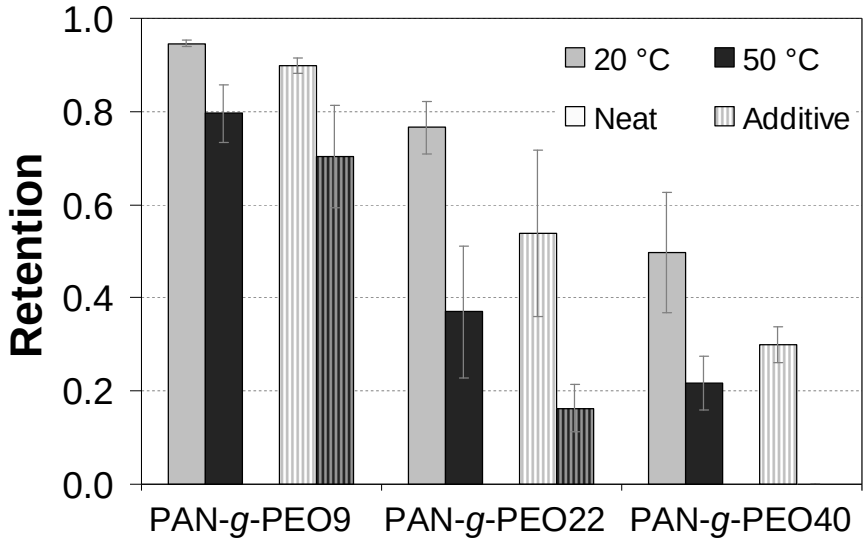

Figure 3.16. Retention of Direct Red 80 (1.07 nm) in 0.2 M NaCl by PAN-*g*-PEO NF membranes (solid bars) and PAN-*g*-PEO membranes prepared with ~4 wt.% PEG additive (striped), at 22 °C (grey) and 50 °C (black). Retentions trend downward with increased temperature, side-chain length and use of additive.

In conditions of reduced PEO-water miscibility, NF membranes made from comb solutions containing PEG additive also show a change in effective pore size. Figure 3.16 shows retention of Direct Red 80 (1.07 nm) in 0.2 M NaCl by PAN-*g*-PEO NF membranes prepared from neat comb solution, and from solutions containing ~4 wt.% PEG additive, measured at 22 and 50 °C. Uniformly, the addition of PEG resulted in lower retentions, while preserving the effect of side chain length. This observation is expected: PEG molecules of the same length as the comb side chains should segregate to the hydrophilic domains, with a peak concentration at the center, during casting [109]. A consequence of this would be an increase

in the characteristic size of the hydrophilic domains formed during the coagulation step of the membrane coating process. Upon eluting from the coating, the effective pore diameter is increased, leading to lower retentions.

3.7. Membrane Stability

One potential limitation of the current implementation of PAN-*g*-PEO membranes was raised at the conclusion of an earlier study [95]: the PEO side chains are tethered to the backbone with an ester bond. Although PEO itself is susceptible to slow oxidative damage [118], ester bonds are susceptible to rapid hydrolysis through acid or base attack. Membrane filtration at extreme pH may be desired to separate acids [123] (for example, electroplating reagents or metals extracted in mining operations), or more generally to chemically clean adsorptive fouling from a system. To evaluate the seriousness of this concern about the ester architecture, PAN-*g*-PEO membranes were subjected to prolonged exposure to acidic (pH 2) and basic (pH 11) conditions. These represent the recommended extremes for PA membranes (*e.g.* NF-90).

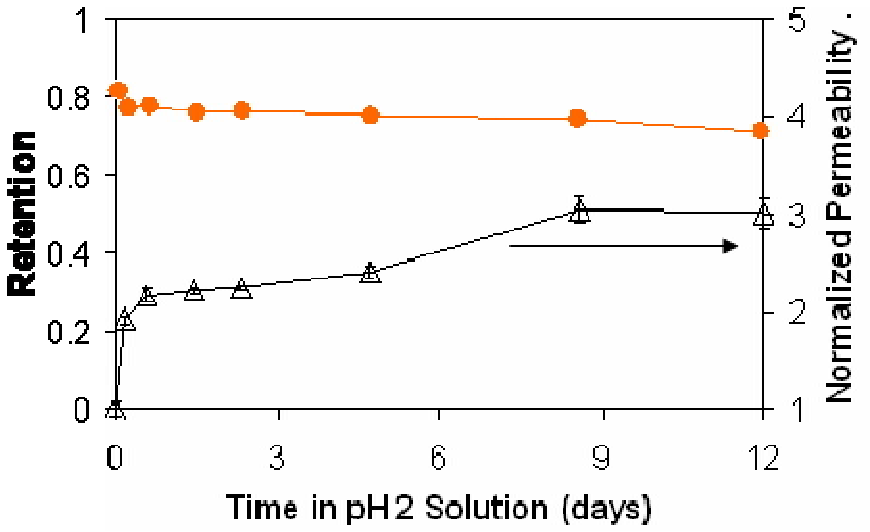

Figure 3.17. Methyl Orange retention (●) and DI water permeability (Δ) of the PAN-*g*-PEO9 membrane with 0.34 MPa pressure after intervals of exposure to pH 2 solution shows a cumulative effect consistent with hydrolysis of the PEO side chain ester linkage.

3.7.1. Permeability and Retention Effects

Figure 3.17 shows the effects of exposure to pH 2 solution on the PAN-*g*-PEO9 membrane over the course of 12 days. A sudden, but small, decrease in retention and simultaneous

increase in permeability occurs within a few hours of acid exposure, followed by a gradual continuation of the same trends. During the course of the experiment, the permeability increased ~300%, while the retention of Methyl Orange decreased by 12%. This is consistent with progressive hydrolysis of the methacrylate ester bonds, reducing density of PEO chains within the fixed nanochannels and increasing the "porosity" for water convection.

In Figure 3.18 (A), the membrane dye retention (filled symbols) is compared with the dye retention of the membranes after 14 days of acid treatment. In the case of the CSB dye in DI water (a), the degree of side-chain hydrolysis was insufficient to allow the dye to pass. However, it did decrease the retention of the Methyl Orange dye in DI water (b) for the PAN-*g*-PEO9 membrane (◊), the neat PAN-*g*-PEO40 membrane (□), and the PEG additive PAN-*g*-PEO40 membrane (Δ), and the degree of hydrolysis was sufficient to differentiate the retention by side chain length. The CSB (c) and Amaranth (d) dyes in 0.2M NaCl are only retained by the PAN-*g*-PEO9 membrane; the retention of both decreases after acid treatment. The relative change in solvent flux during the acid treatment, shown in Fig. 3.18 (B), is large for the PAN-*g*-PEO9 membrane (◊), which had the lowest initial permeability, and small for the PEG additive PAN-*g*-PEO40 membrane (▲), which had the highest initial permeability.

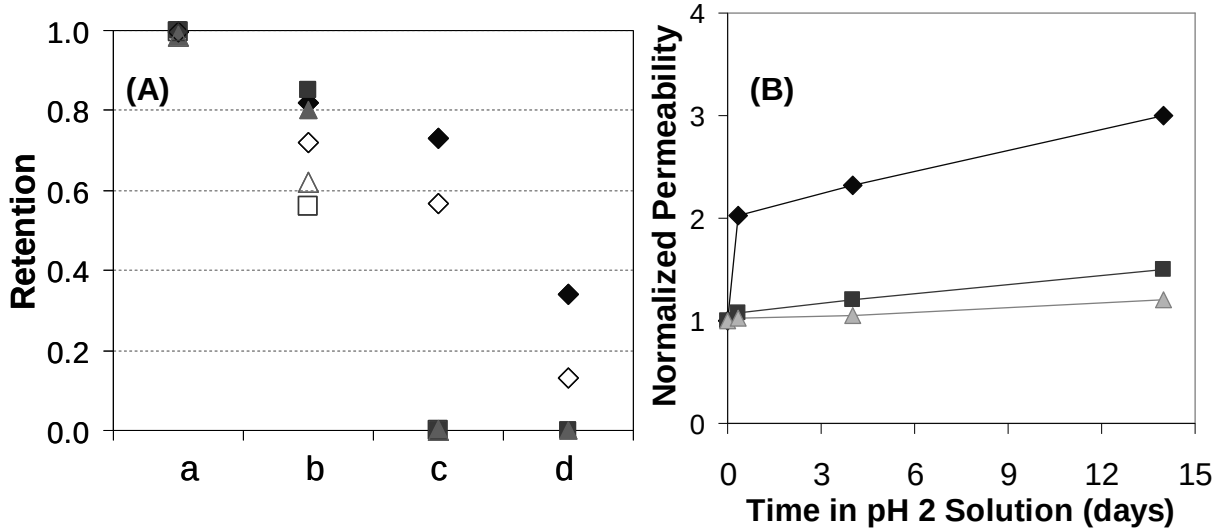

Figure 3.18. The dye retention and permeability of membranes of PAN-*g*-PEO9 (diamonds), neat PAN-*g*-PEO40 (squares) and PAN-*g*-PEO40 with PEG additive (triangles) showing (A) the retention of (a) CSB and (b) Methyl Orange in DI water, and (c) CSB and (d) Amaranth in 0.2M NaCl before (solid symbols) and after (open symbols) 14 days of exposure to pH 2 solution; (B) the DI water flux normalized by the initial flux.

Exposing the membranes to base (pH 11) for two weeks had a smaller and qualitatively different effect on retention and permeability (Figure 3.19). A consistent increase in permeability occurred overall, while the retention was seen to slightly increase, rather than decrease. There are two likely contributing factors to this finding. First, degradation of the comb selective layer and/or PAN base membrane could increase water permeability due to increase in effective porosity. The PAN-400 base membrane is rated for operating between pH 2-10, with only brief exposure recommended at 11.5 pH. In highly basic solutions, such degradation can also be expected to modify the membrane surface chemistry, leading to an increase in membrane surface charge density and dye retention by electrostatic repulsion.

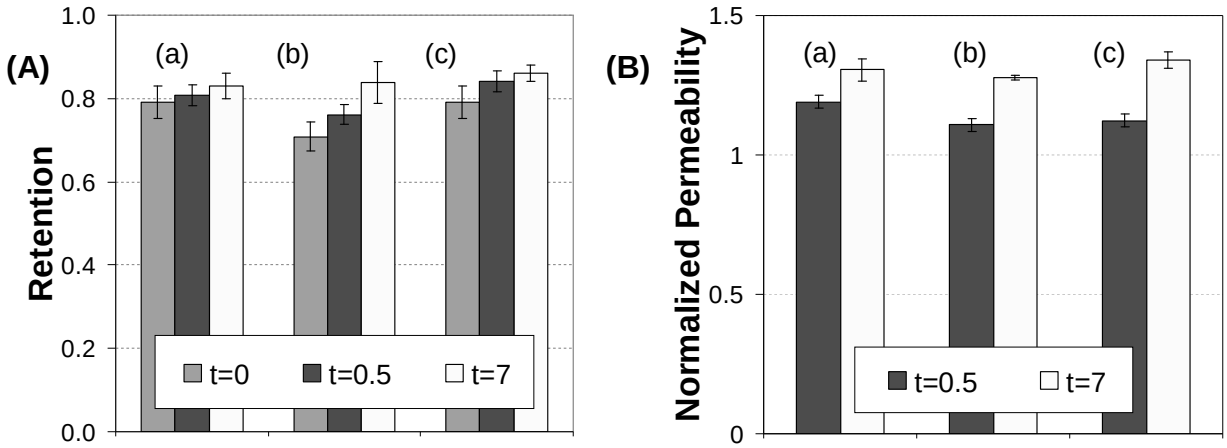

Figure 3.19. The dye retention and permeability of PAN-*g*-PEO9 (a), neat PAN-*g*-PEO40 (b) and PEG additive PAN-*g*-PEO40 (c) membranes showing (A) the retention of Methyl Orange in DI water at 0, 0.5, and 7 days exposure to pH 11 solution; (B) the DI water flux normalized by the initial flux.

3.7.2. Fouling Resistance

The changes in permeability and selectivity with extended exposure to strong acids or bases indicate that significant changes in surface chemistry occur under these conditions. Such changes might be expected to have a significant influence on the fouling resistance of the NF comb membranes. As expected, prolonged exposure to acid compromises the fouling resistance of the membranes (Figure 3.20), consistent with the loss of surface PEO brush coverage due to ester hydrolysis.

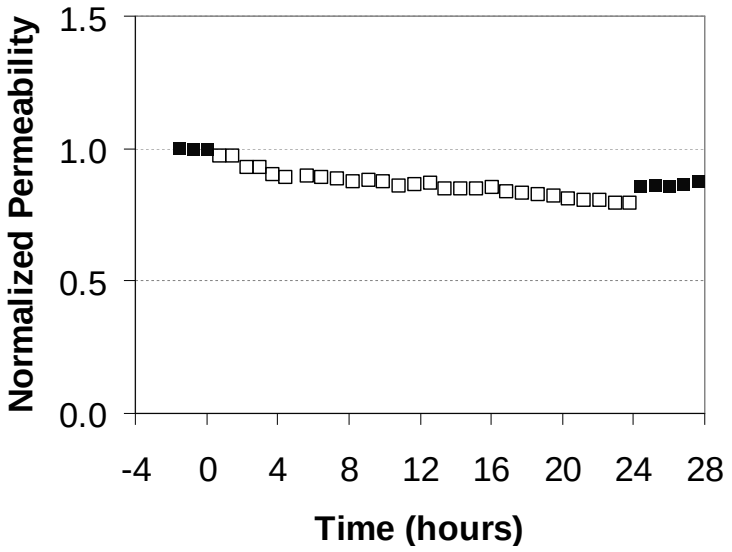

Figure 3.20. The permeability of PAN-*g*-PEO40 membrane to DI water (solid symbols) and 1g/L BSA in PBS (open symbols) at 0.34 MPa after 14 days of exposure to pH 2 solution, normalized by the stabilized DI water permeability.

3.8. Summary and Conclusions

3.8.1. Comb Properties

It was found that PAN-*g*-PEO*n* combs microphase separated for n = 9, 23 and 45, and swelled by over 100% of their weight in water. PAN-*g*-PEO5 did not microphase separate, and was swelled by water only sufficiently to hydrate the PEO. The water contact angle of the combs decreased with side-chain length and was higher for PAN-*g*-PEO9 than for the corresponding PEO9 acrylate comb.

3.8.2. Fouling

AFM measurements of the interaction force between a carboxylate-modified colloid particle tip and the surface of the NF comb membranes found that the PEO brush creates a net repulsive force on all but the 38 wt.% PEO PAN-*g*-PEO9 membrane. The tight adhesion of bacteria to all comb membranes after a one hour exposure was greatly reduced when compared with the PAN base membrane, and decreased with increasing comb side chain length and PEO content. One polyamide control membrane completely prevented tight adhesion during this experiment. We expect that these outcomes are mechanistically different, *i.e.*, that the biofouling resistance is due largely to charge in the case of the NF control

membrane vs. steric repulsion by the PEO brush in the case of the comb membranes. An extended bacterial adhesion study of the membranes could potentially confirm this expectation; given more time to colonize the charged surface, the bacteria should tightly adhere to it [34]. In contrast, long-term resistance of PEO comb copolymer membranes to biofouling has been reported:.a previous ten-day application of a PVDF-*g*-POEM NF membrane in a membrane bioreactor found it had no irreversible fouling, as compared to the UF control [59]; a more direct comparison of commercial NF membranes under such conditions could clarify the effectiveness of the respective approaches to biofouling resistance.

As might be expected from the AFM results, the NF comb membranes completely resisted fouling by BSA in PBS solution over 24 hour dead-end filtrations.

3.8.3. Permeability and Retention

Studies of the retention of rigid molecular probes found that size cutoff in DI water was largely independent of side chain length and temperature. By etching out PEO chains *via* acid hydrolysis of the ester linkage, or reducing the solvent quality with sodium chloride, the size cutoff of the membrane increased, and trended larger with PEO side chain length. A PEG additive also decreased the retention in concert with side chain length. Under conditions that decrease water-PEO miscibility, the retention of the PAN-*g*-PEO membranes also showed a inverse dependence on temperature. The interesting finding that the side chain length has no effect on size cutoff in DI water will be rationalized in Chapter 6.

3.8.4. Hydrolysis Resistance

Exposure to pH 2 or pH 11 conditions led to an increase in membrane permeability and loss of fouling resistance due to loss of the PEO surface brush. The results can be attributed to the hydrolysis of the ester linkage between the PEO side chains and the comb backbone.

4. Precise Size-based Separations with NF Membranes

4.1. Introduction

In Chapter 3, PAN-*g*-PEO membranes were shown to have an effective pore size independent of side chain length in DI water. Precise size-based exclusion was provided by the PEO gel within the microphase-separated morphology. In solutions with high ionic strength, the effective pore size increased proportionally to the side chain length, an effect thought to be due to the destabilization of the PEO-water system which reduces the gel density at the center of the channels. Under these conditions, the effective pore size increased to ~1.2 nm for the tightest membrane (PAN-*g*-PEO9), about 30% larger than that of the control polyamide (PA) thin-film composite NF membranes and much smaller than the PAN-400 base membrane, which retained less than 20% of all the molecular probe sizes.

In contrast, PA TFC NF membranes, which have charged and hydrolysable groups on their surface, respond to changes in pH with a change in charge (and thus electrostatic selectivity) [104]. This characteristic makes their retention properties dependent on both pH and ionic strength (due to the effect of ionic strength on Debye length [17]), which may be undesirable when filtering solutions of materials that have buffering properties or require a specific pH.

The regular nanometer-scale effective pore size and electrostatically neutral chemistry of PAN-*g*-PEO membranes make them capable of separations that may not be practical with available polymer membranes. This chapter will demonstrate this with two types of probes that are useful in current research and development: metal nanoparticles and fluorophore-labeled peptides.

4.2. Nanoparticles

Nanoparticles are gaining interest for biomedical applications and consumer products (*e.g.* titania in sunscreen), but also raising concerns about toxicity and environmental contamination [124,125]. Many of the applications of nanoparticles are highly dependent on

purity and size, which has prompted much effort to improve the purification and fractionation process. Fractionation using ultracentrifugation [126], electrophoresis [127], CO_2-pressurized solvents [128] and dead-end mode nanofiltration [56] have all been reported. A size-selective filtration step could be used to concentrate, desalt, and fractionate nanoparticles in the production stages, and also remove them effectively from wastewater. The former was demonstrated by Sweeney *et al.* using diafiltration, a continuous filtration process common in biological applications, using ultrafiltration polysulfone membranes [129]. They found that five volumes of water were sufficient to purify the ligand-coated particles to the same degree as a combination of solvent extraction, chromatography, and ultracentrifugation.

One of the stated advantages of diafiltration for the nanoparticle purification process is that the continual cross-flow of the solvent reduces concentration polarization and fouling, an important consideration for the hydrophobic membrane material. It is reasonable to expect that a PAN-*g*-PEO membrane with sufficiently large size cutoff could better fill this role due to its improved selectivity and fouling resistance.

4.2.1. Metal Colloid Retention

As a demonstration of this application, metal nanoparticle solutions were filtered through PAN-*g*-PEO45 membranes. In Figure 4.1, TEM micrographs of the feed (a & c) and permeate (b & d) of aqueous 0.7 nm and 2 nm diameter metal nanoparticle solutions are shown. Some permeation of the 0.7 nm silver particles was observed (b), as might be expected from the rigid molecular probe findings for pure water (see 3.6.1; ~0.8 nm size cutoff). Large aggregates (inset) were also observed in the permeate but not the feed. A similar analysis of 2 nm colloidal gold nanoparticles in pure water found no particles in the permeate, consistent with the molecular probe data for DI water for this membrane.

For the same 2 nm Au particles dispersed in methanol, again none were found in the permeate, despite the 2.5 times enhancement in permeability of the PAN-*g*-PEO45 membrane to methanol vs. DI water shown in Fig. 3.11. As mentioned in sec. 3.5.2, most of this difference can be accounted for by the lower viscosity of methanol compared to water. Hence the PAN-*g*-PEO45 size cutoff in methanol might remain below the nominal 2 nm diameter of the test

particles. It is also possible that concentration polarization induced particles to agglomerate before they could permeate the membrane coating.

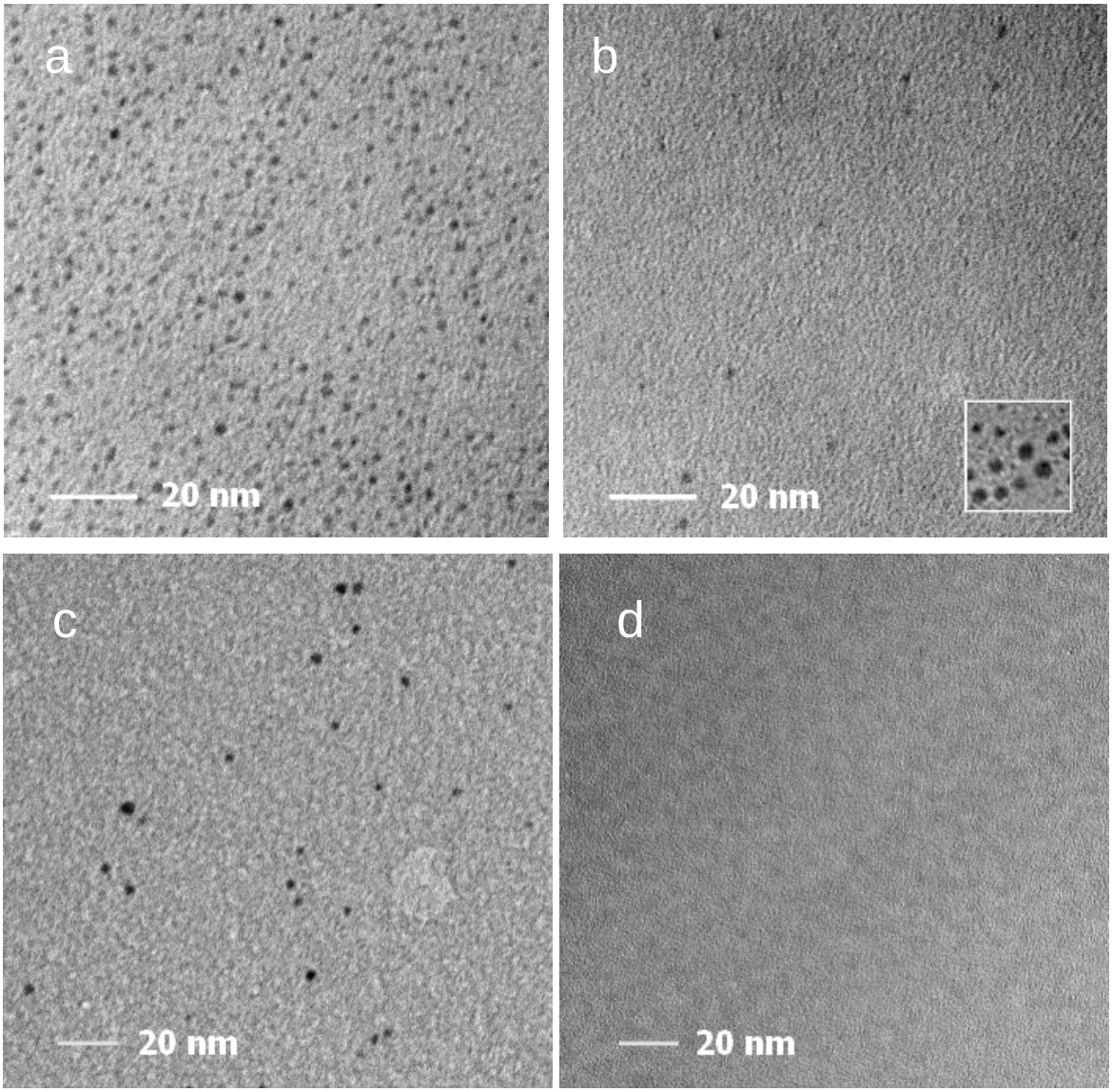

Figure 4.1. TEM micrographs of 0.7 and 2.0 nm metal nanoparticles filtered with a PAN-*g*-PEO45 membrane showing; (a) a feed solution of 0.7 nm Ag nanoparticles magnified 80,000×; (b) 0.7 nm particles in the membrane permeate, with clustered aggregates (inset); (c) a feed containing 2 nm gold nanoparticles at 68,000× magnification; (d) no 2 nm particles in the permeate; the permeation of the particles supports the assignment of a ~0.8 nm size cutoff (see 3.6.1).

4.2.2. Coated Nanoparticle Purification

To eliminate any effects of aggregation, filtration experiments were conducted on ~2 nm gold nanoparticles protected with a monolayer of 11-mercaptoundecanesulfonate and octanethiol

ligands in a 2:1 ratio [97]. These nanoparticles can be completely dried and resuspended without aggregating, and are being investigated for therapeutic use. However, the current purification procedure uses large quantities of alcohols and is time consuming. A single purification/concentration step would expedite the research and simplify adaptation to potential applications.

Figure 4.2 is an analytic ultracentrifugation trace of the feed and retentate solutions using a PAN-*g*-PEO45 NF membrane, and a Sepro NF-20 control. The only statistically significant difference is the complete elimination of the sub-nanometer peak by both membranes. However, the permeability was substantially higher, 52 LMH/MPa for the comb membrane *vs.* 10 LMH/MPa at 0.34 MPa for the control. Moreover, no decrease in permeability (fouling) was observed during the comb membrane filtration, which might be expected for polysulfone membranes due to the organic ligands in the solution. Furthermore, as will be seen in Chapter 5, the comb membrane retains little salt, making it more effective for eliminating any residual salts used in the synthesis.

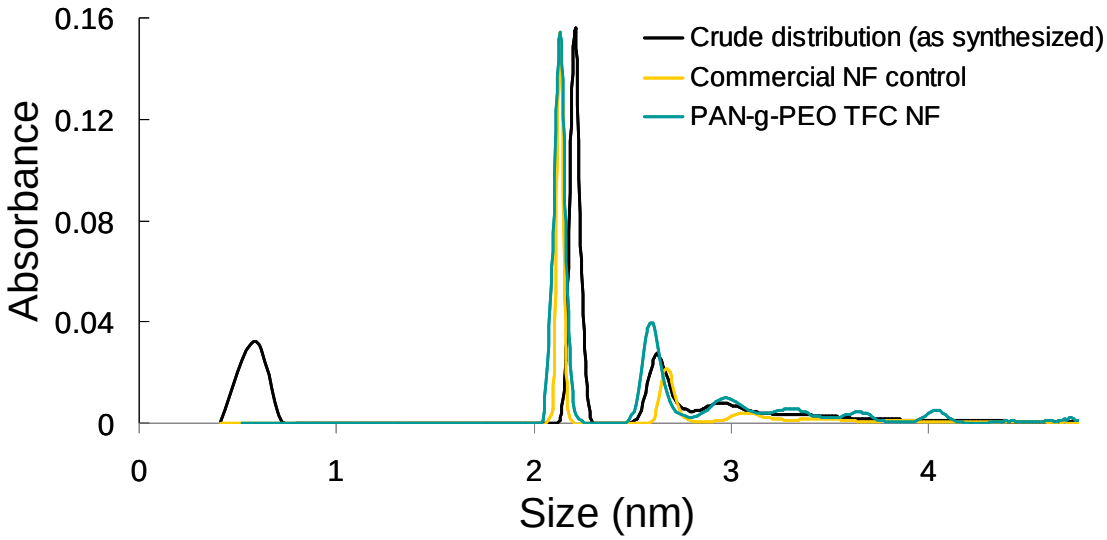

Figure 4.2. Analytic ultracentrifuge trace of a nanoparticle synthesis batch (black) and the retentates of PAN-*g*-PEO45 and NF-20 membrane filtrations; the sub-nanometer components were removed by both membranes; ultracentrifuge analysis and nanoparticles courtesy of Randy Carney (Stellacci group at MIT).

4.3. Peptides

Peptide fractionation with both inorganic [130,131] and polymeric [132] membranes has been reported. In their work to characterize the mechanism of small peptide (< 1 kilodalton (kDa)) nanofiltration using a zirconium oxide membrane, Martin-Orue *et al.* noted that the properties of the solution play a significant role and that charge effects prevail in retention. They then concluded that the number of charges in the peptide, rather than the overall charge, determines its permeation [131]. In another experiment with a ZrO_2 membrane, the retention of selective hydrosylates of β-casein ranging from 0.6 to 6 kDa was found to depend on charge and hydrophobicity [130]. Tsuru *et al.* investigated the utility of various commercial polymer NF membranes for peptide filtration and found that those with molecular weight cutoffs below 300 Da were unsuitable for the purpose [132]. Good separation of peptides was achieved with the membranes rated for 2-3 kDa based on peptide charge. By altering the pH of the solution, researchers were able to shift the retention of peptides of different isoelectric points. Each study reiterated the findings of the first: the retention of the peptides "involves mechanisms other than size exclusion" and that the charge of the membrane plays an important role [130].

Hong and Bruening demonstrated separation of individual neutral amino acids using membranes of porous alumina coated with seven bilayers of polyelectrolyte multilayers [133]. The non-electrostatic, size-based retention of the fouling-resistant comb NF membrane could make possible a rapid size-based fractionation of peptides. Such a technology could constitute an important tool in the rapidly growing field of proteomics, where the shotgun approach to protein characterization depends on rapid separation techniques for protein digests to streamline the process [134].

4.3.1 Labeled Peptide Retention

Figure 4.3 (A) shows retention vs. elution volume for six distinct peptides in 0.1 M NaCl solution filtered through a NF-20 commercial membrane. Each peptide is labeled with the fluorophore carboxytetramethylrhodamine (TMR), and the combined molecular weights of the peptides and label vary from 1.3 to 3.4 kilodaltons (kDa). After reaching steady state, the

various peptides show little difference in retention or connection between retention and molar mass, suggesting that this membrane would not be useful for peptide fractionation.

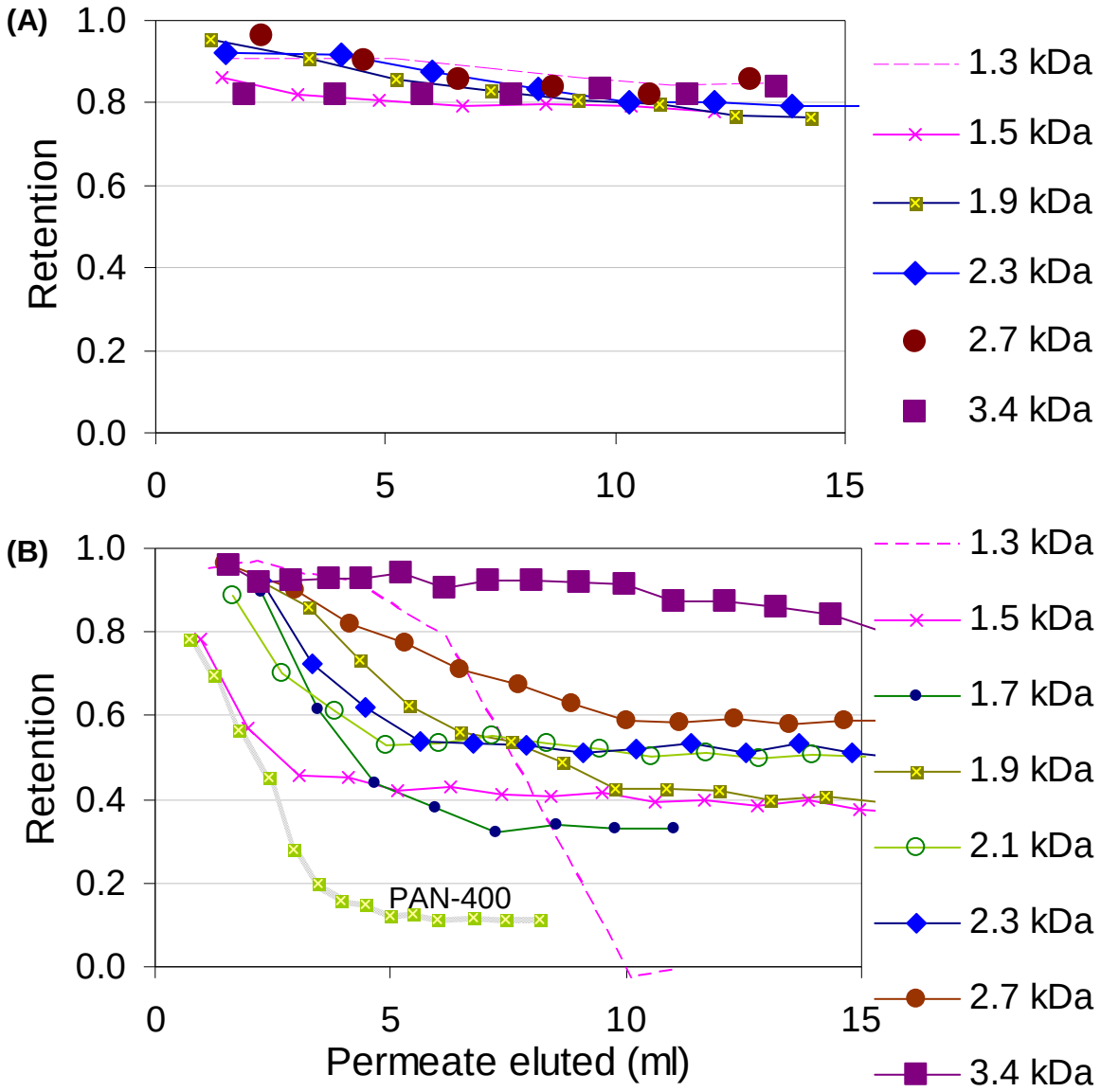

Figure 4.3. Retention of TMR-labeled peptides in 0.1 M NaCl as a function of volume eluted for (A) NF-20 and (B) PAN-*g*-PEO9 and PAN-400 (broad line) membranes shows the potential of the comb membrane for size-based separations by chromatography or conventional filtration.

By contrast, the comb NF membranes, whose pore dimensions are thought to be governed by thermodynamic considerations, show a systematic variation in steady-state retention as a function of peptide molecular weight. Figure 4.3 (B) displays retention vs. elution volume for the same peptides when filtered through the PAN-*g*-PEO9 NF membrane. At steady-state,

retentions range from 0% (1.3 kDa) to 80% (3.4 kDa). The much lower retention of the 1.9 kDa peptide by the PAN-400 base membrane is also plotted for reference.

Prior to reaching steady state rejections, the data exhibit an initial period in which the permeation of the peptides increases with filtration time. This initial period appears to increase with the size of the peptide. This can be explained by the decreased diffusivity and hindered transport of larger peptide molecules. Such differences in "ramp rate" might be exploited to conduct peptide separations chromatographically. Akthakul *et al*.demonstrated separation of two B vitamins through this approach by employing a ~500 micron thick film of PVDF-*g*-POEM as a chromatograph [53].

Figure 4.4 demonstrates the relevance of these results by plotting the peptide properties in order of increasing retention. The properties included are those previously reported to determine nanofiltration retention: overall charge, number of charged residues, and hydrophilicity [130,131]. However, the most consistent trend in the comb membrane filtration is molecular weight, which is nearly monotonic with increasing retention.

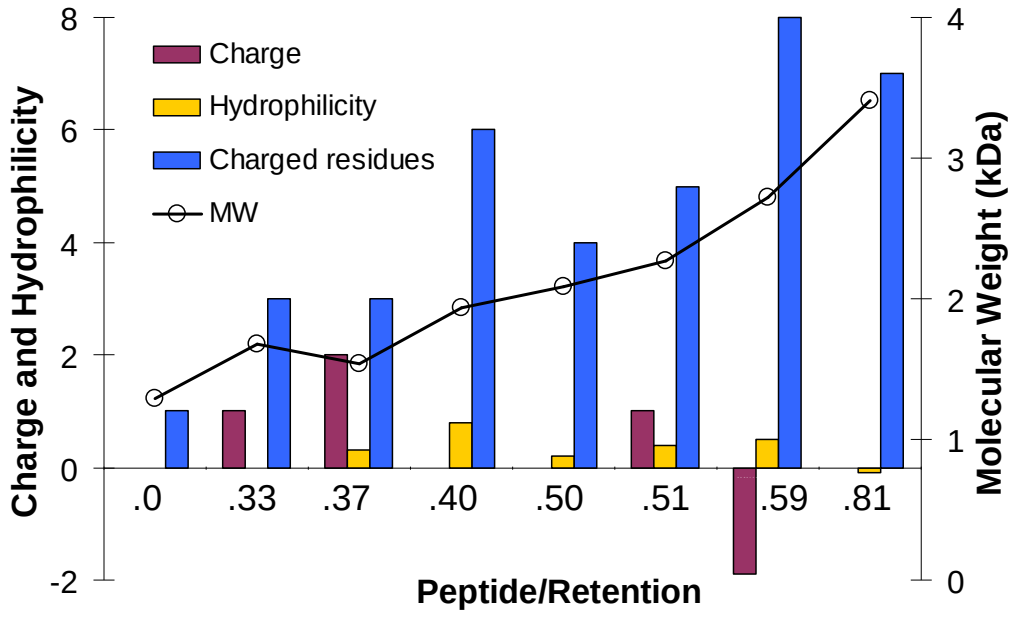

Figure 4.4. Labeled peptide properties relevant to retention ordered by increasing comb membrane retention showing a predominant molecular weight trend.

The smallest peptide filtered (1.3 kDa) did not exhibit the same asymptotic approach to steady state as the larger peptides did (Figure 4.3 (B)), but instead preferentially entered the membrane. The retentate concentration of the other peptides decreased proportionally to the increase in permeate concentration, as might be expected when peptide partitioning into the membrane is less favorable than into solution. However, the decrease in retentate concentration for the 1.3 kDa peptide progressed at a greater rate, and the overall concentration was reduced over time: under the solution conditions used, the peptide was poorly solvated.

Filtrations were performed in different conditions, and it was found that reducing the salt concentration from 100 to 17 mM produced a similar curve to the other peptides (filled circles in Figure 4.5). This finding underscores the potential importance of an NF membrane that works predominantly by a steric rather than an electrostatic mechanism: extended filtrations can be carried out without a buildup of retained salt changing the solvent conditions in the retentate (Table 4.1).

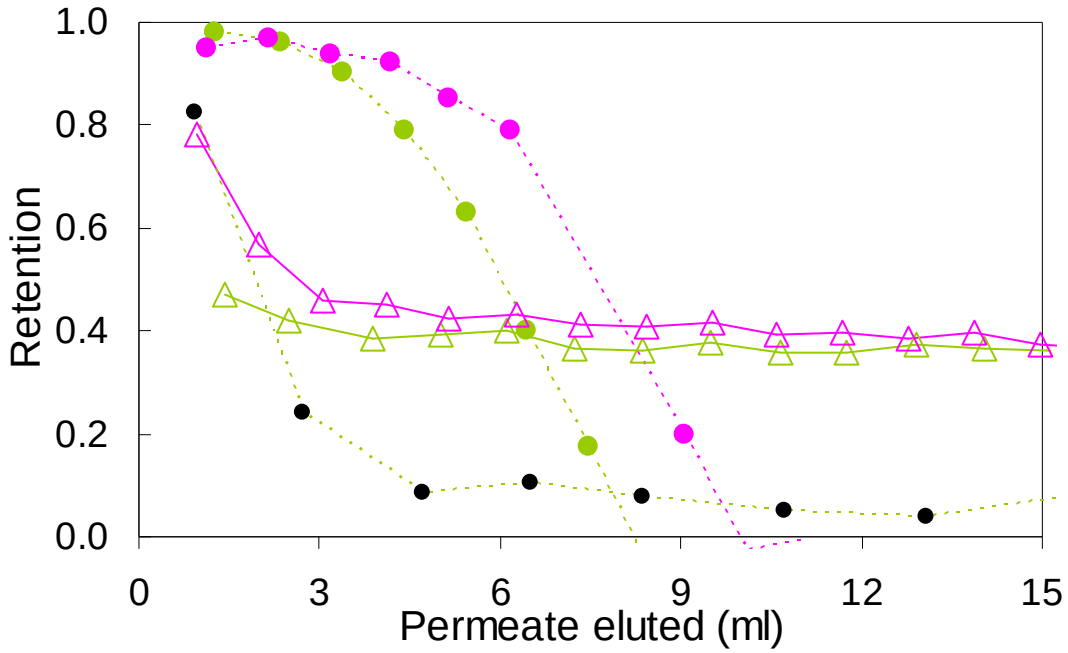

Figure 4.5. The similar FAM (green) and TMR (pink) fluorophores lead to similar retention with 1.3 kDa (●) and 1.5 kDa (Δ) peptide-label pairs; reducing the total concentration of salt to 17 mM changes the behavior of the 1.3 kDa probe (black circles).

Because the only source of possible charge in PAN-*g*-PEO selective layers is *via* limited hydrolysis of its methacrylate and nitrile groups, it only weakly retains sodium sulfate (an effect observed even in the PAN-400 base membrane) due to the divalent anion, while passing the similarly-sized but monovalent chloride ion [13][†]. In contrast, the charged NF-20 membrane retains most sodium sulfate and a measurable amount of sodium chloride.

Table 4.1. Properties of membranes used in peptide filtration experiments.

Membrane Type	**Permeability[*] (LMH/MPa)**	**NaCl Retention[*]**	**Na_2SO_4 Retention[*]**
NF20	11 ± 2	0.10 ± 0.02	0.91 ± 0.03
PAN-*g*-PEO9	50 ± 5	0.01 ± 0.01	0.20 ± 0.05
PAN-400	2300 ± 400	0.00 ± 0.01	0.06 ± 0.01

[*] 1g/L solutions at 0.34 MPa for NF membranes and 0.03 MPa for PAN-400

In preparation for a separation experiment, the retentions of peptides labeled with two different fluorophores were compared. In Figure 4.4, two peptides with either the pink 5-TMR (Figure 4.6 (A)) or green 5-FAM (Figure 4.6 (B)) fluorophore—which are of very similar size—are seen to have similar retention, with slightly higher retention of the larger TMR pairs.

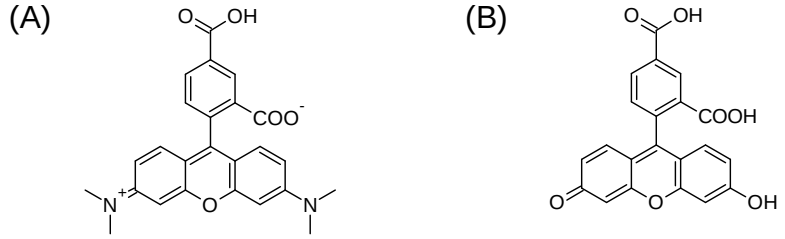

Figure 4.6. A comparison of the structure of the two fluorophore peptide labels showing (A) 5-carboxytetramethylrhodamine (TMR) and (B) 5-carboxyfluorescein (FAM).

4.3.2 Labeled Peptide Fractionation

The systematic variations in retention with peptide molecular weight, thought to arise from the well-defined pore dimensions of comparable size to the peptides, can be exploited to separate peptides by multiple filtrations. To demonstrate this effect, a fractionation (Figure 4.7) was conducted on a FAM-labeled 1.5 kDa peptide and a 1.3 kDa TMR-labeled peptide (Fig. 4.8) in 0.1 M NaCl. The absorbance curves of these labeled peptides are the solid curves

[†] See section 5.1.1 for a discussion of the preferential retention of salts by charged membranes.

on the left (FAM-labeled peptide) and right (TMR-labeled peptide). The dotted curves (a & b) are the absorbances of the retentate and permeate, respectively, from the second filtration generation (Fig. 4.7). After the two filtrations, the ratio of 1.5kDa to 1.3kDa peptide in the retentate (Fig. 4.7 (a)) had increased 6-fold, while the 1.3 kDa to 1.5 kDa ratio in the permeate was found to be 1.5. This is consistent with a retention of 0.28 and 0.11 for the 1.5 kDa and 1.3 kDa peptides, respectively, in the joint filtration conditions. Alternatively, taking the measured retention of 1.5 kDa peptide as 0.37 from the individual filtrations (Figure 4.3), the retention of the erratic 1.3 kDa peptide was 0.15 and the permeation 0.77 (with the difference due to peptide sequestration in the membrane).

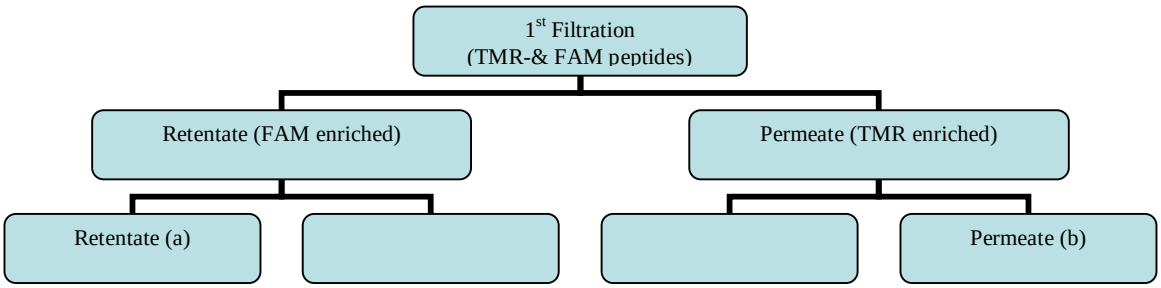

Figure 4.7. Schematic of the peptide filtration

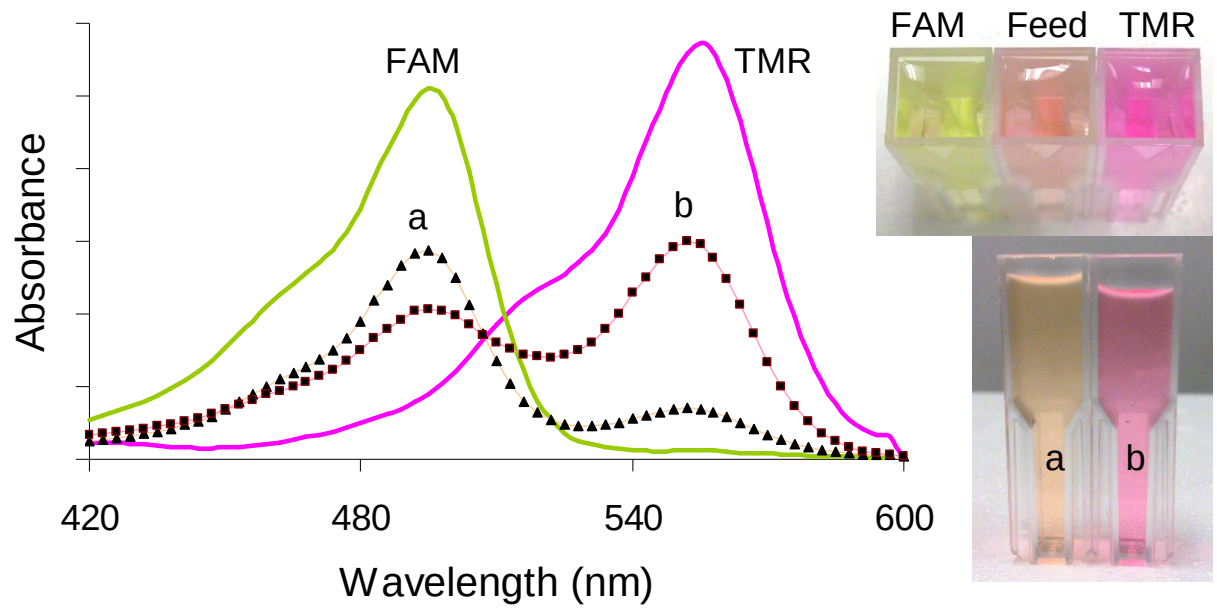

Figure 4.8. Separation of 1.3 kDa and 1.5 kDa peptides *via* PAN-*g*-PEO9 comb membrane filtration: solid curves are absorbances of the pure peptides with their respective FAM and TMR label; fractions from the second generation of filtration (a & b as in Fig. 4.7) contain predominantly one peptide.

4.4. Conclusion

In this chapter, two important materials that overlap the nano- and ultrafiltration realms were filtered with PAN-*g*-PEO membranes. The PAN-g-PEO45 membrane was found to transmit 0.7 nm nanoparticles and retain 2 nm nanoparticles in water, supporting the assignment of a size cutoff > 0.8 nm in Chapter 3. In addition, the membrane was able to quickly purify ligand-coated gold nanoparticles from a synthesis batch by removing all sub-nanometer components. The fouling resistance of the membrane makes it a promising replacement for hydrophobic UF membranes proposed for this role [129].

The peptide properties reported in the literature to be important determinants of retention were hydrophobicity, net charge, and number of charged residues [130-132]. A range of fluorophore-labeled peptides from 1.3 to 3.4 kDa were filtered with PAN-*g*-PEO9. In different sequences these ranged from a hydrophobicity of -0.8 to 0.8 on the Hopp-Woods scale, from 1 to 8 charged residues, and from -2 to 2 net charge, yet the magnitude of their transmission through the membrane followed directly their molecular weight. This is in contrast with the findings of previous studies, and attributable to the uncharged membrane selective layer and regularity of the microphase separated nanochannels. The follow-up demonstration of significant fractionation of two of the peptides *via* two filtration stages confirms that the membrane could potentially replace current batch separation methods used for peptide separation, such as gel electrophoresis and chromatography. When used in combination with charged membranes, peptide mixtures could be fractionated based on both size and isoelectric point, an arrangement described as ideal in a recent review of the field [135].

5. Charge Effects in Amphiphilic Graft Polymer Nanofiltration Membranes

5.1. Introduction

Previous chapters have focused on the size-selective capability of PAN-*g*-PEO membranes and the application possibilities of such membranes. The combination of fouling resistance and ~1 nm regular pores makes fractionations possible that cannot be achieved with conventional polyamide TFC membranes. This demonstration of control over the steric aspect of NF membrane selectivity raises an obvious question: can the electrostatic contribution of the PAN-*g*-PEO membrane selectivity also be controlled? This chapter reports the effects of incorporating fixed negative charges or strong charge polarity into the PAN-*g*-PEO comb.

5.1.1. Desalination Membranes

Polymer membranes have been used for desalination since the Loeb-Sourirajan process made them economically viable (1.3). They eventually differentiated into reverse osmosis (RO) and NF membranes with different aims. RO membranes aim to remove all solutes from the feed; NF membranes preferentially remove certain salts and charged solutes and remove neutral solutes by their size [136]. Full RO is possible when the selective layer has an effective size cutoff below the hydrated radius of even the small chloride ion (0.33 nm [13]); NF membrane desalination works principally by the electrostatic equilibrium principle described by Donnan [137]. Like-charged ions are repulsed by the charged membrane surface, and the counterions are retained due to the energetic cost of charge separation. The Donnan theory provides an idealized expression for the retention of point-charge ions by a charged membrane [17]:

$$R = 1 - \left(\frac{|z_i| c_i}{|z_i| c_i^m + c_x^m} \right)^{|z_i / z_j|} \tag{6}$$

where c_i and c_i^m are the concentrations of like-charged ions in the solution and membrane, c_x^m is the membrane charge concentration, and z is the formal charge of the ion; the j subscript

indicates the counterions. Two of the consequences of this electrostatic retention of ions are that multivalent ions are much more susceptible to exclusion, which is the basis for NF use to separate salts. The relevance of this model to charged PEO comb membranes will be addressed presently.

5.1.2. Developments in Reverse Osmosis Desalination

The water sustainability issue and ready availability of seawater has stimulated research on improved reverse osmosis membrane materials. The problem of fast, exclusive osmotic transport of water was solved by Nature long ago, and the initial exploitation of this was explored by Kumar *et al.* by embedding Aquaporin Z membrane proteins into polymeric vesicles [68]. By measuring the change in size of the vesicles in response to osmotic shock, the researchers were able to calculate that the membranes had a water permeability of ~6,000 L/m^2hMPa, roughly two orders of magnitude better than the ~60 L/m^2hMPa possible with existing RO membranes [9]. In another innovative approach by Zhou *et al.*, lyotropic liquid crystals were cross-linked to leave ~0.75 nm pores which excluded most salts and small molecules [16]. The 40 μm membrane had a thickness-normalized permeability comparable to that of available RO membranes (using an approximation of RO membrane active layer thickness of 0.1 μm).

5.1.3. Novel Nanofiltration Desalination Membranes

The large pore size of PAN-*g*-PEO precludes its use for RO, as it cannot exclude simple salts by size exclusion. Other experimental desalination membranes have been reported that are more directly relevant and comparable. Fornasiero *et al.* formed a membrane from aligned double-walled carbon nanotubes ~1.6 nm wide with negative charges at the entrance and carefully characterized its salt retention properties [17]. They used the retention of salts of different valences, sizes and concentrations to determine the predominant mechanism of salt exclusion. The good agreement of their results with the predictions of the Donnan theory (Equation 6) led them to conclude that the salt retention by the nanotube membranes is predominantly due to electrostatic effects. According to the authors, charges near the opening of the nanotubes effectively exclude ions as long as the Debye length of the solution is at least on the order of the diameter of the nanotubes. As the salt concentration increases, the

increasing ionic strength decreases the Debye length until it is smaller than the charged pore diameter, at which point the retention of the ion rapidly decreases.

Interesting analogies may be drawn between the features resulting in charge exclusion from nanotube membranes and the expected morphology of charged PEO comb membranes, shown schematically in Fig. 5.1. The mechanism of electrostatic salt retention in a charged, microphase separated PEO comb membrane (Figure 5.1) would be expected to work in a similar manner due to the separation of the hydrophobic backbone (and connected charged moieties) from the PEO domain, which conveys the water and solutes.

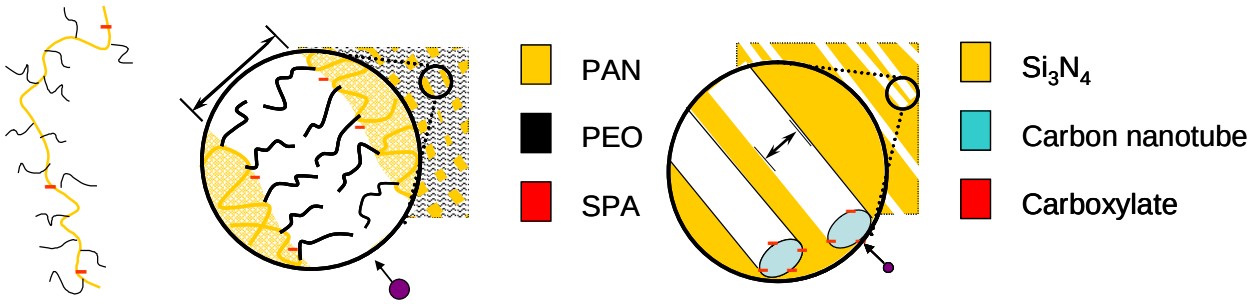

Figure 5.1. Conceptual comparison of P(AN-*r*-SPA)-*g*-PEO) chain and membrane (left) and aligned carbon nanotube membranes (right) showing the displacement of charges from the pore volume; the microphase separation of the comb terpolymer leads to PEO domains surrounded by PAN, with sulfonate charges (SPA) confined to the PAN/PEO-water interface due to their short tether (a propyl group) and attraction to water.

A membrane design more similar to the PAN-*g*-PEO membranes was reported by Koh *et al.*, who "grafted from" a chlorofluoronated polymer backbone with poly(styrene sulfonic acid) (PSSA) to 47 wt.%. They coated a PVDF UF membrane with a 2 µm layer of the resulting microphase-separated copolymer [138] and found that the rejection of salts followed the order predicted by the Donnan model. At a pressure of 0.3 MPa, the membrane retained 83% Na_2SO_4 and 28% NaCl with permeabilities of 60 and 107 LMH/MPa. This membrane will serve as a benchmark for comparison with terpolymer membranes but, because fouling was not addressed, no comparisons can be made of that important aspect.

Studies of fouling on TFC NF membranes are common [24,26,27,36,139] because of the complexity of the problem. Increases in both membrane charge and hydrophobicity can

promote fouling, and it was seen in Chapter 3 that even the very hydrophilic NF-20 membrane was slightly fouled during the 24 hour BSA filtration.

5.2. Terpolymer Comb Membranes

Chapter 2.4 described the synthesis and properties of terpolymers of acrylonitrile, poly(oxyethylene) methacrylate, and a third monomer consisting of a charged group and short tether. That third monomer was either sulfopropyl acrylate (SPA), with a negatively-charged sulfonate group, or *N*,*N*-dimethyl-*N*-(2-methacryloyloxyethyl-*N*-(3-sulfopropyl) ammonium betaine) (SPE), which balances the negative charge of the terminal sulfonate with a quaternary ammonium in the middle of the side chain. Thus, these terpolymers are either negatively charged, or neutral with polar, hydrophilic groups complementing the PEO side chains. Comparison of the selectivity of thin-film composite membranes formed by coating PAN-400 with these terpolymers or the PAN-*g*-PEO copolymer will reveal the effects of charge in the selective layer.

Table 5.1. Amphiphilic Graft Terpolymer and Membrane Properties

Side chain EO units	**Wt. % PEO***	**Wt. % SPA/SPE***	**Permeability† (LMH/MPa) (± 10%)**	**0.1% Na_2SO_4 Retention† (± 0.03)**	**0.1% NaCl Retention† (± 0.02)**
P(AN-*r*-SPA)-*g*-PEO					
9	36	1	50	0.76	0.07
9	46	2	39	0.82	0.09
45	47	1	22	0.72	0.04
P(AN-*r*-SPE)-*g*-PEO					
9	40	5	20	0.46	.02
45	50	4	38	0.40	.01

* ^{1}H NMR; † At 0.34 MPa; reported error is largest std. dev. for the sample set

5.2.1. Salt Retention

Table 5.1 lists the properties of the terpolymer membranes. It can be seen that incorporating even a small quantity of charged groups (SPA) greatly increases the sodium sulfate and sodium chloride retention (compare with 0.2 and 0.01 retention, respectively, for PAN-*g*-PEO

(Table 4.1)). The addition of the polar, zwitterionic SPE has a smaller, but still measurable impact. The desalination properties of each category of membrane tested are summarized in Figure 5.2. The composite plot includes averages of three measurements from one coupon of each of the PAN-*g*-PEO membranes, the three SPA terpolymers, and the two SPE terpolymer membranes, as well as the two controls.

The most salt-retentive terpolymer membrane had 82% retention of sodium sulfate at 1 g/L and 0.34 MPa. The pure water permeability of 39 LMH/MPa was reduced by 16% during that filtration, very nearly equal to reduction in effective transmembrane pressure due to osmotic effects (~13%). It was reduced by 4% while removing 9% of the NaCl (~2% by osmotic pressure). This performance is similar to the 47 wt.% PSSA copolymer membrane reported by Koh *et al.* described earlier [138]. With its much higher concentration of charged groups, that membrane retained 83% of the same sodium sulfate solution at 0.3 MPa, with a permeability of 60 LMH/MPa.

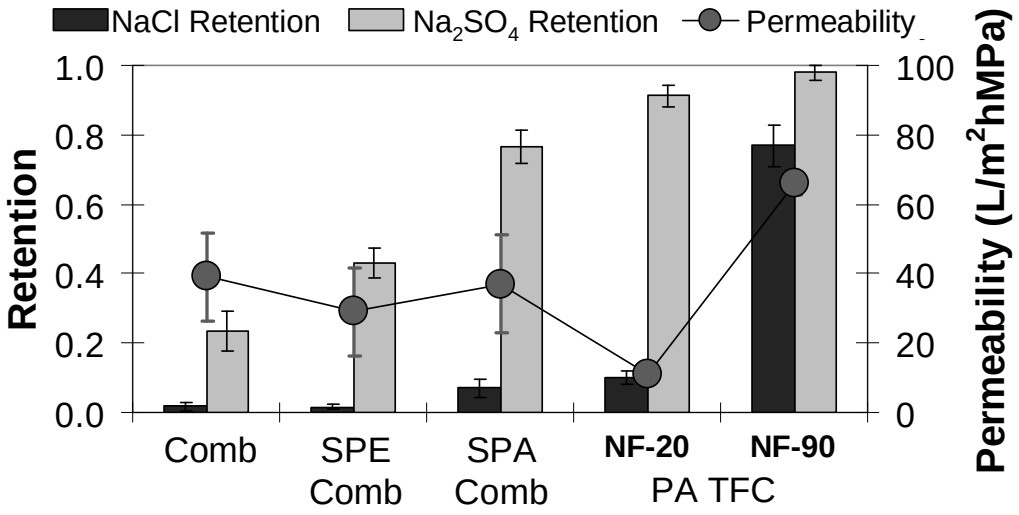

Figure 5.2. The composite salt retention (bars) and DI water permeability (circles) of PAN-*g*-PEO comb membrane, P(AN-*r*-SPE)-*g*-PEO comb membrane, P(AN-*r*-SPA)-*g*-PEO comb membrane, and the two PA TFC control membranes (NF-20 & NF-90) showing the increase in salt retention with charge on the comb membranes.

The membranes differ much more in their retention of sodium chloride, which was three times higher for the PSSA membrane than the terpolymer membrane (28% vs. 9%). This may be accounted for by the higher charge density of the PSSA membrane.

The performance of desalination membranes can often be improved by increasing the pressure, due to preferential partitioning and competitive contributions of diffusion and convection to the retention. To evaluate the effect of increased flux on the salt retention of the P(AN-*r*-SPA)-*g*-PEO9 membrane, it was subjected to higher transmembrane pressures (Figure 5.3). Although the salt retention was increased, the solvent permeation decreased much more than the increased osmotic pressure can explain (from 34 to 29 LMH/MPa with Na_2SO_4) for the terpolymer membrane, most likely due to compaction of the PAN-400 base membrane. The NF-20 membrane's permeability increased from 11 to 12 LMH/MPa over the same interval.

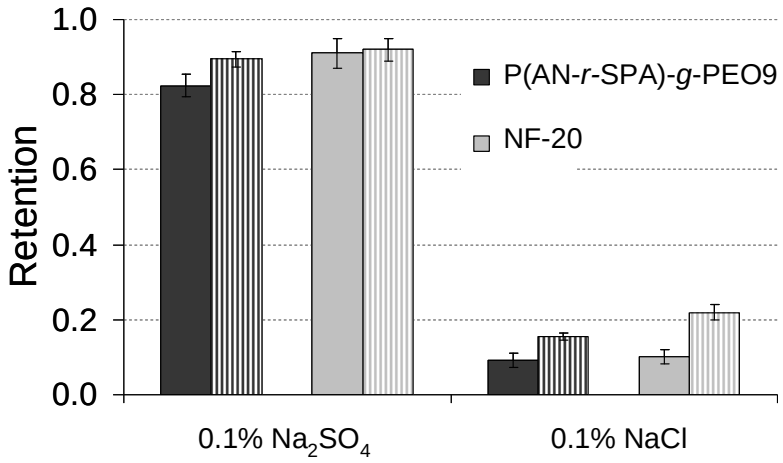

Figure 5.3. Pressure-dependent salt retention of NF membranes showing an increase in retention of Na_2SO_4 for P(AN-*r*-SPA)-*g*-PEO membrane (black bars) from 0.82 at 0.34 MPa (solid bar) to 0.89 at 1 MPa (striped bar), and a similar increase from 0.09 to 0.16 NaCl retention; NF-20 (grey bars) salt retentions were 0.92 and 0.21 at 1 MPa for Na_2SO_4 and NaCl, respectively.

5.2.2. Permeability

Due to the high PEO content of the comb copolymers, little improvement was expected in permeability due to additional hydrophilic groups. As expected, the permeability of the terpolymer membranes was similar to the comb copolymer membranes: permeabilities from 15-50 LMH/MPa were measured. The average thickness-normalized permeability was calculated for P(AN-*r*-SPA)-*g*-PEO9 (46 wt.% PEO) and P(AN-*r*-SPA)-*g*-PEO45 (using average coating thickness estimated from ESEM images) as 64 and 70 LMH-μm/MPa, respectively. This compares favorably to the ~1 and ~8 LMH-μm/MPa, NF-20 and NF-90. Using the reported thickness of 2 μm for the PSSA copolymer membranes by Koh *et al.*, the

thickness normalized pure water permeability of that membrane was over 200 LMH-μm/MPa, (estimated because pure water permeability was not reported).

Unlike the PAN-*g*-PEO comb membranes, which varied little in permeability or retention after 48 hours in the water coagulation bath, the terpolymer membranes exhibited a long-term increase in permeability and concurrent decrease in salt retention (approximately 100% increase in permeability and 10% decrease in Na_2SO_4 retention over the first month). This process begins when the comb is first immersed in water in the coating process, and can be delayed by storing the TFC membrane in the isopropanol bath. One potential mechanism for this phenomenon is a slow approach to the equilibrium swelling state in response to the expansion forces applied by the good solvent for PEO (water) and mutual repulsion of the charged SPA groups. The large population of very long chains in the terpolymers (MW 400-500 kg/mol and PDI ~4; Table 2.2) compared to the copolymers (200-300 kg/mol and PDI ~ 2; Table 2.1) would prolong this process.

5.2.3. Fouling Resistance

When challenged with the BSA model foulant solution, two types of behavior were observed (Figure 5.4). The P(AN-*r*-SPA)-*g*-PEO membrane with 36 wt.% PEO (circles) had a small irreversible decrease in permeability. The SPA comb membranes with higher PEO content, represented by the 46 wt.% P(AN-*r*-SPA)-*g*-PEO9 (triangles), and the P(AN-*r*-SPE)-*g*-PEO membranes (squares) have a decrease in permeability that is slowly recovered after the DI water feed resumes. The delayed recovery is likely a result of a more tightly adhered cake fouling layer (due to the charged surface) compared with membranes coated with the PAN-*g*-PEO copolymer. Because the residual foulant molecules are only weakly adsorbed to the surface, they are eventually released when immersed in DI water and subjected to the motion of the PEO brush and shear forces from the stirring. As in the case of the copolymer comb, all the membranes completely retained BSA after three hours filtration.

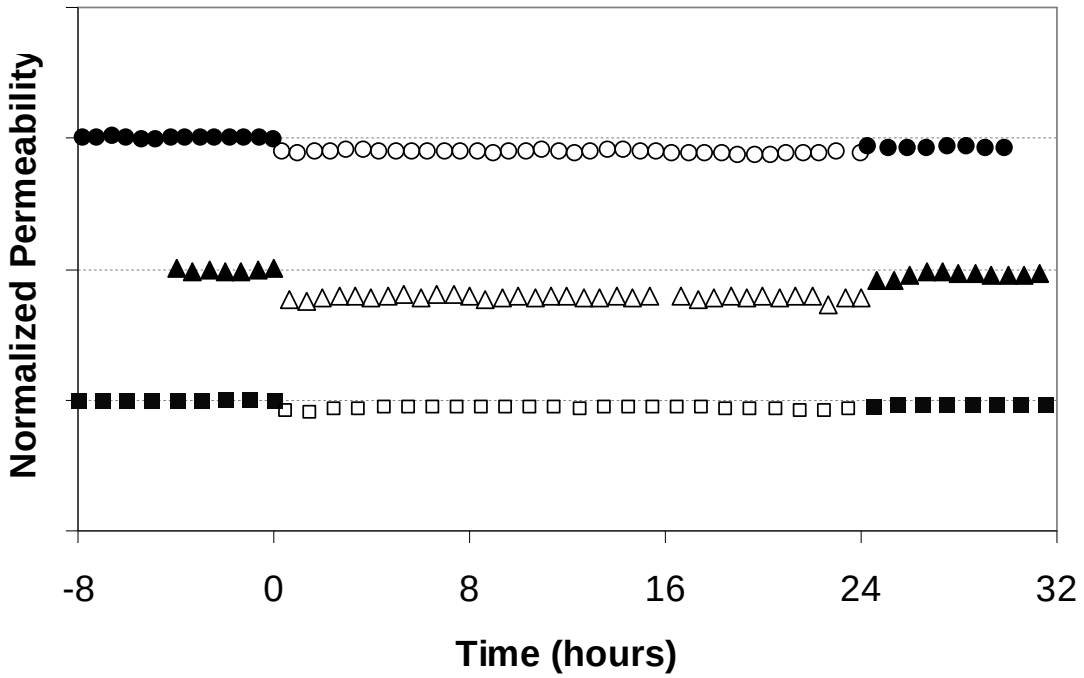

Figure 5.4. The dead-end filtration of 1 g/L BSA solution (open symbols) and deionized water (filled symbols) through terpolymer NF membranes with permeability normalized by the initial pure water permeability showing a 3% loss of permeability in the 36 wt.% PEO P(AN-*r*-SPA)-*g*-PEO membrane (circles); a 5% permeability loss quickly recovered to 2% for the 46 wt.% PEO P(AN-*r*-SPA)-*g*-PEO membrane (triangles); a 5% loss in permeability in the SPE comb membranes followed by gradual recovery to 2% within six hours (squares). BSA retention, R_{BSA}=1.0.

5.3. Double Layer Membranes

In order to shield the electrostatically active layer of the P(AN-*r*-SPA)-*g*-PEO membrane from the foulants in solution, a TFC membrane was made with two coatings of comb polymer (Table 5.2). The first layer was the 36 wt.% PEO SPA terpolymer, followed by a layer of PAN-*g*-PEO45 (Table 3.1). A portion of the membrane was left with only the first coating to better compare the results.

As is seen in Table 5.2, two sequential copolymer coatings can be performed without adversely affecting the membrane properties. The second layer, (PAN-*g*-PEO45) did not increase the salt retention of the membrane at the same pressure, but did decrease the permeability by approximately 50%. Considering the high permeability of the PAN-400 base membrane, this is a reasonable outcome for two equally thick resistors to flux in series.

Table 5.2 Double Layer Membrane Properties

Active Layer	Permeability (LMH/MPa)*	0.1% Na_2SO_4 Retention*	0.1% NaCl Retention*
P(AN-*r*-SPA)-*g*-PEO9	44 ± 3	0.72 ± 0.03	0.07 ± 0.02
PAN-*g*-PEO45 / P(AN-*r*-SPA)-*g*-PEO9	21 ± 2	0.72 ± 0.04	0.05 ± 0.02

* At 0.34 MPa; three separate measurements of one coupon from each membrane.

When used to filter BSA for a 24-hour fouling experiment, the membrane with both layers was found to experience less fouling compared to the single charged layer, but did not completely prevent it. This may be due to imperfect coverage of the second coating, and warrants further investigation.

5.4. Conclusion

The salt retention of PEO comb polymer membranes, especially of the divalent sulfate ion, was much increased by incorporating a small fraction (2 %) of fixed negative charges into the polymer composition *via* charged monomers. Incorporating 5% zwitterionic monomers also enhanced the Na_2SO_4 retention to a lesser degree.

Although the membranes were found to be reduced in permeability by exposure to BSA solution, the degree of fouling was less than for either PA TFC commercial membrane and was gradually, largely recovered for the higher PEO-content terpolymers.

A double coating was made using an uncharged comb on top of a charged terpolymer. The double coated membrane had the same salt retention and improved fouling resistance over the membrane coated only with terpolymer. Additional experiments are needed to explore the utility and effectiveness of this approach.

The membranes had high (divalent) sodium sulfate selectivity compared to sodium chloride, presumably due to the inherently low charge density of the membranes.

As was expected from the ~1 nm pore size of PAN-*g*-PEO membranes, reverse osmosis type salt exclusion was not achieved. Instead, adding charge to the selective layer by incorporating a small fraction of sulfopropyl acrylate in the comb polymer synthesis produces a terpolymer that makes desalination membranes similar to NF-20 in salt retention and permeability, along with excellent fouling resistance. PEO comb terpolymer membranes optimized for charge content and active layer thickness could potentially be competitive for water softening and applications where salt specificity is an asset.

6. Summary and Conclusions

This thesis has presented further studies of the properties of amphiphilic graft copolymer membranes that were developed in this laboratory. Previous studies explored ultrafiltration and nanofiltration membranes composed of variations on a PEO macromonomer theme, with poly(methyl methacrylate) [60,140], poly(vinylidene fluoride) [54,53,56,57,59,79], polysulfone [141] and polyacrylonitrile (PAN) [55,58] as the rigid structural backbone component. The most recent evolution, PAN-*g*-PEO, has the desirable properties of facile synthesis involving inexpensive materials. The excellent fouling resistance and permeability of PAN/PAN-*g*-PEO UF membranes inspired the creation of a start-up company, Clean Membranes, to seek to commoditize them.

6.1. Findings

6.1.1. The Questions

The promise of PAN-*g*-PEO as a membrane material raises questions worthy of pursuit:

- Can the size- and charge-selective properties of the membranes be controlled?
- Do the resulting membranes have fouling resistant properties?
- What applications might the membranes have?

It was with these questions that this work commenced.

6.1.2. Controlling Size Cutoff

In Chapter 3, control over the steric portion of membrane selectivity was achieved by two methods—variation of side chain length and inclusion of a PEG additive—but with a caveat: to truly differentiate the effective pore size of the membranes prepared by the methods reported here, the PEO-water gel must be destabilized, *e.g.*, by increasing the ionic strength of the feed. This surprising result may diminish the utility of the size control, but invites further exploration of membrane coating and additive parameters to qualify. For example, changing the solvent quality of the casting solution or the properties of the nonsolvent used in the

coagulation bath might change the size of the PEO domains formed when precipitating out of solution.

6.1.2 Understanding PAN-g-PEO Membrane Size Selectivity

The simple model of PEO domain width as the determinant of membrane size cutoff presented in Chapter 3 cannot explain the molecular probe filtration findings: (1) size cutoff is independent of comb side-chain length in good solvent conditions for PEO; (2) when the solvent quality is reduced by the addition of 0.2 M NaCl, retention becomes a function of side chain length. To possibly account for these observations, it is useful to develop a model of the microphase morphology adopted by the amphiphilic comb coating. A schematic illustration of the coating morphology is presented in Figure 6.1, where the glassy PAN domains (rust) form a rigid network onto which swollen PEO chains (black) are anchored at some average spacing ξ.

Microphase separation of the comb's backbone and randomly-spaced side chains results in a quasi-periodic bicontinuous morphology with hydrophilic domains of an average size given by *D*. The magnitude of *D* is a strong function of the number of EO segments per side-chain, *n*, as well as the solvent content. From ESEM studies in section 3.3.1, the coating thickness appears to be fixed during its formation, when it is precipitated in isopropanol and subsequently transferred to DI water. To estimate *D*, we might therefore assume a water content associated with the equilibrium brush structure, as measured by the swelling ratios reported in Table 3.1. Permeation of solutes through the selective layer coating is absolutely limited by the boundaries of the hydrophilic domains (*i.e.* the domain size *D*).

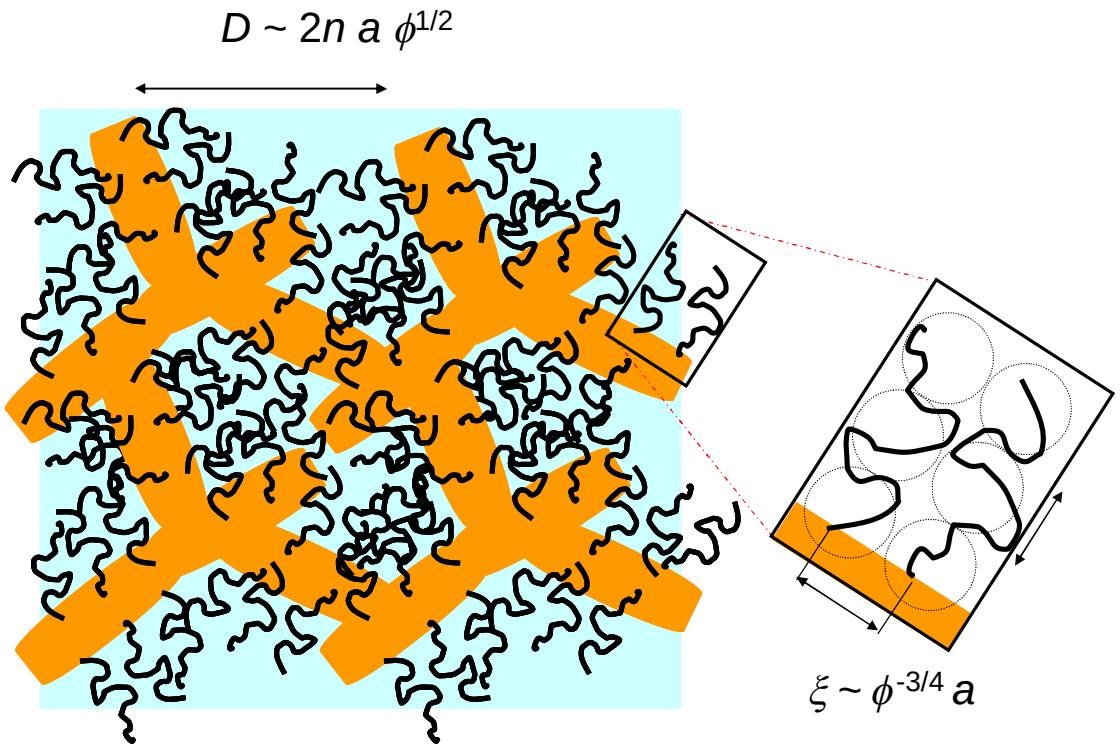

Figure 6.1. A schematic illustration of the bicontinuous PAN-*g*-PEO*n* comb morphology in good solvent conditions showing two length scales of size exclusion: the nanochannel width (*D)* bounded by glassy PAN (rust) domains established during membrane casting; and the mesh size ξ, which characterizes the physical gel created within the hydrophilic domains due to the high packing density of grafted PEO chains on the PAN surface.

In addition to this hard limitation, however, the swollen PEO chains within the hydrophilic domains also act as a size-selective barrier. The effective obstruction posed by the PEO gel depends on the mesh size, or characteristic distance between chains, ξ. [142] Following the scaling model of Alexander and DeGennes, ξ for the PEO brush is a function of polymer volume fraction ϕ_{PEO} :

$$\xi \cong a\phi_{PEO}^{-3/4} \tag{7}$$

where a = 0.35 nm [119] is the EO segment length. We approximate the PEO domain width as that of two opposing, contacting brushes [119] (*i.e.* $D = 2L$, where L is the Alexander-DeGennes brush height):

$$D \cong 2na\phi_{PEO}^{1/2} \tag{8}$$

Using values of ϕ_{PEO} calculated from the swelling data in Table 3.1, along with the known values of n for the various PAN-*g*-PEO copolymers, estimates can be made for D and ξ. Comparison of the tabulated values for the combs (Table 6.1) reveals similar mesh sizes for all of the combs, qualitatively consistent with the probe filtration results for DI water, which gave a size cutoff in the 1 nm range, independent of side-chain length.

When salt is added to the solution, the reduction in solvent quality reduces the brush height proportionately to side chain length [143], opening the hydrophilic domains, whose size is fixed by the neighboring PAN domains, to the passage of larger molecules. For the PAN-*g*-PEO9 NF membrane, the shift in cutoff size of ~0.4 nm represents a small collapse of the brush, causing a shift from mesh- to microphase-based size selectivity. Although the cutoff size for the PAN-*g*-PEO23 and PAN-*g*-PEO45 membranes in 0.2 M NaCl fell outside the range of probe molecule sizes investigated here, Akthakul *et al.* reported nanoparticle size cutoffs in the range of 3-4 nm for PVDF-*g*-POEM23 NF membranes in organic solvents which were shown to swell the comb much less than water [56,101]. Consequently, the effective pore size is closer to the theoretical maximum, d_{max}, calculated by subtracting the PEO hard-core volume from the swollen domain volume, as reported in Table 6.1.

Table 6.1. Estimates of PEO mesh size and domain size for PAN-*g*-PEO combs

Comb	n	ϕ_{PEO}	ξ **(nm)**	D **(nm)**	d_{max} **(nm)***
PAN-*g*-PEO9 (38%)	9	0.21	1.1	2.9	2.7
PAN-*g*-PEO9 (44%)	9	0.19	1.2	2.8	2.6
PAN-*g*-PEO22	22	0.13	1.7	5.5	5.3
PAN-*g*-PEO40	40	0.15	1.5	10.8	10.2

* Void size created within hydrophilic domains by PEO collapse to bulk density.

6.1.3. Applications

Even with the limitations in effective pore size, applications could benefit from the improved water permeability possible with longer side chains and PEG additives. Even in low ionic strength solution, the ~1 nm effective pore size of PAN-*g*-PEO membranes means they occupy the open niche of larger uncharged NF membranes. The ability to separate peptides by

size, in spite of the differences in hydrophobicity and charge (Chapter 4), is a specific demonstration of the possibilities. There are also filtration processes carried out in saline or aliphatic solvent conditions that could directly employ the control of size cutoff.

6.1.4. Fouling Resistance

The fouling resistance of the membranes investigated here is good, but may be reduced somewhat from the acrylate-based PAN-*g*-PEO9 reported previously, particularly for the shorter side chains. Whether this is due to the decreased hydrophilicity of POEM-based (methacrylate) comb or architectural differences (*e.g.* due to differences in monomer reactivities) is not clear; however, it appears that a higher fraction of PEO is needed in the POEM-based PAN-*g*-PEO to maximize fouling-resistant properties. This difference was seen in the bacterial adhesion and AFM experiments, but not the BSA filtration experiments.

In any case, the ready availability of POEM was the main reason for its use. The approach used here for controlling the size cutoff with side chain length should be equally valid with acrylate PEO macromonomers. It has also been demonstrated using a different backbone (PVDF) [53,56], and may be possible with others. The ability of the resulting membranes to resist fouling is another matter: PMMA-*g*-PEO, one of the PEO combs studied previously by our group, was shown to provide incomplete fouling resistance when used as a surface-segregating additive in PVDF UF membranes [60].

6.1.5. pH Stability

Because exposure to acidic (pH 2) or basic (pH 11) conditions changes the membrane properties and greatly reduces its antifouling character, PAN-*g*-PEO membranes are best used in systems that have no other components with a susceptibility to fouling, or as a prefilter for such components [4]. Acid hydrolysis of the ester linkages of the PEO side chains opens up the effective pore size (Figure 3.18), which could be due to both increased mesh size due to a reduction in graft density and a partal opening of the domain center by the resulting decrease in brush height, thus allowing the domain size to play a role.

6.1.6. Controlling Charge Selectivity

Adding a small fraction of charge to the comb (Chapter 5) gave salt retention capability comparable to current commercial nanofiltration membranes. Both the fouling behavior and salt retention of this terpolymer membrane is similar to that of the NF-20 control membrane. The much more effective desalination control (NF-90) did not perform as well in fouling resistance.

6.2. Prospective

The possibilities of the two-dimensional parameter space available with control of both steric and electrostatic selectivity have not been evaluated. As a possible application, a matrix of membranes spanning both axes could be used to fractionate biomolecule samples prior to additional characterization. This kind of automated, sample-space resolving tool is a central paradigm of shotgun proteomics [134].

The complex problem of fouling resistance, the different properties that promote it in different environments, and the myriad current and potential applications of polymer filtration membranes leaves room for many useful applications of PAN-*g*-PEO NF membranes and future improvements.

6.3. Future Directions

Several of the concepts and findings developed in this work could be extended to improve the utility, understanding and application scope of amphiphilic graft copolymer membranes. The bacterial adhesion and AFM studies of the comb membranes by collaborators at Yale and the BSA filtration experiments confirmed that the membranes have excellent fouling resistance properties. However, the susceptibility of the ester PEO linkage to hydrolysis in acid and basic conditions restricts the membranes to pH conditions less extreme than those possible with polyamide NF membranes. The ether linkages of PEO itself are less susceptible to hydrolysis. The effect of pH on the PA NF membranes is to change the surface potential, making the electrostatic properties vary. A membrane capable of size-based separation not affected by pH could be valuable. For this application, a comb copolymer based on a vinyl

PEO macromonomer would be ideal, thus eliminating the ester while maintaining the pairing with PAN (which has been found to be more biofouling-resistant than PVDF and polyethersulfone, two other common UF membrane materials [144]). The utility of such a polymer depends upon its availability; unlike the methacrylate macromonomer of PEO, vinyl-functionalized PEO does not appear to be available through common suppliers. One alternative is to prepare PEO-functionalized styrene macromonomers, which can be done with good yield [145]. The good copolymerizability of styrene and acrylonitrile make the approach plausible, but the properties of such a comb could be very different due to the phenyl ring and the material impractical as a commercial coating due to the involved preparation.

There are still open questions regarding the size exclusion mechanism of PAN-*g*-PEO NF membranes. Model predictions of a side-chain length-dependent size cutoff in poor solvents could not be tested due to a lack of rigid molecule probes of size > 1.3 nm. As an alternative, membranes could be tested using a distribution of appropriately-functionalized and coated nanoparticles in a poor solvent for PEO, such as an ether or aliphatic hydrocarbon. If the size cutoff is found to be directly proportional to the side chain molecular weight, it would support the model and also provide a measure of the hydrophilic domain size, that has proved difficult to obtain by conventional x-ray scattering methods. It could also provide a useful approach to quantify the effect of PEG additive on the coated membrane morphology.

The size cutoff under those conditions could be very precise due to the regularity and rigidity of the collapsed, PEO-coated PAN domains in the microphase-separated structure [56]. The first step in pursuing this course would be to test the feasibility of using a MF membrane as the base support. As was seen in the PAN-400 control filtrations, the broad distribution of pores extends to sufficiently small sizes to retain a significant amount of the ~1 nm dyes (Figure 3.11, 3.12). It would thus restrict the passage of coated nanoparticles, adding ambiguity to the results.

A more direct measure of the microphase domain size could be obtained by transmission electron microscopy. Another alternative for characterizing the comb morphology in both the dry and hydrated states is neutron scattering, which unlike x-ray and electron methods doesn't

rely on electron density for contrast. Through the use of selective deuteration, scattering contrast can be manipulated in a system of several components (PAN, PEO and water) to determine their relative spatial locations within the microphase-separated structure. The limitation of this characterization technique is the infrastructure required to produce a beam of thermalized neutrons; using it requires a grant of instrument time at a facility with a reactor or collider.

Active membranes are membranes imbued with catalytic or reactive components that mediate a reaction with solutes passing through. The self-assembled nature of the comb membranes makes them interesting candidates as hosts for active components. By modifying a fraction of PEO side chain ends with ligands, it might be possible to add catalytic nanoparticles to the polymer solution or synthesize nanoparticles *in situ* to form an active membrane with homogenous distribution of liganded particles throughout. Polymer and alumina active membranes have been investigated for hydrogenation reactions and provided advantages over slurry reactor and fixed-bed reactor methods [146-148]. Another application is for water treatment: catalytic nitrate removal [149], a potentially important application due to the extent of fertilizer runoff contamination of surface water.

There are still new applications and scientific understanding to be derived from PEO amphiphilic comb copolymer membranes. It is hoped that the potential will continue to be recognized and investigated.

Glossary

amphiphilic: having both hydrophobic and hydrophilic components
brush: a surface consisting of many individual chains spaced closely enough that they mutually interact
BSA: bovine serum albumin, a 66 kDa protein derived from cow blood
comb: a polymer morphology having side chains attached at intervals to the main backbone
copolymer: a polymer with two component monomers
coupon: an individual section of a membrane
DMF: dimethyl formamide, a polar organic solvent
DMSO: dimethyl sulfoxide, a polar organic solvent with low toxicity
graft: a polymer architecture having one or more side chains
LMH: L/m^2h, a common unit for flux. LMH/MPa (L/m^2hMPa) is a unit of permeability.
macromonomer: a monomer that includes a polymer or other complex structure
monomer: a molecule with a functional group that can participate in polymerization
neat: a pure substance; a neat polymer has no additives
NF: nanofiltration, the regime between reverse osmosis and ultrafiltration and defined as up to 2 nm size cutoff
PA: polyamide, more specifically an aromatic, carboxylate-bearing polyamide interfacially polymerized to make thin-film composite membranes (Figure 1.1.B)
PAN: polyacrylonitrile, in inexpensive polymer
PAN-*g*-PEO: polyacrylonitrile-*graft*-poly(ethylene oxide), an amphiphilic comb copolymer
PBS: phosphate-buffered saline, a common pH 7.4 buffer
PEG: poly(ethylene glycol), another name for low molecular weight PEO
PEO: poly(ethylene oxide), a water-soluble polymer
POEM: poly(oxyethylene) methacrylate, a PEO macromonomer using a methacrylate group
PSSA: poly(styrene sulfonic acid), a negatively charged polymer
PVDF: poly(vinylidene fluoride), a hydrophobic, thermally and mechanically robust membrane material
SPA: sulfopropyl acrylate, a monomer with a negative fixed charge
SPE: *N*,*N*-dimethyl-*N*-(2-methacryloyloxyethyl-*N*-(3-sulfopropyl) ammonium betaine, a very presumptuous zwitterionic monomer
TEA: triethyl amine, a tertiary amine commonly used to neutralize acid produced during a chemical synthesis
terpolymer: a polymer with three component monomers
TFC: thin-film composite, a membrane consisting of a support base membrane and thin selective layer (Figure 1.1.B)
Thickness-normalized permeability: a measure of membrane permeability that includes the thickness of the active layer; permeability in NF is inversely proportional to active layer thickness
UF: ultrafiltration, membrane process for solutes 2-200 nm in size; typified by mesoporous phase inverse membranes
zwitterion: a molecule with both negative and positively charged groups coexisting

Bibliography

[1] K. Ranganathan, K. Karunagaran, D.C. Sharma, Recycling of wastewaters of textile dyeing industries using advanced treatment technology and cost analysis - Case studies, Resources Conservation and Recycling. 50 (2007) 306-318.

[2] W. Lau, A. Ismail, Polymeric nanofiltration membranes for textile dye wastewater treatment: Preparation, performance evaluation, transport modelling, and fouling control -- a review, Desalination. 245 (2009) 321-348.

[3] B. Lesjean, E. Huisjes, Survey of the European MBR market: trends and perspectives, Desalination. 231 (2008) 71-81.

[4] P. Eriksson, M. Kyburz, W. Pergande, NF membrane characteristics and evaluation for sea water processing applications, Desalination. 184 (2005) 281-294.

[5] C. Christy, S. Vermant, The state-of-the-art of filtration in recovery processes for biopharmaceutical production, Desalination. 147 (2002) 1-4.

[6] T. Burnouf, M. Radosevich, Nanofiltration of plasma-derived biopharmaceutical products, Haemophilia. 9 (2003) 24-37.

[7] Progress on Sanitation and Drinking Water, (n.d.).

[8] The Center of Advanced Materials for the Purification of Water with Systems (WaterCAMPWS), (n.d.).

[9] R.W. Baker, Membrane Technology and Applications, Chichester, John Wiley, 2004.

[10] S. Loeb, S. Sourirajan, Sea water demineralization by means of an osmotic membrane, in: Saline Water Conversion—II, Washington, D. C., American Chemical Society, 1963: pp. 117-132.

[11] J. Cadotte, R. Petersen, R. Larson, E. Erickson, A new thin-film composite seawater reverse osmosis membrane, Desalination. 32 (1980) 25-31.

[12] B. Van Der Bruggen, J. Schaep, D. Wilms, C. Vandecasteele, A comparison of models to describe the maximal retention of organic molecules in nanofiltration, Separation Science and Technology. 35 (2000) 169-182.

[13] E.R. Nightingale, Phenomenological theory of ion solvation. Effective radii of hydrated ions, The Journal of Physical Chemistry. 63 (1959) 1381-1387.

[14] H.Y. Ng, M. Elimelech, Influence of colloidal fouling on rejection of trace organic contaminants by reverse osmosis, Journal of Membrane Science. 244 (2004) 215-226.

[15] Nguyen Thanh D., K. Chan, T. Matsuura, S. Sourirajan, Effect of shrinkage on pore size and pore size distribution of different cellulosic reverse osmosis membranes, Industrial & Engineering Chemistry Product Research and Development. 23 (1984) 501-508.

[16] M.J. Zhou, P.R. Nemade, X.Y. Lu, X.H. Zeng, E.S. Hatakeyama, R.D. Noble, et al., New type of membrane material for water desalination based on a cross-linked bicontinuous cubic lyotropic liquid crystal assembly, Journal of the American Chemical Society. 129 (2007) 9574-9575.

[17] F. Fornasiero, H.G. Park, J.K. Holt, M. Stadermann, C.P. Grigoropoulos, A. Noy, et al., Ion exclusion by sub-2-nm carbon nanotube pores, Proceedings of the National Academy of Sciences of the United States of America. 105 (2008) 17250-17255.

[18] J. Warczok, M. Ferrando, F. Lopez, C. Guell, Concentration of apple and pear juices by nanofiltration at low pressures, Journal of Food Engineering. 63 (2004) 63-70.

[19] S. Banvolgyi, S. Horvath, E. Bekassy-Molnar, G. Vatai, Concentration of blackcurrant (Ribes nigrum L.) juice with nanofiltration, Desalination. 200 (2006) 535-536.

[20] A. Hinkova, Z. Bubnik, P. Kadlec, J. Pridal, Potentials of separation membranes in the sugar industry, Separation and Purification Technology. 26 (2002) 101-110.

[21] V. Gekas, G. Baralla, V. Flores, Applications of membrane technology in the food industry, Food Science and Technology International. 4 (1998) 311-328.

[22] N. Hilal, H. Al-Zoubi, N. Darwish, A. Mohamma, M. Abu Arabi, A comprehensive review of nanofiltration membranes:Treatment, pretreatment, modelling, and atomic force microscopy, Desalination. 170 (2004) 281-308.
[23] M.F.A. Goosen, S.S. Sablani, H. Al-Hinai, S. Al-Obeidani, R. Al-Belushi, D. Jackson, Fouling of Reverse Osmosis and Ultrafiltration Membranes: A Critical Review, Separation Science and Technology. 39 (2005) 2261-2297.
[24] M. Mänttäri, L. Puro, J. Nuortila-Jokinen, M. Nyström, Fouling effects of polysaccharides and humic acid in nanofiltration, Journal of Membrane Science. 165 (2000) 1-17.
[25] H.C. Flemming, Biofouling in water systems - cases, causes and countermeasures, Applied Microbiology and Biotechnology. 59 (2002) 629-640.
[26] P. Xu, J.E. Drewes, T. Kim, C. Bellona, G. Amy, Effect of membrane fouling on transport of organic contaminants in NF/RO membrane applications, Journal of Membrane Science. 279 (2006) 165-175.
[27] D. Violleau, H. Essis-Tome, H. Habarou, J. Croué, M. Pontié, Fouling studies of a polyamide nanofiltration membrane by selected natural organic matter: an analytical approach, Desalination. 173 (2005) 223-238.
[28] A. Ramesh, D.J. Lee, J.Y. Lai, Membrane biofouling by extracellular polymeric substances or soluble microbial products from membrane bioreactor sludge, Applied Microbiology and Biotechnology. 74 (2007) 699-707.
[29] M. Herzberg, M. Elimelech, Physiology and genetic traits of reverse osmosis membrane biofilms: a case study with Pseudomonas aeruginosa, Isme J. 2 (2007) 180-194.
[30] H. Flemming, Biofouling in water systems – cases, causes and countermeasures, Applied Microbiology and Biotechnology. 59 (2002) 629-640.
[31] J.S. Baker, L.Y. Dudley, Biofouling in membrane systems -- A review, Desalination. 118 (1998) 81-89.
[32] H. Miyama, H. Shimada, N. Fujii, Y. Nosaka, Y. Noishiki, Graft copolymerization of methoxypoly(ethylene glycohol) methacrylate onto polyacrylonitrile and evaluation of nonthrombogenicity of the copolymer, Journal of Applied Polymer Science. 35 (1988) 115-125.
[33] M. Ulbricht, G. Belfort, Surface modification of ultrafiltration membranes by low temperature plasma II. Graft polymerization onto polyacrylonitrile and polysulfone, Journal of Membrane Science. 111 (1996) 193-215.
[34] V. Kochkodan, N. Hilal, V. Goncharuk, L. Al-Khatib, T. Levadna, Effect of the surface modification of polymer membranes on their microbiological fouling, Colloid Journal. 68 (2006) 267-273.
[35] M. Taniguchi, J.E. Kilduff, G. Belfort, Modes of natural organic matter fouling during ultrafiltration, Environmental Science & Technology. 37 (2003) 1676-1683.
[36] L.D. Nghiem, C. Espendiller, G. Braun, Influence of organic and colloidal fouling on the removal of sulphamethoxazole by nanofiltration membranes, Water Science and Technology. 58 (2008) 163-169.
[37] R.R. Sharma, R. Agrawal, S. Chellam, Temperature effects on sieving characteristics of thin-film composite nanofiltration membranes: pore size distributions and transport parameters, Journal of Membrane Science. 223 (2003) 69-87.
[38] W.H. Fissell, A. Dubnisheva, A.N. Eldridge, A.J. Fleischman, A.L. Zydney, S. Roy, High-performance silicon nanopore hemofiltration membranes, Journal of Membrane Science. 326 (2009) 58-63.
[39] H. Susanto, M. Ulbricht, Photografted thin polymer hydrogel layers on PES ultrafiltration membranes: Characterization, stability, and influence on separation performance, Langmuir. 23 (2007) 7818-7830.
[40] J.S. Louie, I. Pinnau, I. Ciobanu, K.P. Ishida, A. Ng, M. Reinhard, Effects of polyether-polyamide block copolymer coating on performance and fouling of reverse osmosis membranes, Journal of Membrane Science. 280 (2006) 762-770.

[41] C. Hobbs, S.K. Hong, J. Taylor, Effect of surface roughness on fouling of RO and NF membranes during filtration of a high organic surficial groundwater, Journal of Water Supply Research and Technology-Aqua. 55 (2006) 559-570.
[42] S.P. Nunes, M.L. Sforca, K.V. Peinemann, Dense hydrophilic composite membranes for ultrafiltration, Journal of Membrane Science. 106 (1995) 49-56.
[43] S.J. Sofia, V. Premnath, E.W. Merrill, Poly(ethylene oxide) grafted to silicon surfaces: Grafting density and protein adsorption, Macromolecules. 31 (1998) 5059-5070.
[44] W. Norde, D. Gage, Interaction of bovine serum albumin and human blood plasma with PEO-tethered surfaces: Influence of PEO chain length, grafting density, and temperature, Langmuir. 20 (2004) 4162-4167.
[45] D.J. Irvine, A.M. Mayes, S.K. Satija, J.G. Barker, S.J. Sofia-Allgor, L.G. Griffith, Comparison of tethered star and linear poly(ethylene oxide) for control of biomaterials surface properties, Journal of Biomedical Materials Research. 40 (1998) 498-509.
[46] W.T.E. Bosker, P.A. Iakovlev, W. Norde, M.A.C. Stuart, BSA adsorption on bimodal PEO brushes, Journal of Colloid and Interface Science. 286 (2005) 496-503.
[47] H. Ju, B.D. McCloskey, A.C. Sagle, Y.H. Wu, V.A. Kusuma, B.D. Freeman, Crosslinked poly(ethylene oxide) fouling resistant coating materials for oil/water separation, Journal of Membrane Science. 307 (2008) 260-267.
[48] H.B. Park, B.D. Freeman, Z.B. Zhang, M. Sankir, J.E. McGrath, Highly chlorine-tolerant polymers for desalination, Angewandte Chemie-International Edition. 47 (2008) 6019-6024.
[49] H. Ju, B.D. McCloskey, A.C. Sagle, V.A. Kusuma, B.D. Freeman, Preparation and characterization of crosslinked poly(ethylene glycol) diacrylate hydrogels as fouling-resistant membrane coating materials, Journal of Membrane Science. 330 (2009) 180-188.
[50] D.S. Wavhal, E.R. Fisher, Modification of polysulfone ultrafiltration membranes by CO2 plasma treatment, Desalination. 172 (2005) 189-205.
[51] H. Iwata, M.I. Ivanchenko, Y. Miyaki, Preparation of anti-oil stained membrane by grafting polyethylene-glycol macromer onto polysulfone membrane, Journal of Applied Polymer Science. 54 (1994) 125-128.
[52] D. Leckband, S. Sheth, A. Halperin, Grafted poly(ethylene oxide) brushes as nonfouling surface coatings, J Biomater Sci Polym Ed. 10 (1999) 1125-1147.
[53] A. Akthakul, R.F. Salinaro, A.M. Mayes, Antifouling polymer membranes with subnanometer size selectivity, Macromolecules. 37 (2004) 7663-7668.
[54] J.F. Hester, A.M. Mayes, Design and performance of foul-resistant poly(vinylidene fluoride) membranes prepared in a single-step by surface segregation, Journal of Membrane Science. 202 (2002) 119-135.
[55] A. Asatekin, E.A. Olivetti, A.M. Mayes, Fouling resistant, high flux nanofiltration membranes from polyacrylonitrile-graft-poly(ethylene oxide) (PAN-g-PEO), Journal of Membrane Science. 332 (2009) 6-12.
[56] A. Akthakul, A.I. Hochbaum, F. Stellacci, A.M. Mayes, Size fractionation of metal nanoparticles by membrane filtration, Advanced Materials. 17 (2005) 532-535.
[57] A. Asatekin, A.M. Mayes, Responsive pore size properties of composite NF membranes based on PVDF graft copolymers, Separation Science and Technology. 44 (2009) 3330-3345.
[58] A. Asatekin, S. Kang, M. Elimelech, A.M. Mayes, Anti-fouling ultrafiltration membranes containing polyacrylonitrile-graft-poly (ethylene oxide) comb copolymer additives, Journal of Membrane Science. 298 (2007) 136-146.
[59] A. Asatekin, A. Menniti, S.T. Kang, M. Elimelech, E. Morgenroth, A.M. Mayes, Antifouling nanofiltration membranes for membrane bioreactors from self-assembling graft copolymers, Journal of Membrane Science. 285 (2006) 81-89.
[60] J.F. Hester, P. Banerjee, A.M. Mayes, Preparation of protein-resistant surfaces on poly(vinylidene fluoride) membranes via surface segregation, Macromolecules. 32 (1999) 1643-1650.

[61] L.P. Zhu, L. Xu, B.K. Zhu, Y.X. Feng, Y.Y. Xu, Preparation and characterization of improved fouling-resistant PPESK ultrafiltration membranes with amphiphilic PPESK-graft-PEG copolymers as additives, Journal of Membrane Science. 294 (2007) 196-206.
[62] I.V. Berlinova, A. Amzil, N.G. Vladimirov, Amphiphilic graft-copolymers with poly(oxyethylene) side-chains - synthesis via phthalimidoacrylate prepolymers, Journal of Polymer Science Part a-Polymer Chemistry. 33 (1995) 1751-1758.
[63] J.Y. Park, M.H. Acar, A. Akthakul, W. Kuhlman, A.M. Mayes, Polysulfone-graft-poly(ethylene glycol) graft copolymers for surface modification of polysulfone membranes, Biomaterials. 27 (2006) 856-865.
[64] M.H. Keefe, J.L. O'Donnell, R.C. Bailey, S.T. Nguyen, J.T. Hupp, Permeable, microporous polymeric membrane materials constructed from discrete molecular squares, Advanced Materials. 15 (2003) 1936-1939.
[65] S.Y. Yang, I. Ryu, H.Y. Kim, J.K. Kim, S.K. Jang, T.P. Russell, Nanoporous membranes with ultrahigh selectivity and flux for the filtration of viruses, Advanced Materials. 18 (2006) 709-+.
[66] L. Chen, W.A. Phillip, E.L. Cussler, M.A. Hillmyer, Robust Nanoporous Membranes Templated by a Doubly Reactive Block Copolymer, Journal of the American Chemical Society. 129 (2007) 13786-13787.
[67] X. Peng, J. Jin, Y. Nakamura, T. Ohno, I. Ichinose, Ultrafast permeation of water through protein-based membranes, Nat Nano. 4 (2009) 353-357.
[68] M. Kumar, M. Grzelakowski, J. Zilles, M. Clark, W. Meier, Highly permeable polymeric membranes based on the incorporation of the functional water channel protein Aquaporin Z, Proceedings of the National Academy of Sciences of the United States of America. 104 (2007) 20719-20724.
[69] J.A. Quinn, J.L. Anderson, W.S. Ho, W.J. Petzny, Model pores of molecular dimension - preparation and characterization of track-etched membranes, Biophysical Journal. 12 (1972) 990-1007.
[70] S. Yu, S.B. Lee, M. Kang, C.R. Martin, Size-based protein separations in poly(ethylene glycol)-derivatized gold nanotubule membranes, Nano Letters. 1 (2001) 495-498.
[71] K.B. Jirage, J.C. Hulteen, C.R. Martin, Nanotubule-based molecular-filtration membranes, Science. 278 (1997) 655-658.
[72] Y. Lu, T. Suzuki, W. Zhang, J.S. Moore, B.J. Mariñas, Nanofiltration membranes based on rigid star amphiphiles, Chemistry of Materials. 19 (2007) 3194-3204.
[73] B. Van der Bruggen, M. Mänttäri, M. Nyström, Drawbacks of applying nanofiltration and how to avoid them: A review, Separation and Purification Technology. 63 (2008) 251-263.
[74] S. Kang, A. Asatekin, A.M. Mayes, M. Elimelech, Protein antifouling mechanisms of PAN UF membranes incorporating PAN-g-PEO additive, Journal of Membrane Science. 296 (2007) 42-50.
[75] Z. Xu, F. Nie, C. Qu, L. Wan, J. Wu, K. Yao, Tethering poly(ethylene glycol)s to improve the surface biocompatibility of poly(acrylonitrile-co-maleic acid) asymmetric membranes, Biomaterials. 26 (2005) 589-598.
[76] J.H. Koh, K.J. Lee, J.A. Seo, J.H. Kim, Amphiphilic polymer electrolytes consisting of PVC-g-POEM comb-like copolymer and LiCF3SO3, Journal of Polymer Science Part B: Polymer Physics. 47 (2009) 1443-1451.
[77] J.Z. Dawson, Physicochemical characterization of PEG-based comb-like amphiphilic copolymer structures for possible imaging and therapeutic applications, MIT, 2008.
[78] Plastics News, (2010).
[79] J.F. Hester, P. Banerjee, Y.Y. Won, A. Akthakul, M.H. Acar, A.M. Mayes, ATRP of amphiphilic graft copolymers based on PVDF and their use as membrane additives, Macromolecules. 35 (2002) 7652-7661.
[80] Y. Shen, H. Tang, S. Ding, Catalyst separation in atom transfer radical polymerization, Progress in Polymer Science. 29 (2004) 1053-1078.

[81] A. Adout, S. Kang, A. Asatekin, A.M. Mayes, M. Elimelech, Ultrafiltration membranes incorporating amphiphilic comb copolymer additives prevent irreversible adhesion of bacteria, Environmental Science & Technology. 44 (2010) 2406-2411.
[82] D. Neugebauer, Graft copolymers with poly(ethylene oxide) segments, Polymer International. 56 (2007) 1469-1498.
[83] I. Taniguchi, W.A. Kuhlman, L.G. Griffith, A.M. Mayes, Macromonomer purification strategy for well-defined polymer amphiphiles incorporating poly(ethylene glycol) monomethacrylate, Macromolecular Rapid Communications. 27 (2006) 631-636.
[84] M.E.E. Garcia, R. Nobrega, C.M.F. Oliveira, Polyacrylonitrile-graft-poly(ethylene oxide) .1. Synthesis and characterization of copolymers obtained in N,N-dimethyl formamide solution, Polymer Bulletin. 37 (1996) 437-442.
[85] K. Ito, H. Tsuchida, A. Hayashi, T. Kitano, E. Yamada, T. Matsumoto, Reactivity of poly(ethylene oxide) macromonomers in radical copolymerization, Polymer Journal. 17 (1985) 827-839.
[86] G.F. Meijs, E. Rizzardo, Reactivity of macromonomers in free-radical polymerization, Journal of Macromolecular Science-Reviews in Macromolecular Chemistry and Physics. C30 (1990) 305-377.
[87] B. Geetha, A.B. Mandal, T. Ramasami, Synthesis, characterization, and micelle formation in an aqueous-solution of methoxypoly(ethylene glycol) macromonomer, homopolymer, and graft copolymer, Macromolecules. 26 (1993) 4083-4088.
[88] X. Fan, L. Lin, P.B. Messersmith, Cell fouling resistance of polymer brushes grafted from Ti substrates by surface-initiated polymerization: Effect of ethylene glycol side chain length, Biomacromolecules. 7 (2006) 2443-2448.
[89] Grafted poly(ethylene oxide) brushes as nonfouling... [J Biomater Sci Polym Ed. 1999] - PubMed result, (n.d.).
[90] R. Jiang, Y. Kuang, X. Sun, S. Zhang, An improved catalytic system for recycling OsO4 and chiral ligands in the asymmetric dihydroxylation of olefins, Tetrahedron: Asymmetry. 15 (2004) 743-746.
[91] H. Xie, M. Cui, J. Guo, Some properties and morphology of poly(2-vinyl pyridine)-g-polyoxyethylene, European Polymer Journal. 33 (1997) 1537-1542.
[92] A.G. Ruzette, P.P. Soo, D.R. Sadoway, A.M. Mayes, Melt-formable block copolymer electrolytes for lithium rechargeable batteries, Journal of The Electrochemical Society. 148 (2001) A537-A543.
[93] M.E.E. Garcia, R. Nobrega, C.M.F. Oliveira, Polyacrylonitrile-graft-poly(ethylene oxide) .2. Membranes of polyacrylonitrile and polyacrylonitrile-graft-poly(ethylene oxide) blends for separation of water/ethanol mixtures by pervaporation, Polymer Bulletin. 37 (1996) 519-523.
[94] P. Gramain, Y. Frere, Preparation of monomethoxy-poly(ethylene oxide) acrylate and methacrylate and its polymerization - self-gelling polymers, Polymer Communications. 27 (1986) 16-18.
[95] A. Asatekin Alexiou, Improved Filtration Membranes through Self-Organizing Amphiphilic Comb Copolymers, MIT, 2009.
[96] G. Moad, D.H. Solomon, Copolymerization, in: The Chemistry of Radical Polymerization (Second Edition), Amsterdam, Elsevier Science Ltd, 2005: pp. 333-412.
[97] O. Uzun, Y. Hu, A. Verma, S. Chen, A. Centrone, F. Stellacci, Water-soluble amphiphilic gold nanoparticles with structured ligand shells, Chem. Commun. (2008) 196.
[98] H.E. Gottlieb, V. Kotlyar, A. Nudelman, NMR chemical shifts of common laboratory solvents as trace impurities, The Journal of Organic Chemistry. 62 (1997) 7512-7515.
[99] A. Volkov, D. Stamatialis, V. Khotimsky, V. Volkov, M. Wessling, N. Platé, Poly[1-(trimethylsilyl)-1-propyne] as a solvent resistance nanofiltration membrane material, Journal of Membrane Science. 281 (2006) 351-357.
[100] P.S. Singh, V.K. Aswal, Compacted nanoscale blocks To build skin layers of reverse osmosis

and nanofiltration membranes: A revelation from small-angle neutron scattering, The Journal of Physical Chemistry C. 111 (2007) 16219-16226.
[101] A. Akthakul, Design of Chemistry and Morphology of Polymer Filtration Membranes, MIT, 2003.
[102] A.S. Kenyon, M.J. Rayford, Mechanical relaxation processes in polyacrylonitrile polymers and copolymers, Journal of Applied Polymer Science. 23 (1979) 717-725.
[103] A.V. Rajulu, P.M. Sab, Refractometric studies in water/polyethylene glycol-300 mixtures, European Polymer Journal. 34 (1998) 31-32.
[104] J. Tanninen, M. Mänttäri, M. Nyström, Effect of salt mixture concentration on fractionation with NF membranes, Journal of Membrane Science. 283 (2006) 57-64.
[105] M.L. Ferrer, R. Duchowicz, B. Carrasco, J.G. de la Torre, A.U. Acuña, The conformation of serum albumin in solution: A combined phosphorescence depolarization-hydrodynamic modeling study, Biophysical Journal. 80 (2001) 2422-2430.
[106] X.F. Wang, D.F. Fang, K. Yoon, B.S. Hsiao, B. Chu, High performance ultrafiltration composite membranes based on poly(vinyl alcohol) hydrogel coating on crosslinked nanofibrous poly(vinyl alcohol) scaffold, Journal of Membrane Science. 278 (2006) 261-268.
[107] J. Hester, S.C. Olugebefola, A.M. Mayes, Preparation of pH-responsive polymer membranes by self-organization, Journal of Membrane Science. 208 (2002) 375-388.
[108] D. Stamatialis, N. Stafie, K. Buadu, M. Hempenius, M. Wessling, Observations on the permeation performance of solvent resistant nanofiltration membranes, Journal of Membrane Science. 279 (2006) 424-433.
[109] A.M. Mayes, T.P. Russell, S.K. Satija, C.F. Majkrzak, Homopolymer distributions in ordered block copolymers, Macromolecules. 25 (1992) 6523-6531.
[110] S. Saeki, N. Kuwahara, M. Nakata, M. Kaneko, Phase separation of poly(ethylene glycol) water salt systems, Polymer. 18 (1977) 1027-1031.
[111] H.S. Ashbaugh, M.E. Paulaitis, Monomer hydrophobicity as a mechanism for the LCST behavior of poly(ethylene oxide) in water, Industrial & Engineering Chemistry Research. 45 (2006) 5531-5537.
[112] G.D. Smith, D. Bedrov, Roles of enthalpy, entropy, and hydrogen bonding in the lower critical solution temperature behavior of poly(ethylene oxide)/water solutions, Journal of Physical Chemistry B. 107 (2003) 3095-3097.
[113] J.H. Sung, D.C. Lee, H.J. Park, Conformational characteristics of poly(ethylene oxide) (PEO) in methanol, Polymer. 48 (2007) 4205-4212.
[114] J. Santos, A. Hidalgo, R. Oliveira, S. Velizarov, J. Crespo, Analysis of solvent flux through nanofiltration membranes by mechanistic, chemometric and hybrid modelling, Journal of Membrane Science. 300 (2007) 191-204.
[115] S. Darvishmanesh, A. Buekenhoudt, J. Degrève, B. Van der Bruggen, General model for prediction of solvent permeation through organic and inorganic solvent resistant nanofiltration membranes, Journal of Membrane Science. 334 (2009) 43-49.
[116] J. Geens, K. Peeters, B. Van der Bruggen, C. Vandecasteele, Polymeric nanofiltration of binary water-alcohol mixtures: Influence of feed composition and membrane properties on permeability and rejection, Journal of Membrane Science. 255 (2005) 255-264.
[117] S. Bekiranov, R. Bruinsma, P. Pincus, Solution behavior of polyethylene oxide in water as a function of temperature and pressure, Phys. Rev. E. 55 (1997) 577-585.
[118] R. Smith, B. Ellis, Polymers: A Property Database, 2nd ed., CRC Press, 2007.
[119] P. Hansen, J. Cohen, R. Podgornik, V. Parsegian, Osmotic properties of poly(ethylene glycols): Quantitative features of brush and bulk scaling laws, Biophysical Journal. 84 (2003) 350-355.
[120] M. Zhou, T. Kidd, R. Noble, D. Gin, Supported lyotropic liquid-crystal polymer membranes: Promising materials for molecular-size-selective aqueous nanofiltration, Advanced Materials. 17 (2005) 1850-1853.
[121] Y. Yuan, J.E. Kilduff, Hydrodynamic modeling of NOM transport in UF: Effects of charge

density and ionic strength on effective size and sieving, Environmental Science & Technology. 43 (2009) 5449-5454.
[122] E.M.V. Hoek, M. Elimelech, Cake-enhanced concentration polarization: A new fouling mechanism for salt-rejecting membranes, Environmental Science & Technology. 37 (2003) 5581-5588.
[123] J. Tanninen, M. Mänttäri, M. Nyström, Effect of electrolyte strength on acid separation with NF membranes, Journal of Membrane Science. 294 (2007) 207-212.
[124] S. Hall, T. Bradley, J.T. Moore, T. Kuykindall, L. Minella, Acute and chronic toxicity of nano-scale TiO2 particles to freshwater fish, cladocerans, and green algae, and effects of organic and inorganic substrate on TiO2 toxicity, Nanotoxicology. 3 (2009) 91-97.
[125] M. Auffan, M. Pedeutour, J. Rose, A. Masion, F. Ziarelli, D. Borschneck, et al., Structural degradation at the surface of a TiO2-based nanomaterial used in cosmetics, Environmental Science & Technology. 44 (2010) 2689-2694.
[126] J.P. Novak, C. Nickerson, S. Franzen, D.L. Feldheim, Purification of molecularly bridged metal nanoparticle arrays by centrifugation and size exclusion chromatography, Analytical Chemistry. 73 (2001) 5758-5761.
[127] A.C. Templeton, D.E. Cliffel, R.W. Murray, Redox and fluorophore functionalization of water-soluble, tiopronin-protected gold clusters, Journal of the American Chemical Society. 121 (1999) 7081-7089.
[128] S.R. Saunders, C.B. Roberts, Size-selective fractionation of nanoparticles at an application scale using CO 2 gas-expanded liquids, Nanotechnology. 20 (2009) 475605.
[129] S.F. Sweeney, G.H. Woehrle, J.E. Hutchison, Rapid purification and size separation of gold nanoparticles via diafiltration, Journal of the American Chemical Society. 128 (2006) 3190-3197.
[130] F. Nau, F.L. Kerhervé, J. Leonil, G. Daufin, Selective separation of tryptic beta-casein peptides through ultrafiltration membranes: Influence of ionic interactions, Biotechnology and Bioengineering. 46 (1995) 246-253.
[131] C. Martin-Orue, S. Bouhallab, A. Garem, Nanofiltration of amino acid and peptide solutions: mechanisms of separation, Journal of Membrane Science. 142 (1998) 225-233.
[132] T. Tsuru, T. Shutou, S. Nakao, S. Kimura, Peptide and amino acid separation with nanofiltration membranes, Separation Science and Technology. 29 (1994) 971-984.
[133] S.U. Hong, M.L. Bruening, Separation of amino acid mixtures using multilayer polyelectrolyte nanofiltration membranes, Journal of Membrane Science. 280 (2006) 1-5.
[134] W.H. McDonald, J.R. Yates, Shotgun proteomics and biomarker discovery, Disease Markers. 18 (2002) 99-105.
[135] J.Y. Han, J.P. Fu, R.B. Schoch, Molecular sieving using nanofilters: Past, present and future, Lab on a Chip. 8 (2008) 23-33.
[136] Y. Lanteri, P. Fievet, A. Szymczyk, Evaluation of the steric, electric, and dielectric exclusion model on the basis of salt rejection rate and membrane potential measurements, Journal of Colloid and Interface Science. 331 (2009) 148-155.
[137] F.G. Donnan, The theory of membrane equilibria, Chemical Reviews. 1 (1924) 73-90.
[138] J.H. Koh, Y.W. Kim, J.T. Park, B.R. Min, J.H. Kim, Nanofiltration membranes based on poly(vinylidene fluoride-co-chlorotrifluoroethylene)-graft-poly(styrene sulfonic acid), Polymers for Advanced Technologies. 19 (2008) 1643-1648.
[139] M.A. Seman, M. Khayet, N. Hilal, Nanofiltration thin-film composite polyester polyethersulfone-based membranes prepared by interfacial polymerization, Journal of Membrane Science. 348 (2010) 109-116.
[140] C. Devereaux, Self-healing properties of water filtration membranes containing amphiphilic comb polymer, MIT, 2004.
[141] J.Y. Park, M.H. Acar, A. Akthakul, W. Kuhlman, A.M. Mayes, Polysulfone-graft-poly(ethylene glycol) graft copolymers for surface modification of polysulfone membranes,

Biomaterials. 27 (2006) 856-865.
[142] P. Gennes, Scaling concepts in polymer physics, Ithaca N.Y., Cornell University Press, 1979.
[143] K. Binder, Scaling concepts for polymer brushes and their test with computer simulation, The European Physical Journal E - Soft Matter. 9 (2002) 293-298.
[144] G. Zhang, S. Ji, X. Gao, Z. Liu, Adsorptive fouling of extracellular polymeric substances with polymeric ultrafiltration membranes, Journal of Membrane Science. 309 (2008) 28-35.
[145] Y. Gnanou, P. Rempp, Macromonomer synthesis. New functionalization methods, Die Makromolekulare Chemie. 188 (1987) 2111-2119.
[146] L. Gröschel, R. Haidar, A. Beyer, H. Cölfen, B. Frank, R. Schomäcker, Hydrogenation of propyne in palladium-containing polyacrylic acid membranes and its characterization, Industrial & Engineering Chemistry Research. 44 (2005) 9064-9070.
[147] A. Schmidt, A. Wolf, R. Warsitz, R. Dittmeyer, D. Urbanczyk, I. Voigt, et al., A pore-flow-through membrane reactor for partial hydrogenation of 1,5-cyclooctadiene, AIChE Journal. 54 (2008) 258-268.
[148] Y. Zhou, H. Ye, R. Schomacker, Selective hydrogenation of 1,5-cyclo-octadiene over porous Pd/alpha-Al2O3 active membrane, Chinese Journal of Catalysis. 28 (2007) 715-719.
[149] B.P. Chaplin, E. Roundy, K.A. Guy, J.R. Shapley, C.J. Werth, Effects of natural water ions and humic acid on catalytic nitrate reduction kinetics using an alumina supported Pd−Cu catalyst, Environmental Science & Technology. 40 (2006) 3075-3081.

Appendix A. Sepro PAN-400 Base Membrane Properties

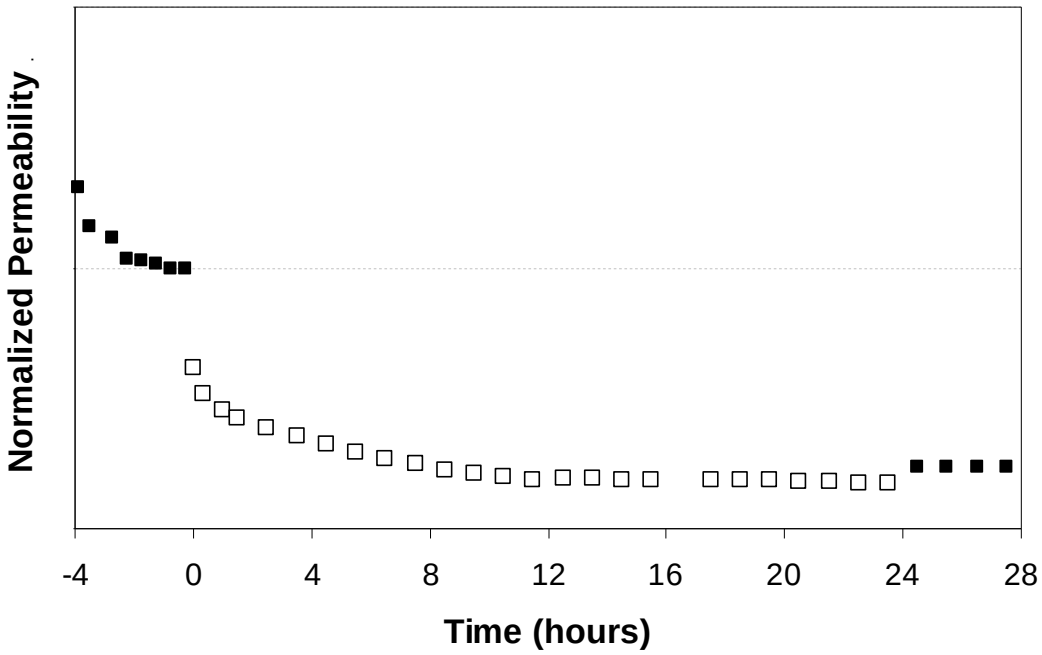

Figure A.1. Dead-end filtration at 0.03 MPa of 1 g/L BSA solution (open symbols) and deionized water (filled) through PAN-400 with permeability normalized by the initial pure water permeability. Exposure to the protein solution causes a 76% decrease in the initial permeability of 2,600 L/m^{2}hMPa.

Table A.1. PAN-400 Properties

Permeability (10^3 LMH/MPa)	**0.1% Na_2SO_4 Retention***	**0.1% NaCl Retention***	**Final BSA Retention**
2.3 ± 0.4	0.06 ± 0.01	0.00 ± 0.01	0.95

* 1 g/L at 154 LMH flux

Appendix B. Thickness-Normalized Permeability Data

Table B.1. Thickness-normalized permeabilities for PAN-*g*-PEO comb membranes

Comb	Permeability (LMH/MPa)	Thickness (μm)	Thickness-Normalized Permeability (LMH-µm/MPa)
PAN-*g*-PEO9 (38% PEO)	39 ±1	2.4 ±0.2	92 ±9
	40 ±1	1.0 ±0.1	40 ±5
PAN-*g*-PEO9 (44% PEO)	60 ±9	1.0 ±0.3	60 ±20
	63 ±8	1.7 ±0.3	110 ±30
PAN-*g*-PEO22	44 ±1	2.5 ±0.4	110 ±20
PAN-*g*-PEO40	34 ±2	0.8 ±0.1	28 ±5
PAN-*g*-PEO40 + 10% PEG45	25 ±1	1.7 ±0.2	44 ±5

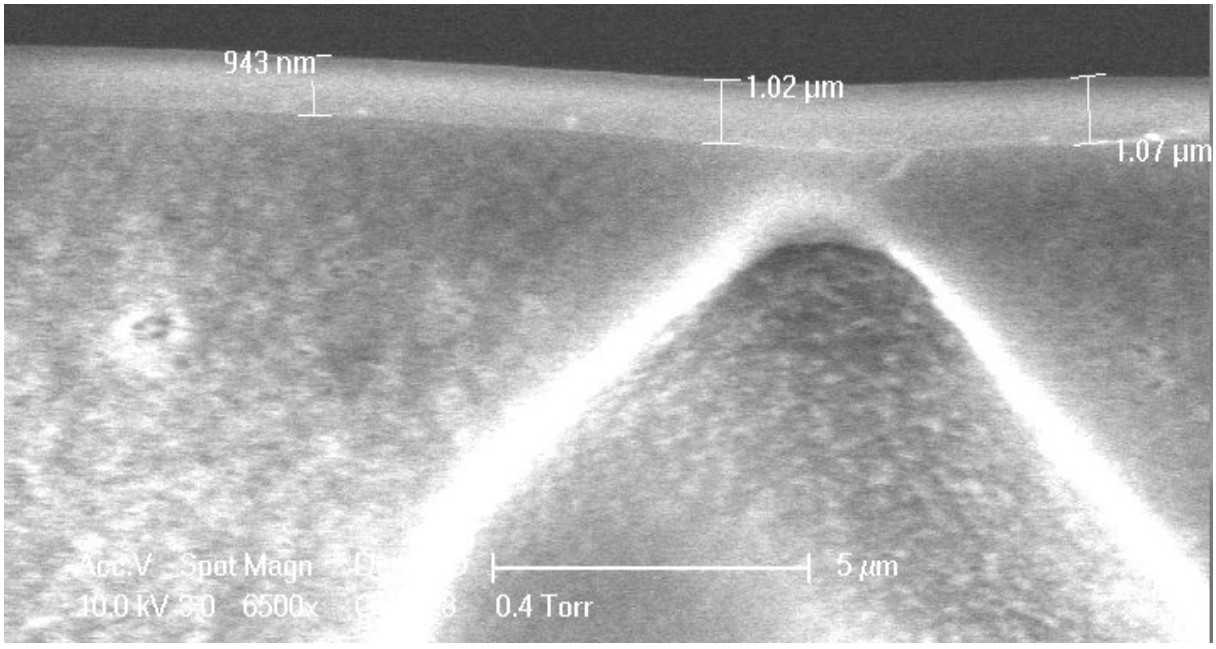

Figure B.1. ESEM micrograph, using 10 kV beam potential and GSE detector, of PAN-*g*-PEO40 comb coating on PAN-400 membrane.

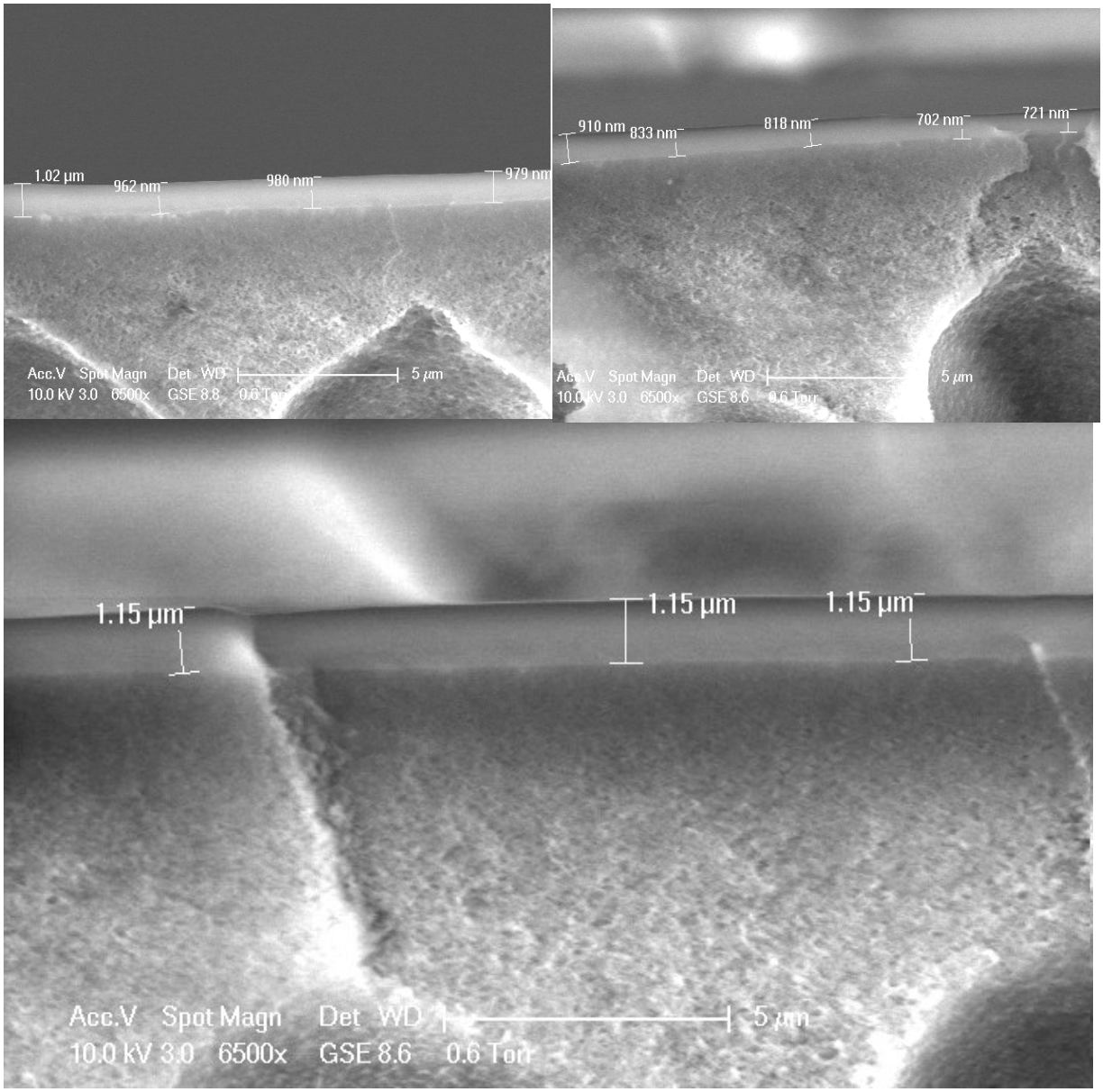

Figure B.2. ESEM micrographs, using 10 kV beam potential and GSE detector, of PAN-*g*-PEO9 comb coating on PAN-400 membrane.